UNIL | Université de Lausanne

Faculté de Biologie
et de Médecine

DEPARTEMENT DE PHARMACOLOGIE ET DE TOXICOLOGIE

ROLE OF INTRACELLULAR CYSTEINES IN ENAC FUNCTION

Thèse de Doctorat ès Sciences de la Vie (PhD)

présentée en co-tutelle à la Faculté de Biologie et de Médecine de l'Université de Lausanne (Suisse) et l'Ecole Doctorale de Physiologie et Physiopathologie de l'Université Pierre et Marie Curie, Paris VI (France)

par

Armelle-Natsuo TAKEDA

diplomée d'Etudes Approfondies de Physiopathologie Cellulaire et Moléculaire, Université Pierre et Marie Curie, Paris VI, France

Jury

Prof. Giampietro CORRADIN, President
Professeur Laurent SCHILD, Directeur de thèse (UNIL)
Docteur Alain VANDEWALLE, Directeur de thèse (Paris VI)
Dr. Ian FORSTER, Expert
Dr. Stefan GRÜNDER, Expert
Pr. Jacques TEULON, Expert

Lausanne 2009

Imprimatur

Vu le rapport présenté par le jury d'examen, composé de

Président	Monsieur	Prof.	Giampietro	**Corradin**
Directeur de thèse	Monsieur	Prof.	Laurent	**Schild**
Co-directeur de thèse	Monsieur	Dr	Alain	**Vandewalle**
Experts	Monsieur	Prof.	Stefan	**Gruender**
	Monsieur	Prof.	Jacques	**Teulon**
	Monsieur	Dr	Ian C.	**Forster**

le Conseil de Faculté autorise l'impression de la thèse de
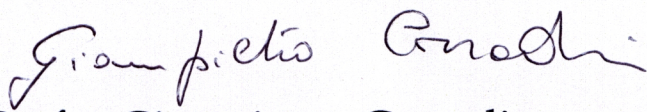
Madame Armelle-Natsuo Takeda

titulaire d'un DEA de l'Université Pierre et Marie Curie, Paris VI, France

intitulée

Role of intracellular cysteines
in ENaC function

Lausanne, le 1 mai 2009

pour Le Doyen
de la Faculté de Biologie et de Médecine

Prof. Giampietro Corradin

ACKNOWLEDGMENTS

ABSTRACT

Role of intracellular cysteines in ENaC function

Armelle TAKEDA, Department of Pharmacology and Toxicology (CH) and Biomedical Research Centre Bichat-Beaujon (F).
Thesis performed in co-supervision between the <u>Faculty of Biology and Medicine</u> of the University of Lausanne, Switzerland and the <u>Doctoral Institute of Physiology and Physiopathology</u> of the University Pierre & Marie Curie of Paris, France.

The epithelial sodium channel (ENaC) regulates the sodium reabsorption in the collecting duct principal cells of the nephron. ENaC is mainly regulated by hormones such as aldosterone and vasopressin, but also by serine proteases, Na^+ and divalent cations. The crystallization of an ENaC/Deg member, the Acid Sensing Ion Channel, has been recently published but the pore-lining residues constitution of ENaC internal pore remains unclear. It has been reported that mutation αS589C of the selectivity filter on the αENaC subunit, a three residues G/SxS sequence, renders the channel permeant to divalent cations and sensitive to extracellular Cd^{2+}. We have shown in the first part of my work that the side chain of αSer589 residue is not pointing toward the pore lumen, permitting the Cd^{2+} to permeate through the ion pore and to coordinate with a native cysteine, γCys546, located in the second transmembrane domain of the γENaC subunit. In a second part, we were interested in the sulfhydryl-reagent intracellular inhibition of ENaC-mediated Na^+ current. Kellenberger *et al.* have shown that ENaC is rapidly and reversibly inhibited by internal sulfhydryl reagents underlying the involvement of intracellular cysteines in the internal regulation of ENaC. We set up a new approach comprising a Substituted Cysteine Analysis Method (SCAM) using intracellular MTSEA-biotin perfusion coupled to functional and biochemical assays. We were thus able to correlate the cysteine-modification of ENaC by methanethiosulfonate (MTS) and its effect on sodium current. This allowed us to determine the amino acids that are accessible to intracellular MTS and the one important for the inhibition of the channel.

RESUME

Rôle des cysteines intracellulaires dans la fonction d'ENaC

Armelle TAKEDA, Département de Pharmacologie et de Toxicologie (CH) et Centre de Recherche Biomédical Centre Bichat-Beaujon (F).
Thèse effectuée en co-tutelle entre la Faculté de Biologie et de Médecine de l'Université de Lausanne, Suisse et l'Ecole Doctorale de Physiologie et de Physiopathologie de l'Université Pierre & Marie Curie de Paris, France.

Le canal épithélial sodique ENaC est responsable de la réabsorption du sodium dans les cellules principales du tubule collecteur rénal. Ce canal est essentiellement régulé par voie hormonale *via* l'aldostérone et la vasopressine mais également par des sérines protéases, le Na^+ lui-même et certains cations divalents. La cristallisation du canal sodique sensible au pH acide, ASIC, un autre membre de la famille ENaC/Deg, a été publiée mais les acides aminés constituant le pore interne d'ENaC restent indéterminés. Il a été montré que la mutation αS589C du filtre de sélectivité de la sous-unité αENaC permet le passage de cations divalents et l'inhibition du canal par le Cd^{2+} extracellulaire. Dans un premier temps, nous avons montré que la chaine latérale de la αSer589 n'est pas orientée vers l'intérieur du pore, permettant au Cd^{2+} de traverser le canal et d'interagir avec une cysteine native du second domaine transmembranaire de la sous-unité γENaC, la γCys546. Dans un second temps, nous nous sommes intéressés au mécanisme d'inhibition d'ENaC par les réactifs sulfhydryl internes. Kellenberger *et al.* ont montré l'implication de cystéines intracellulaires dans la régulation interne d'ENaC par les réactifs sulfhydryl. Nous avons mis en place une nouvelle approche couplant la méthode d'analyse par substitution de cystéines (SCAM) avec des perfusions intracellulaires de MTSEA-biotine. Ainsi, nous pouvons mettre en corrélation les modifications des cystéines d'ENaC par les réactifs methanethiosulfonates (MTS) avec leur effet sur le courant sodique, et donc mettre en évidence les acides aminés accessibles aux MTS intracellulaires et ceux qui sont importants dans la fonction du canal.

RESUME DESTINE A UN LARGE PUBLIC

Rôle des cysteines intracellulaires dans la fonction d'ENaC

Armelle TAKEDA, Département de Pharmacologie et de Toxicologie (CH) et Centre de Recherche Biomédical Centre Bichat-Beaujon (F).

La cellule, unité fonctionnelle du corps humain, est délimitée par une membrane plasmique servant de barrière biologique entre le milieu extracellulaire et le milieu intracellulaire. Cette membrane est imperméable aux nutriments indispensables au fonctionnement de la cellule et donc du corps. Mais la survie de la cellule dépend, entre autres, du maintien de la teneur en ions dans chacun des milieux intracellulaire et extracellulaire et les ions doivent pouvoir être réabsorbés ou sécrétés selon les besoins de la cellule. Ainsi, la cellule synthétise des protéines qui s'insèrent dans la membrane et forment un canal laissant passer spécifiquement, dans un sens ou dans l'autre, certains ions. L'ion sodium (Na^+), présent dans la plupart des aliments et dans le sel, est spécifiquement absorbé dans les cellules du rein grâce à un canal à Na^+ épithélial appelé ENaC. Dans le cas d'ENaC, les ions Na^+ sont réabsorbés de l'urine primaire vers l'intérieur de la cellule. Ils passent ensuite, grâce à un autre canal, de l'intérieur de la cellule vers le sang. C'est entre autres par cette réabsorption de Na^+ que se fait la régulation et le maintien de la concentration sodique du plasma sanguin. Le rôle crucial d'ENaC dans le maintien de l'équilibre sodique dans le corps sous-entend une haute régulation de ce canal dans les cellules. Certains cas de canal ENaC hyperactif ont déjà été rapportés comme dans des maladies telles que l'hypertension et la mucoviscidose. Pour parer à ces dysfonctionnements, il est essentiel de connaitre les mécanismes et fonctionnements de ce genre de protéines. Ainsi, nous nous sommes intéressés aux mécanismes qui régissent l'activité de ce canal. Comment ENaC peut-il être aussi sélectif aux ions Na^+ sans laisser passer les autres ions? Par quels mécanismes et interactions avec les autres protéines ENaC peut-il être activé ou désactivé? Une protéine est une macromolécule biologique composée d'une chaîne d'acides aminés. Parmi les 22 acides aminés présents chez l'homme, la cystéine présente un groupe particulier, le groupe sulfhydryl, capable de former une liaison spécifique et stable avec un autre groupe sulfhydryl. Ces liaisons sont souvent impliquées dans la structure tridimensionnelle de la protéine. Nous avons utilisé cette caractéristique afin d'étudier l'accessibilité et le rôle des cystéines présentes dans ENaC et donc, établir la structure du canal et la corréler avec sa fonction.

KEY WORDS

Epithelial Sodium Channel (ENaC), Regulation, Ion Pore, Cadmium (Cd^{2+}), Methanethiosulfonate (MTS), Cysteine.

MOTS CLEFS

Canal épithélial sodique (ENaC), Régulation, Pore ionique, Cadmium (Cd^{2+}), Methanethiosulfonate (MTS), Cystéine.

TABLE OF CONTENTS

LIST OF FIGURES

ABBREVIATIONS

Å	Angstrom
ADH	Anti-Diuretic Hormone
AIT	Aldosterone-Induced Transcript
ASL	Airway Surface Liquid
ASIC	Acid-Sensing Ion channel
BMOE	bis(maleimido)ethane
cΔASIC	chicken N- and C-termini truncated ASIC
CAP	Channel Activating Protease
CCD	Cortical Collecting Duct
CFTR	Cystic Fibrosis transmembrane conductance regulator
CRD	Cysteine-Rich Domain
Cter_ΔCys	channel mutated in the C-terminus cysteines
Deg	Degenerin
DCT	Distal Convoluted Tubule
DRG	Dorsal Root Ganglion
DTME	dithio-bis-maleimidoethane
DTT	Dithiothreitol
ENaC	Epithelial Sodium Channel
FaNaC	FMRF-amide-gated sodium channel
FMRF	Phe-Met-Arg-Phe
$g(Na^+)$, $g(Li^+)$	unitary channel conductance for Na^+ or Li^+
IC_{50}	half maximal inhibitory concentration
Int_ΔCys	channel mutated in the N- and C-termini and TM1 & 2 cysteines
K_D	dissociation constant
K_m	Half maximal conductance
MBS	Modified Barth's Saline
MR	Mineralocorticoid Receptor
MTS	Methanethiosulfonate
MTSEA	N-Biotinylaminoethyl MTS
MTSET	2-(trimethylammonium)ethyl MTS

NaTT	Sodium Tetrathionate
NCC	Na^+, Cl^- cotransporter
Nedd4-2	Neural Precursor cells-expressed developmentally down-regulated 4-isoform 2
NKCC2	Na^+, K^+, $2Cl^-$ cotransporter
NMDA	N-methyl-D-aspartique
NMDG	N-methyl-D-glucosamine
Nter_ΔCys	channel mutated in the N-terminus cysteines
PCL	Periciliary Liquid
PCT	Proximal Convoluted Tubule
PcTX1	Psalmotoxin 1
$pH_{0.5}$	pH for half-maximal activation
PHA-1	Pseudohypoaldosteronism type 1
pS	pico Siemens
ROMK	Renal Outer Medullary Potassium channel
SCAM	Substitution Cysteine Analysis Method
SDS	Sodium Dodecyl Sulfate
SDS-PAGE	SDS-Polyacrylamide Gel Electrophoresis
Sgk1	Serum and Glucocorticoid regulated Kinase isoform 1
TAL	Thick-walled Ascending Limb
TEV	Two-Electrode Voltage Clamp
TM	Transmembrane domain
VP	Vasopressin
WT	Wild-type

LIST OF AMINO ACIDS

Ala	A	Alanine
Arg	R	Arginine
Asn	N	Asparagine
Asp	D	Aspartate
Cys	C	Cysteine
Gln	Q	Glutamine
Glu	E	Glutamate
Gly	G	Glycine
His	H	Histidine
Ile	I	Isoleucine
Leu	L	Leucine
Lys	K	Lysine
Met	M	Methionine
Phe	F	Phenylalanine
Pro	P	Proline
Ser	S	Serine
Thr	T	Threonine
Trp	W	Tryptophan
Tyr	Y	Tyrosine
Val	V	Valine

INTRODUCTION

The Epithelial Sodium Channel (ENaC) belongs to the ENaC/Degenerin gene family discovered in the beginning of the 1990s. Two genes, *deg-1* and *mec-4*, were first discovered in *Caenorhabditis elegans*. Chalfie *et al.* have shown that gain-of-function of these two degenerin ion channel genes results in a toxic gene product. This causes the degeneration of several neurons (23) and renders mutants incapable of mechanosensation. Then, the sequence of the ENaC α subunit was isolated from epithelial cells of rat distal colon and identified by functional expression in *Xenopus laevis* oocytes (19), quickly followed by the two other β and γ ENaC subunits (20). Sequence alignment of ENaC α, β and γ subunits with *mec-4* and *deg-1* had underlined a high sequence homology, presuming that proteins product by these three genes are members of the same cation channel family. To this new family, numerous additional genes appeared to share sequence homology. Neuronal degenerin from human and rat brain were cloned and described as amiloride-sensitive cation channels for which phylogenetic analysis indicated that they were equally divergent from all other members of the ENaC/DEG family. These genes are expressed predominantly in the peripheral and central nervous system and thus, their encoding protein were called mammalian degenerins (MDEG) or brain Na$^+$ channels (BNaC1, BNaC2) (42). After the discovery of their activation by rapid extracellular acidification (128), their name was changed to Acid-Sensing Ion Channel (ASIC). In parallel, it had been shown that in the nervous tissue of the snail *Helix aspersa*, the FMRFamide-gated sodium channel (FaNaC) could be blocked by amiloride. This protein shares a low sequence identity with ENaC subunits and degenerins but displays the same overall structural organization (79), forming its own subfamily within the ENaC/DEG family. It has also been shown that the gene dGNaC1 is expressed specifically in the gonads and early embryo in

Drosophila melanogaster and thus, seems to be implicated in gametogenesis and early embryogenesis in drosophila.

Studies of sequence alignment between all the members of ENaC/Deg family led to a potential phylogenetic tree proposed in Figure 1 (70). Related sequences are organized into subfamilies. We can distinguish seven branches, with three main subfamilies of genes encoding for: (i) the four ENaC subunits (α, β, γ and δ); (ii) the four ASIC subunits (+ splice variants); and (iii) the *C. elegans* degenerins (DEG, DEL, MEC and UNC). The amino sequence identity between the different ENaC/Deg subfamilies is 15-20 %. Within subfamilies, identities are 30 % for ENaC subunits and 45-60 % for the four ASIC genes (1 to 4). Between species, identities of amino sequences are 85 % between human and rat orthologs of ENaC, almost 100 % between human and rat orthologs of ASIC1, 2 and 4 and 85 % for ASIC3 (70). Although functionally different, members of ENaC/Deg family share the same structure and functional domains that are involved in the control of the channel activity and in the formation of the pore.
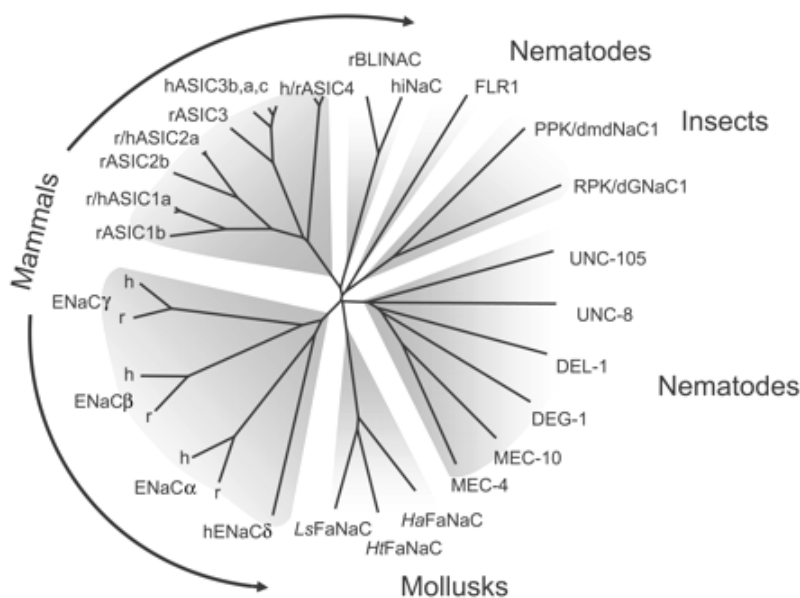
Figure 1: Phylogenetic tree of the ENaC/Deg family. *Kellenberger and Schild, Physiol. Rev., 2002*

I/ ENaC

I-1) Localization of ENaC

ENaC is located at the apical membrane of polarized cells in different tissues, *i.e.* the kidney, the lung, the skin, salivary glands and the tongue. It mediates the Na^+ transport across the membrane to permit its vectorial transcellular transport. This electrogenic Na^+ absorption is necessary to maintain the composition and the volume of the fluid on either side of the epithelium. For example, in the kidney, this active transepithelial transport is essential for the maintenance of blood Na^+ and K^+ levels and their homeostasis. In the lung, it permits to maintain the volume of the luminal fluid.

I-1-i) *The kidney*

The kidney is a natural filter that maintains the homeostatic balance in the body by excreting metabolites and organic wastes in urine along with water (Figure 2). It regulates the blood pressure by regulating the plasma concentration of ions such as Na^+ and K^+, and the levels of compounds like glucose and bicarbonate. The nephron is the renal functional unit. Millions of nephrons join together in collecting ducts to pour out the secreted urine in the ureter (Figure 2A).
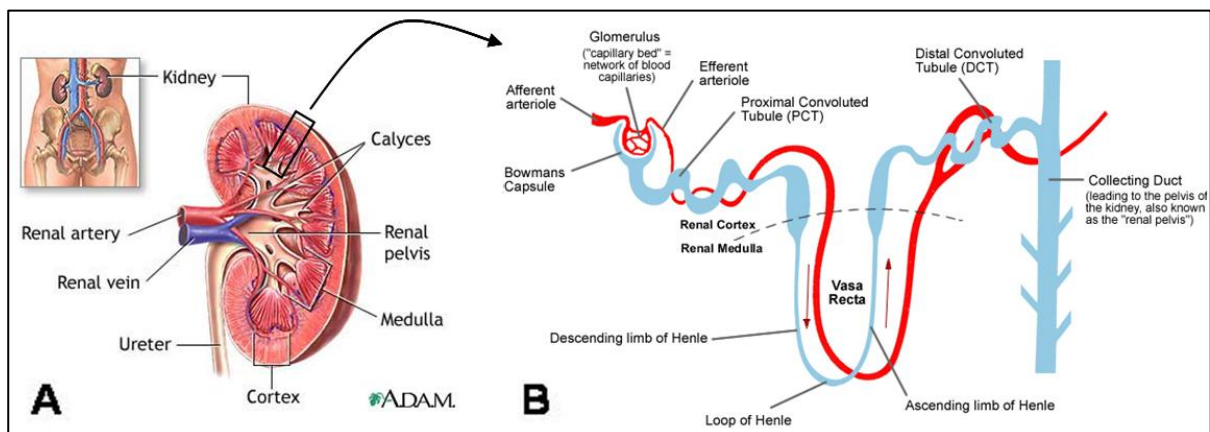
Figure 2: (A) Schematic representation of the kidney (*http://health.nytimes.com***) (B)** Schematic representation of a nephron (*http://www.ivy-rose.co.uk*)

The glomerulus is a network of blood capillaries that filter the blood thanks to the high permeability of its capillaries to water and electrolytes. The filtrate flows along the nephron (Figure 2B) and water and small molecules are reabsorbed from the filtrate into the blood. At the basolateral membrane of proximal convoluted tubule (PCT) cells, the Na^+,K^+-ATPase actively pump Na^+ out of the cell into the blood leading to a strong electrochemical gradient in the cell. This gradient provides a potential to allow isoosmotic Na^+ reabsorption (65 % of filtered sodium) from the lumen to the cell. In the loop of Henle, water is reabsorbed into the hyperosmotic medullary interstitium leading to the concentration of urine. Approximately 25 % of filtered sodium is reabsorbed in the thick-walled ascending limb (TAL) *via* the $Na^+,K^+,2Cl^-$ cotransporter (NKCC2), organized in parallel with the apical K^+ channel ROMK. Then, in the distal convoluted tubule (DCT), about 10 % of sodium is reabsorbed by the Na^+,Cl^- cotransporter. The collecting ducts connect the nephrons to the ureter. In humans, the system accounts for 4-5 % of the kidney's reabsorption of sodium and 5 % of the kidney's reabsorption of water. The cortical collecting ducts (CCD) cells are largely impermeable to water without the presence of antidiuretic hormone (or vasopressin), and are sensitive to aldosterone which stimulates active sodium reabsorption. They are composed of two types of cells: (i) the principal cells, mediating the sodium-potassium balance, and (ii) the intercalated cells (α and β), participating in the acid-base homeostasis. In the principal cells of CCD (Figure 3), sodium is reabsorbed from urine by ENaC which colocalizes with the K^+ channel ROMK. Sodium is then driven to blood *via* the basolateral Na^+,K^+-ATPase pump. This absorption is regulated by the expression of ENaC at the surface of the apical membrane.
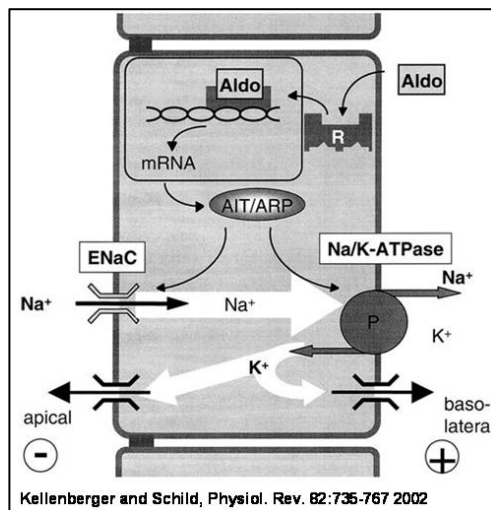
Figure 3: Transepithelial ion transport in a principal cell of the cortical collecting duct. R, mineralocorticoid receptor; AIT, aldosterone-induced transcripts; ARP, aldosterone-repressed protein. *from Kellenberger & Schild, Physiol. Rev., 2002 (70)*

I-1-ii) *The lung*

On the apical surface of the airway epithelium (Figure 4A), there is a glycocalyx, a network of polysaccharides that coats the apical cell surface, and a film of liquid, the periciliary liquid (PCL) layer through which cilia beat freely. This is overlaid by a mucus layer, a gel generated by the high molecular weight mucins, which entraps particles to be transported by coordinated ciliary movement. Altogether, PCL and mucus layers form the Airway Surface Liquid (ASL). The PCL is likely a polyanionic gel layer that allows the cilia to beat. During their strokes, the tips of the cilia contact the underside of the mucous blanket. They propel mucous with entrapped particles to the mouth where everything can be expectorated. This allows the surface of the airways to be kept clean. The viscoelasticity of the mucus is determined by the mucins themselves, their interaction with "sticker" proteins and by the hydration of the layer. This hydration is mediated by a balance between Na^+ absorption *via* ENaC, and Cl^- secretion *via* the cystic fibrosis transmembrane conductance regulator (CFTR) (Figure 4B). The hydration of the mucus is the most important variable in controlling the

efficiency of mucus clearance (15). CFTR belongs to the ABC (ATP-binding cassette) family transporter ATPases and is the only ion channel of the family. It has been shown that CFTR inhibits ENaC activity (122) and stabilizes ENaC at the plasma membrane (82). Moreover, a direct physical association of CFTR and ENaC has been assessed with the fluorescence resonance energy transfer technique (FRET) (8).
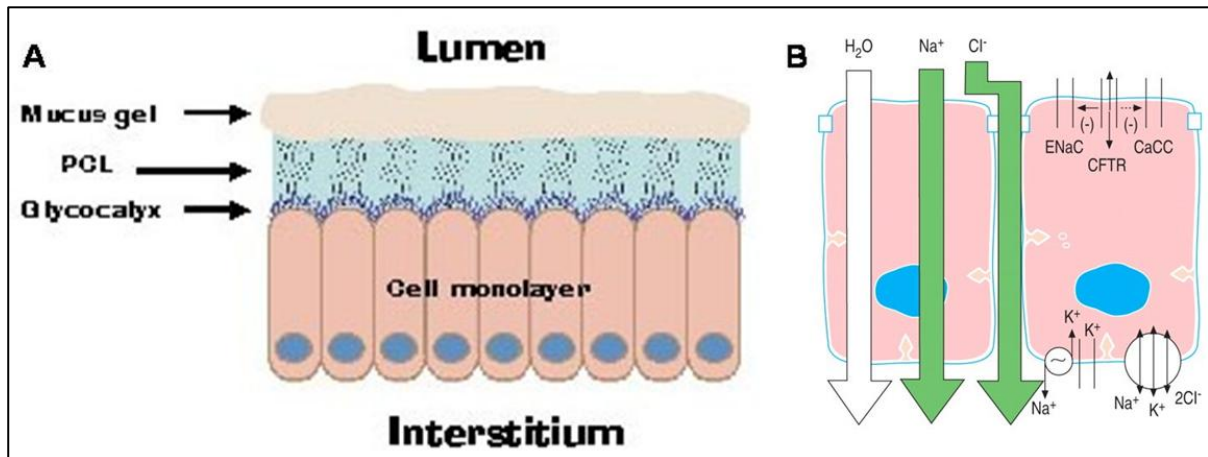
Figure 4: Schematic representation of lung cells. (**A**) The airway surface liquid (ASL) is partitioned into three open compartments, a glycocalyx, a periciliary liquid (PCL) layer and a mucus layer. *from http://www.med.unc.edu/cystfib/Staff/paradiso.htm* (**B**) Regulation of the volume of PCL by active ion transport. *from Boucher, Eur. Respir. J, 2004 (14).*

I-2) Biophysical properties of ENaC

ENaC discriminates among cations based on their size. Small cations such as sodium, lithium and protons are permeant whereas larger cations like potassium or ammonium are not ($Li^+ > Na^+ \gg K^+$). Moreover, ENaC is not permeable to divalent cations. In CCD and *Xenopus laevis* oocytes expressing $\alpha\beta\gamma$ ENaC, 140 mM of extracellular Na^+ leads to a unitary conductance (*g*) of 5 pS and 150 mM of extracellular Li^+, to a $g(Li^+)$ of 10 pS. Calculation of the concentration for half-maximal conductance (K_m) shows that the apparent affinity is higher for Na^+ than for Li^+, with $K_m(Na^+)$ of 20-50 mM and $K_m(Li^+)$ of 90 mM in CCD and 120 mM in *Xenopus laevis* oocytes. This lower affinity and higher conductance of Li^+ is explained by a

higher dissociation rate of Li$^+$ from its binding site in the channel pore compared with Na$^+$. The single-channel conductance changes with the subunit composition of ENaC. In oocytes expressing αβ ENaC, the single-channel conductance is 4-5 pS at 150 mM Na$^+$ or Li$^+$. With αγ ENaC, the Na$^+$ conductance is still 4-5 pS but Li$^+$ conductance is 9-10 pS, as with αβγ ENaC (70). Measurement of the voltage-dependence of the conductance through ENaC has been accounted for in large part by the concentration gradient for Na$^+$ across the apical cell membrane. ENaC is characterized by a slow kinetic of the gating, *i.e.* long spontaneous open and closed times in the range of 0.5-5 seconds at room temperature. In rat CCD, at 37 °C, the gating of the cloned rat ENaC speeds up (hundreds of milliseconds in duration) (43).

I-3) Regulations of ENaC

The main role of ENaC in polarized epithelial cells is to allow the vectorial transcellular transport of Na$^+$ in order to maintain the composition and the volume of the fluid on either side of the epithelium. The entry of Na$^+$ through ENaC at the apical membrane induces a favourable electrochemical gradient that allows the secretion of K$^+$ in the tubule lumen. ENaC represents the rate-limiting step in this process and is regulated by different factors. As other proteins, ENaC follows general process of protein biosynthesis and degradation. Biosynthesis of ENaC subunits is under the control of aldosterone, as explained below, and degradation occurs *via* the ubiquitination of the subunits. Ubiquitination is a posttranslational modification involving the ligation of ubiquitin polypeptides and plays an essential role in many kinds of cellular function. The process of ubiquitination consists of 3 main steps (Figure 5): (i) the ubiquitin is activated by ATP and then transferred to the E1 ubiquitin-activating enzyme where it binds to E1 sulfhydryl group *via* a thioester linkage releasing a molecule of AMP; (ii) the ubiquitin is transferred from E1 to the cysteine residue of E2 ubiquitin-conjugating enzyme; (iii) the E3 ubiquitin-protein

ligase interacts with both E2 and the substrate and allows the transfer of ubiquitin to a lysine residue present on the substrate. Substrate can be monoubiquitinated or polyubiquitinated leading to different signals for protein recycling or degradation. A target protein must be labelled with at least four ubiquitin monomers (in the form of a polyubiquitin chain) before it is recognized by the proteasome, where unneeded or damaged proteins are degraded by proteolysis. The E3 ubiquitin ligase of ENaC has been shown to be the Neural Precursor cells-expressed developmentally down-regulated 4, Nedd4-2 (125). Nedd4-2 interacts specifically with ENaC subunits *via* its PY motif but mechanisms of Nedd4-2-mediated regulation of ENaC will be detailed later (*cf. 'Liddle syndrome' and 'PY motif'*). USP2-45 has been recently identified as the deubiquitinating enzyme that increases ENaC activity in Xenopus oocytes (35), *i.e.* the antagonist enzyme of Nedd4-2.
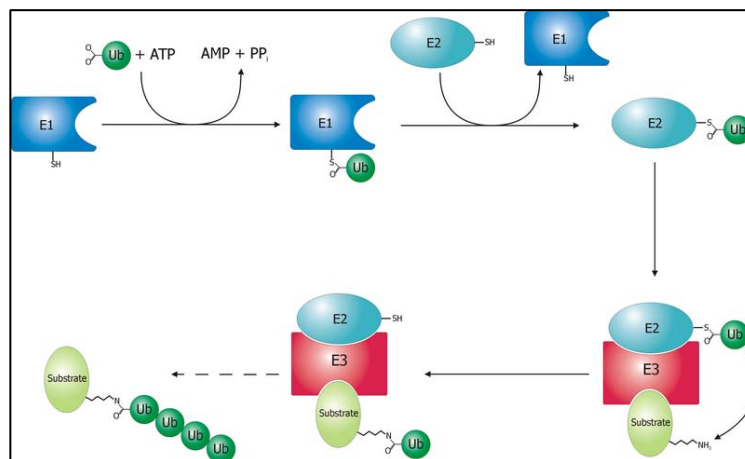
Figure 5: The ubiquitination system. *from http://upload.wikimedia.org/wikipedia/commons/7/7f/Ubiquitylation.png*

I-3-i) *Hormonal regulation*

I-3-i-a) Aldosterone

Aldosterone is a hormone synthesized in the cortex of the adrenal glands in response to the renin-angiotensin system that regulates blood pressure by controlling the extracellular fluid

volume of the body. The renin-angiotensin system is itself activated by a decrease in renal blood pressure or decrease in dietary Na^+ (98). In the principal cells of the cortical collecting duct (CCD), aldosterone regulates the Na^+ reabsorption by its binding to the mineralocorticoid receptor (MR) (Figure 6) (121). The activated complex MR/aldosterone is translocated to the nucleus where it binds to the MR/GR responsive element within the promoter of aldosterone-induced transcripts. It has been recently shown by surface biotinylation of renal cells in rat kidney and by membrane fractionation that increasing the levels of aldosterone in the animals, by feeding a low-Na^+ diet or infusing them directly with hormone, increased the expression of ENaC subunits at the surface by two- to fivefold (41). Among the synthesis of αENaC, α1 and β1 Na^+,K^+-ATPase subunits during the late phase of aldosterone-response (> 3 hours) (85; 86), aldosterone increases ENaC activity by increasing the number of channels at the cell surface in two different ways: (i) stimulation of pathway increasing channel insertion at the cell surface, (ii) inhibition of pathway removing channel expressed at the cell surface. During the early phase (45 min to 3 hours), aldosterone induces the synthesis of several proteins that mediate the cell surface expression of ENaC (100).
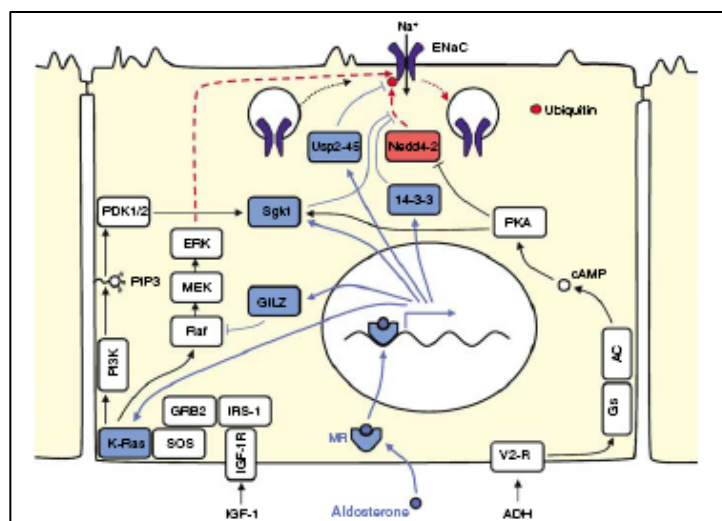
Figure 6: Model for the regulation of ENaC surface expression. Effect of aldosterone and vasopressin on Sgk1, K-Ras, GILZ, 14-3-3, Nedd4-2 and USP2-45 regulations. *from Verrey et al., Kidney Int., 2008 (125).*

The Serum and Glucocorticoid regulated Kinase isoform 1 (**Sgk1**) plays a role in preventing apoptosis and promoting cell proliferation (88). It has been identified as a primary aldosterone-induced transcript in amphibian and mammalian renal epithelia (25; 90). Sgk1 knock-out (*Sgk1⁻/⁻*) mice studies did not present an abnormal phenotype at standard NaCl intake, with an aldosterone-mediated increase of the amiloride-sensitive sodium current similar in wild-type (WT) and *Sgk1⁻/⁻* mice (36; 87; 133). In contrast, in a low salt diet, *Sgk1⁻/⁻* revealed a significant urinary salt wasting despite increases in plasma aldosterone levels, suggesting that lack of Sgk1 prevented the upregulation of ENaC. However, Fejes-Tóth *et al.* have shown that the change in salt wasting should be due to a significant decrease in the Na^+,Cl^+-cotransporter (NCC) which mediates sodium transport in early distal tubules. *In vitro*, the stimulatory effect of aldosterone on ENaC has been related to Sgk1 (80). First, a direct interaction between Sgk1 and ENaC has been suggested in inside-out membrane patches of *Xenopus laevis* oocytes where deletion of the αENaC C-terminus significantly reduced the stimulatory effect of Sgk1 (32). Second, the phosphorylation by Sgk1 of the ubiquitine ligase Nedd4-2, involved in the internalisation of ENaC from the cell surface for recycling or degradation (*cf. 'Liddle syndrome' and 'PY motif'*), has been shown to increase the cell surface expression of ENaC (30; 117). **K-Ras2** is a small G protein that stimulates the ENaC activity *via* its effector protein PI3-kinase and likely also *via* direct effects of its phospholipid product, the phosphatidylinositol 3,4,5-triphosphate (PIP3) on ENaC function (119). The glucocorticoid-induced leucine zipper (**GILZ**) is a leucine zipper protein whose expression is augmented by dexamethasone. It prevents the activation of Raf, another downstream effector of Ras, and thereby prevents the inhibitory action of Erk1/2 on ENaC. Erk-mediated inhibition involved ENaC phosphorylation that stimulates Nedd4-2 interaction with ENaC. Thus, GILZ stimulates the release of ENaC from the inhibition mediated by Nedd4-2 (10). **14-3-3** protein has been shown to potentially participate in the inhibition of Nedd4-2 mediated by Sgk1 (125).

I-3-i-b) Vasopressin

Vasopressin (VP), or antidiuretic hormone (ADH), regulates the water conservation in the body by increasing the permeability to water in the last portion of the nephron (7). VP is stored in the neurohypophysis and released after changes in the osmotic pressure, detected by baroreceptor in the hypothalamus. In the kidney, VP targets the principal cells of the CCD where it acts *via* two specific receptors: the V2 receptor (V2R) located in the basolateral membrane with cyclic adenosyl monophosphate (cAMP) as second messenger, and the V1a receptor (V1aR) located in the apical membrane with Ca^{2+} as second messenger (1) (Figure 7). The antidiuretic action of VP occurs *via* V2R, leading to an increase of water and urea permeability and sodium transport. The V2R-induced increase of cAMP leads to the insertion in the apical membrane of preformed vesicles containing AQP2 and an increase of the apical membrane Na^+ conductance achieved through ENaC (7). Altogether, water and sodium reabsorption lead to the concentration of the luminal fluid in the CCD and thus, to an increase of the urine osmolality. The hydroosmotic effect of basolateral VP can be inhibited by a luminal action of VP mediated by V1aR. Apical VP stimulates prostaglandin (PGs) synthesis *via* an increase of intracellular Ca^{2+} (16).

Bankir, Cardiovascular Research 51:372-390 2001
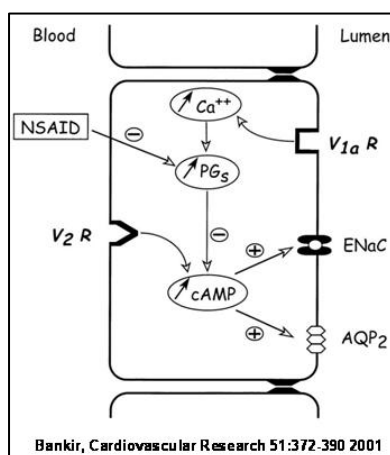
Figure 7: Effect of vasopressin on mammalian CCD cells. Representation of V2R and V1aR effects on AQP2 and ENaC. V2R induces the activation of both channels by an increase of intracellular cAMP. This can be attenuated by the combined action of VP from the luminal side

on V1aR which induces an increase of Ca^{2+} and thus of prostaglandins (PGs). The antidiuretic action of VP can be reinforced with non-steroid anti-inflammatory drugs (NSAID) by inhibiting the PGs. *from Bankir, Cardiovasc. Res., 2001 (7)*

I-3-ii) *Proteolytic activation of ENaC*

Although aldosterone and vasopressin play a key role in the regulation of ENaC, there are also others factors that regulate ENaC. The first evidence of proteolytic activation was the activation of ENaC by extracellular addition of the serine protease **trypsin** (27). Membrane-bound serine proteases had been identified that act as **channel activating proteases** (CAP) (127). The first, CAP-1 in the mouse model or **prostasine** in human, is a glycophosphatidylinositol-anchored protein (24). The two others are mCAP-2, the mouse homolog of the human transmembrane serine protease TMPRSS4, and mCAP-3, or matriptase (126). Each of them is able to increase the sodium current 6 to 10 fold in *Xenopus laevis* oocytes by increasing ENaC open probability. It has also been shown that co-expression of mCAP1, 2 or 3 with Sgk1 leads to a synergistic activation of ENaC (126). Other proteases also activate ENaC like the ubiquitous subtilisin-like proprotein convertase **furin**, cleaving both the α and γ subunits (58), and the neutrophil and pancreatic **elastase**, cleaving at two different sites, both distal to the furin cleavage site on the γ subunit (51).

The activation of ENaC involves the furin-dependant cleavage of the extracellular loop at two sites within the α subunit and at a single site within the γ subunit (60). This cleavage permits the release of two inhibitory domains, one of 26 amino acids located between the two sites on the α subunit (22), and a second one of 43 amino acids between the furin and prostasine cleavage sites on the γ subunit (17). It has been shown that the furin-mediated cleavage of the α subunit affected the basal sodium current, whereas cleavage of the γ subunit affected the overall

expression levels (52). Complete activation was obtained with the combined action of trypsin cleaving the γ subunit (31; 91). Further studies suggested that the proteolytic processing of the γ subunit has a dominant role in activating the channel (21). The β subunit does not undergo any proteolytic cleavage but seems to play an important role in ENaC activation *via* furin-independent activation. The proteolysis of α and γ subunits occurs within the *trans*-Golgi network but both cleaved and uncleaved channels are expressed at the cell membrane (59).
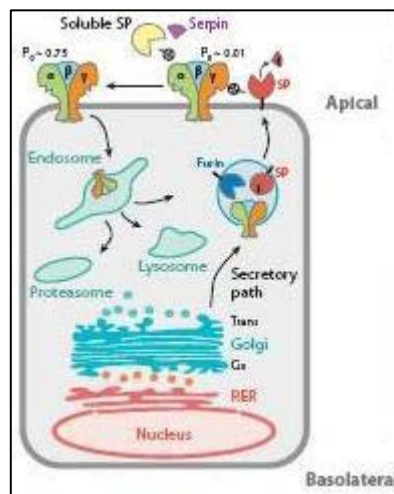
Figure 8: Schematic representation of proteolytic regulation of ENaC. Convertases and ENaC are expected to cotraffic along the same trans-Golgi path, potentially partially proteolized ENaC heteromers to be delivered to the cell surface. At the cell surface, channel-activating serine proteases (SP) become activated and, if appropriately colocalized, can complete proteolytic activation. *from Rossier and Stutts, Annu. Rev. Physiol., 2008 (101)*

Cleaved ENaC is used to exhibit long open and closed states. A population of amiloride-sensitive channels presenting a long closed time and short open times was predicted to be the non-cleaved pool of expressed channels which are able to be activated by extracellular proteases (18). It has to be noticed that more than the proteases, inhibitors of proteases play also a role in the regulation of ENaC. For example, the protease nexin 1 (PN-1) is an endogenous serine protease inhibitor (serpin) that inhibits prostasine as other proteases and, in this way, regulates the expression of selected proteases. In the lungs, the air surface liquid volume is highly regulated by the balance of proteases and protease inhibitors that modulate ENaC activity (89).

I-3-iii) *Ion regulation of ENaC*

I-3-iii-a) Na$^+$ self- & feedback inhibitions

The activity of ENaC is strongly regulated by sodium itself *via* two distinct phenomena: self-inhibition and feedback inhibition. Self-inhibition is the quick return of inward sodium current to a lower steady state value after the rapid increase of extracellular sodium concentration. This model proposes that external sodium has an inhibitory effect on ENaC activity, thereby protecting the cell from Na$^+$ overload. Mechanisms remain unclear but Palmer *et al* (94) proposed that self-inhibition likely induces a decrease in the open probability of ENaC. Bize and Horisberger (11) have recently demonstrated by outward sodium current measurements that self-inhibition and saturation of the conduction site play a significant role in the inhibition of ENaC by extracellular Na$^+$. Using ENaC chimera, Babini *et al.* (6) showed the involvement of the proximal part of the extracellular loop in the Na$^+$ self-inhibition. Moreover, two histidine and several cysteine residues have been proposed as crucial structural determinants for the Na$^+$ self-inhibition (106; 110). Recently, αGly481 and γMet438 in mouse ENaC subunits have been identified as functional determinants of Na$^+$ self-inhibition and of ENaC gating (83). Self-inhibition can be prevented by extracellular proteases (26), such as furin (107), or by extracellular Zn^{2+} (113) or protons (28). The feedback inhibition displays a slow time course (time constant 10-20 min) due to the increase of intracellular sodium concentration. The inhibition occurs *via* a reduction of the ENaC open probability, limiting the sodium entry when concentration of intracellular Na$^+$ ions is high (3). Kellenberger *et al.* (65) have shown that the Liddle mutations of the PY motif on the β and γ subunits, involved in the Nedd-4 regulation of ENaC, lead to a mutant channel less sensitive to inhibition by intracellular Na$^+$. It has been recently shown that intracellular Na$^+$ regulates ENaC cleavage by altering the accessibility of ENaC cleavage sites to proteases (72).

I-3-iii-b) intracellular pH

Maintenance of cell pH depends on the gradient of Na^+ from outside to inside the cell. Thus, elevation of intracellular Na^+ due to a stimulation of Na^+ entry can lead to the acidification of the intracellular medium. Cell pH is therefore a candidate to mediate feedback inhibition. Indeed, it has been shown in frog skin that the sodium permeability is highly sensitive to cytoplasmic pH (53). However, the role of pH in mediating control over Na^+ channels may differ from tissue to tissue (43).

I-3-iii-c) redox regulation

It has been shown that nitric oxide (NO) inhibits ENaC activity in lung alveolar type 2 cells (54) and that in human lung carcinoma cells, the H_2O_2-mediated oxidative stress suppresses the dexamethasone-dependent αENaC transcriptional activation (130). These results suggested that the oxygen-sensitive regulation of ENaC is potentially a key mechanism for regulation of epithelial Na^+ transport during hypoxia. It has been shown recently that ENaC is inhibited in mouse CCD cells by application of intracellular heme mimicking hypoxia conditions (131). This inhibition occurs *via* a decrease in ENaC open probability with no change in the unitary current amplitude. When hemeoxygenase is active, *i.e.* when hemes are catabolised, activity of ENaC is stimulated (131). It has thus been proposed that hemeoxygenase permits the oxygen-sensitive regulation of ENaC. The site on ENaC by which heme should exert its inhibition has not been determined. Furthermore, no known binding site has been found on ENaC but histidine, methionine and cysteine residues are known to provide sites of interaction with heme iron. Study of protein sequences alignment underlined the presence of intracellularly accessible cysteines in the N- and C-termini of α, β and γENaC subunits. Especially in the N-terminus, five cysteine residues are conserved among species and flanked a highly conserved HG motif that plays a role in ENaC gating. Cysteine-substitution and

modification experiments have shown that ENaC is inhibited by intracellular thiol reagents and thiol oxidation (64). This suggests the involvement of intracellular cysteines of ENaC in the thiol-mediated inhibition and, above all, suggests the possibility that changes in intracellular redox potential modulate ENaC activity and transepithelial sodium transport. The mechanisms of the thiol-mediated inhibition of ENaC will be investigated in this work.

I-4) Physiopathology involving ENaC

I-4-i) *Pseudohypoaldosteronism type 1*

Pseudohypoaldosteronism type 1 (PHA1) is an inheritable disorder characterized by severe neonatal salt-wasting, metabolic acidosis, hyperkalemia, dehydration and elevated plasma aldosterone and renin activities. We distinguish two distinct clinical features (50): (i) the autosomal dominant form, linked to the mineralocorticoid receptor; (ii) the recessive systemic form, linked to ENaC. This latter is due to frameshift or missense mutations that lead to a loss of channel function. Several mutations have been identified in human ENaC subunits, for example: (i) the missense mutation βG37S, in the highly conserved domain HG, located in the N-terminus of the β subunit. Homologous mutations into α and γ subunits also significantly reduce the ENaC sodium current (44); (ii) 2 frameshifts (1449delC and 729delA) and 1 missense mutation resulting in the substitution of serine 562 for leucine in the alpha subunit (αS562L) (103); (iii) the mutation αR508Stop leading to a truncated α subunit missing the second transmembrane and C-terminus domains (12); (iv) the mutation αR492Stop leading also to a truncated form of the α subunit (13).

I-4-ii) *Liddle syndrome*

This syndrome took the name of the endocrinologist Grant W. Liddle that described the first time in 1963 patients presenting *'A familial renal disorder simulating primary aldosteronism but with negligible aldosterone secretion'* (77). This autosomal dominant Mendelian hypertension is characterized by severe hypertension, hypokalemia, suppressed plasma renin activity and low urinary level of aldosterone. Mineralocorticoid antagonist such as spironolactone has no effect but a specific blocker of ENaC, trimaterene, normalized blood pressure and hypokalemia. The linkage of the Liddle syndrome with the β subunit of ENaC has underlined a premature stop codon in the C-terminus of the β subunit (115). This leads to the deletion of almost all the C-terminus of the β subunit, particularly the PY motif, involved in the Nedd4-2 ubiquitin ligase regulation (*cf. 'Regulation of ENaC' & 'PY motif'*). Alteration of internalisation of ENaC results in an increase of its surface expression and thus, an increase in sodium reabsorption (39). The conserved sensitivity of ENaC Liddle mutant to aldosterone and vasopressin contribute to the increase of Na^+ absorption (5). Several other mutations, on the rat β and γ subunits, have been described: (i) the βR564Stop mutation identified from the first Liddle patients (104); (ii) the γW574Stop that deletes the last 76 amino acids of the γENaC C-terminus (48); (iii) the βP616L, a *de novo* missense mutation of the β subunit (49). Mutations in the extracellular loop (the insertion of a single nucleotide in the exon 13 of βENaC leading to a frameshift abrogating the PY motif, and γN530S) had been identified from a patient with Liddle syndrome and associated with an increased ENaC activity (56).

The first evidence *in vivo* of the constitutive hyperactivity of ENaC in CCD from mice harbouring Liddle mutation was provided with mice expressing the mutated form of βENaC found by Liddle (9; 97). Another model of Liddle mice was obtained with mice deficient in the ubiquitin ligase Nedd4-2 (114). These mice express hypertension *via* ENaC hyperactivity since:

(i) the three ENaC subunits are highly expressed in kidney, in contrast with other Na^+ transporters; (ii) the down-regulation of ENaC function is impaired; and (iii) the salt-sensitive hypertension is substantially reduced in presence of amiloride.

I-4-iii) *Cystic fibrosis lung disease*

Ninety percent of cystic fibrosis (CF) cases are due to a deletion at position Phe508 in the CFTR protein. CF disease evolves from small-airway obstruction, airway inflammation and intermittent infection into chronic bacterial infection, bronchiectasis and ultimately death. Phe508 mutation prevents the achievement of the native global conformation and leads to a misfolding and failure of translocation of CFTR to the apical membrane (14). Mice deficient in CFTR do not have a spontaneous pulmonary disease phenotype but overexpression of ENaC in mice inducing ASL depletion, increased mucus concentration, delayed mucus transport and mucus adhesion to airway surfaces (84). It has been shown that the ASL volume modulates the activity of ENaC by modification of the serine proteases-protease inhibitors balance and that alterations of this balance leads to an excessive Na^+ absorption like in CF (89). Altogether, these observations suggest that airway surface hydration is the most important variable in controlling the efficiency of mucus clearance. Pharmaceutical companies are looking to develop new treatments for diseases such as CF, like derivative of amiloride, the specific inhibitor of ENaC, that is 60-100 fold more potent than amiloride (57).

II/ ASIC

Four Acid-Sensing Ion Channels, or ASIC, genes have been identified (ASIC 1 to 4) and three of them have splice variants: ASIC1 a/b, ASIC2 a/b, ASIC3 a/b/c. ASIC are ligand-gated ion channels activated by protons with different pH sensitivity and kinetics depending of the subunit composition of the multimer.

II-1) Localization of ASIC

ASIC is expressed at the membrane of epithelial cells in the central and peripheral nervous systems. ASIC1a, ASIC2a and ASIC2b each show a widespread distribution pattern in brain. Highest levels of expression, and coexpression with ASIC4, are found in the hippocampus (involved in short term memory, navigation), the cerebellum (sensory reception, coordination, motor control), in the pyramidal neurones of the neo- (sensory perception) and allocortical (olfaction) regions, the main olfactory bulb (olfaction), the habenula (olfaction) and the basolateral amygdaloid nuclei (memory, emotional reaction). The strongest expression of ASIC4 is in the pituitary gland (70). In the peripheral nervous system, ASIC localize to neurons innerving skin, heart, gut and muscle. They have also been detected in the eye, ear, taste buds and bone. In cutaneous neurons, ASICs, especially ASIC3, have been detected in large, medium and small dorsal root ganglion (DRG) neurons (132).

II-2) Biophysical properties of ASIC

In contrary to ENaC that is constitutively active, ASIC is gated by extracellular protons and thus sensitive to extracellular pH. They are low conductance channels that mainly conduct Na^+ ($g(Na^+)$ of 10-15 pS) (78). Homomeric ASIC1a channels respond to low external pH by mediating a fast and transient inward current with a threshold pH of 6.9 and the pH for half-

maximal activation ($pH_{0.5}$) at 6.2. In addition, ASIC1a is permeable to Ca^{2+} and K^+ ($Na^+ > Ca^{2+} > K^+$) and desensitizes rapidly (inactivation time = 1.4 sec). ASIC1b responds with a similar transient current compared with ASIC1a and a $pH_{0.5}$ of 5.9. Homomeric ASIC2a channels have low sensitivity to protons with a $pH_{0.5}$ of 4.4. ASIC 3 are highly sensitive to protons and have a $pH_{0.5}$ of 6.7 (134). ASIC2b and ASIC4 do not form homomeric channels. However, they associate with other subunits to form heteromeric ASIC with distinct properties that we will not detail here. Typical inward sodium currents obtained with homomeric ASIC1a, ASIC1b, ASIC2a and ASIC3 are presented in figure 9.
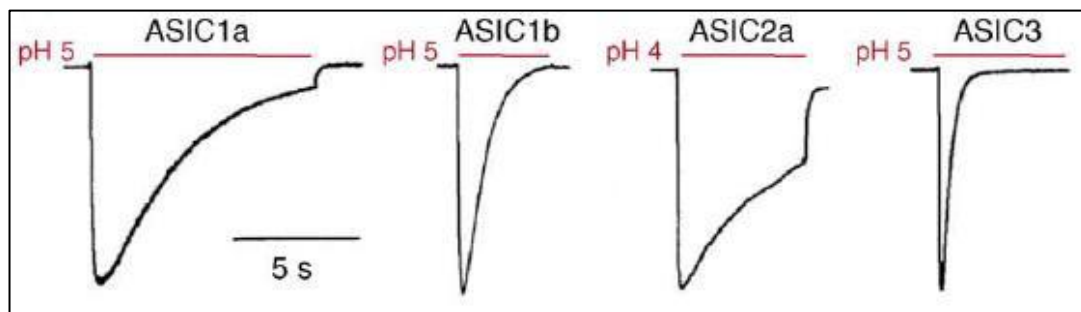
Figure 9: Acid-evoked currents in heterologous cells (Cos-7) expressing the indicated ASIC subunits. *from Wemmie et al., Trends in Neurosciences, 2006 (132)*

II-3) Modulation of ASIC

ASIC activity can be modulated by interacting proteins. Physiological relevance of these interactions remains unclear but they have been described either *in vitro* or *in vivo* by immunofluorescence. ASIC subunits contain a PDZ binding motif at their C-terminal part and interact with several PDZ-containing proteins. For example, PICK1 (Protein interacting with C-kinase 1) colocalizes with ASIC in the nervous system and associates with ASIC1 and ASIC2. *In vitro*, it participates at the protein kinase C (PKC)-mediated up regulation of ASIC2a and ASIC3. During inflammation, ASIC3 is up-regulated by activators of the PKC pathway released (78) such as NHERF-1, Na/H exchange regulatory factor-1, which associates with ASIC3 and increases its surface expression. Most of these proteins colocalize with ASIC3 in DRG neurons suggesting their association *in vivo*. ASIC also interact with non-PDZ proteins. An association

of CaMKII, calcium/calmodulin-dependent protein kinase II, and ASIC1a has been described in brain, which is enhanced by ischemia and leads to an increase of ASIC1a current by CaMKII phosphorylation (78). The Figure 10 shows proteins interacting with ASIC. Peripheral inflammation also increases the ASIC transcript levels in DRG and spinal cord. Synaptically released protons could activate ASICs in the postsynaptic and, possibly, the presynaptic membrane (insert, Figure10).

FMRF-amide is a neuropeptide known to lead to a potentiation of the H^+-gated currents by increasing the peak amplitude and/or slowing inactivation of ASIC1 and ASIC3 but not ASIC2a. FMRF-amide is not present itself in mammals, but FMRF-amide-related proteins (NPFF, NPAF, NPSF) are largely expressed in the central nervous system. However, modulation of ASIC requires FMRF-amide addition at pH 7.4, *i.e.* when the channel is closed, raising questions about how these peptides could affect ASIC *in vivo* (78).
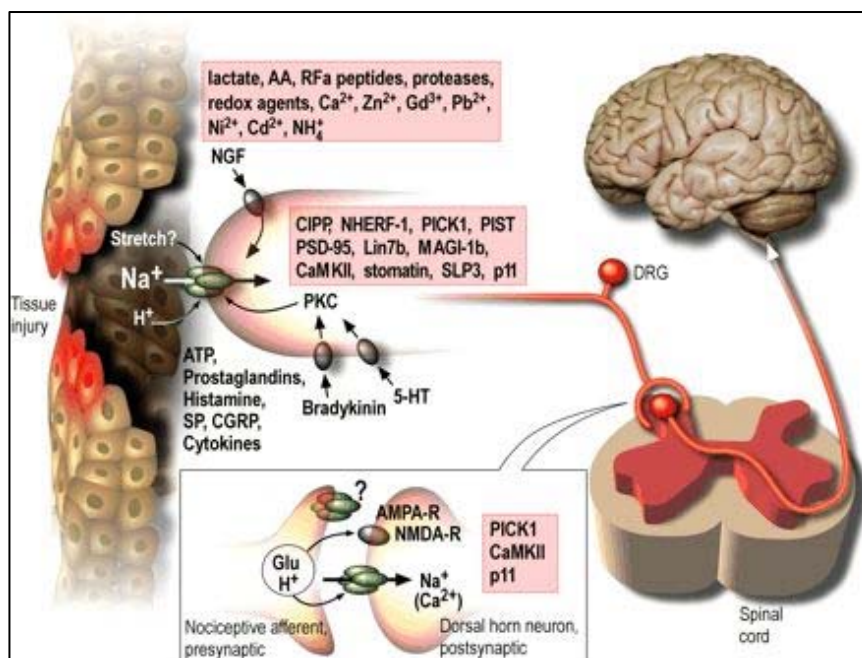
Figure 10: ASICs in primary afferent nociceptors and spinal cord neurons. Interacting proteins and extracellular modulators are shown. AA, Arachidonic Acid; NGF, Nerve Growth Factor; PKC, Protein Kinase C;SP, Substance P; CGRP, Calcitonin gene-related peptide; 5-HT, Serotonin. *From Lingueglia, JBC, 2007 (78)*

II-4) <u>Pharmacology of ASIC</u>

II-4-i) *PcTX1*

The Psalmotoxin 1, or PcTX1, is the most specific blocker of ASIC1a. It has been isolated from the venom of South American tarantula *Psalmopoeus Cambridge*. PcTX1 is a peptide of 40 amino acids cross-linked by three disulfide bridges. It inhibits ASIC1a mediated sodium current in nanomolar concentrations ($IC_{50} < 1nM$). PcTX1 acts as a gating modifier by binding on cysteine-rich domains I and II (CRDI and CRDII; *cf. below, 'Cysteine-Rich Domain'*) of the extracellular loop. It shifts the channel from its resting state towards the inactivated state through an increase of its apparent affinity for protons. This shift is Ca^{2+}-dependent, where increasing extracellular Ca^{2+} results in a decrease of the PcTX1 inhibition (134).

II-4-ii) *APETx2*

APETx2 is a 42 amino acids peptide toxin isolated from sea anemone *Anthopleura elegantissima*. It specifically inhibits homomeric ASIC3 ($IC_{50} = 63$ nM in rat and 175 nM in human) and ASIC3 containing channels (ASIC3/1a, $IC_{50} = 2$ μM; ASIC3/1b, $IC_{50} = 900$ nM; ASIC3/2b, $IC_{50} = 117$ nM). Others channels are not sensitive to APETx2. The mode of action remains unknown (134).

II-4-iii) *Non-specific blockers of ASIC*

Amiloride is a diuretic agent that specifically blocks ENaC in the nanomolar range. It is a non specific blocker of ASIC with an IC_{50} of 10-50 μM (compared with 0.1-1 μM for ENaC). As for ENaC, amiloride binds in the pre-TM2 region and inhibits the current by direct blockage of the channel (*cf. below 'Amiloride binding site'*). A-317567 is a non-selective blocker of ASIC1a-like, ASIC2a-like and ASIC3-like currents in rat DRG neurons with IC_{50} of 2-30 μM.

Finally, non-steroid anti-inflammatory drugs (NSAIDs) are known to inhibit ASIC at therapeutic doses for analgesic effects. For example, Ibuprofen inhibits ASIC1a with an IC_{50} of 350 μM, and Aspirin, ASIC3 containing channels with IC_{50} of 260 μM (134).

Isoform	Tissue distribution	pH$_{0.5\ act}$	Blockers	Modulators	Physiology	Pathology
ASIC1a	PNS, brain, spinal cord, retina, taste cells, bone	6.2-6.8	amiloride, NSAIDs, A-317567, PcTx1	RFa peptides, lactate, spermine, AA, proteases	visceral mechanoperception, visual transduction, synaptic plasticity, fear conditioning, nociception? (PNS and CNS)	upregulated by inflammation in DRG and spinal cord, tissue damage after brain ischemia, downregulated in a rat model of neuropathic pain, downregulated in a rat model of epilepsy, detected in gliomas
ASIC1b	PNS, taste cells, cochlear hair cells	5.1-6.2	amiloride	PcTx1, spermine, proteases	nociception?	upregulated by inflammation in DRG
ASIC2a	PNS (including specialized mechanoreceptors), brain, spinal cord, retina, cochlear spiral ganglion, taste cells (rat), bone	4.1-5.0	amiloride, A-317567	zinc	ASIC1a modulation in the CNS, visual transduction, cutaneous and visceral mechanoperception, suprathreshold hearing, taste	upregulated by inflammation in spinal cord, protects against light-induced retinal degeneration, upregulated in rat brain during ischemia, detected in gliomas
ASIC2b	PNS, brain, spinal cord, retina, taste cells	n/a	n/a		ASIC2a and ASIC3 modulation	upregulated by inflammation in DRG, downregulated in a rat model of epilepsy
ASIC3	PNS (including specialized mechanoreceptors), taste cells, retina, testis, lung epithelial cells, inner ear, bone	6.2-6.7	amiloride, NSAIDs, A-317567, APETx2	RFa peptides, lactate, AA, amiloride	nociception, cutaneous and visceral mechanoperception, hearing	upregulated by inflammation in DRG, acid sensing and inflammatory and non-inflammatory mechanical hyperalgesia in muscle, possible role in angina
ASIC4	PNS (low), brain, spinal cord, retina, pituitary gland, inner ear	n/a	?	?	?	?

Table 1: Properties of ASIC channels. n/a, non applicable. *from Lingueglia, JBC, 2007 (78)*

II-5) Physiopathology linked to ASIC

II-4-i) *Pain*

The suggestion of the involvement of ASIC in visceral pain came with the observation that ASIC3 is expressed in cardiac afferents, likely mediating the pain of ischemia angina (123). In addition, ASIC affects the response to gut distension. ASIC might be also involved in pain at several locations. They are expressed in nerves innervating joints and bones suggesting that they sense the acidosis induced by chronic inflammatory arthritides and cancer metastases. Moreover, ASIC in muscle afferents may detect the lactic acidosis due to severe or intense exercise. Altogether, these observations suggest that ASIC should be a good target for the treatment of pain. But mouse data showed that disrupting ASIC might increase sensitivity to

painful stimuli. Explanations are unclear but might include variability in genetic background and species, differences in testing paradigms and environmental variability (132).

II-5-ii) *Ischemic stroke*

During ischemia, increased anaerobic glycolysis because of reduced oxygen supply leads to lactic acid accumulation. Accumulation of lactic acid, along with increased H^+ release from ATP hydrolysis, causes a decrease in brain pH, or acidosis. During brain ischemia, extracellular pH falls to 6.5 or lower. Because of its permeability to Ca^{2+} and it sensitivity to pH, the activation of ASIC1a plays a role in the pathology of acidosis-mediated and ischemic brain injury. It is also known that N-methyl-D-aspartic acid (NMDA) receptors and subsequent Ca^{2+} toxicity are involved in ischemic brain injury. Compared to ASIC1a or NMDA blockade alone, co-application of NMDA and ASIC1a blockade produces additional neuroprotection. Therefore, Ca^{2+}-permeable ASIC1a represents a novel pharmacological target for ischemic brain injury (134).

II-5-iii) *Other diseases*

ASIC1a is located at synapses and particularly abundant in the amygdala (emotional reaction), and modulation of synaptic physiology is likely to have behavioural consequences. Loss of ASIC1a has pronounced effects on fear-related behaviour. Moreover, analysis of mice overexpressing ASIC1a suggests that human gain-of-function mutations might be prone to fearful behaviour and supersensitive to acidosis. Therefore, manipulating ASIC1a function pharmacology might provide a novel strategy for reducing fear and anxiety in patients (132). Moreover, a significant drop of brain pH during intense neuronal excitation or seizure activity

suggests that ASIC1a activation might play a role in the generation and maintenance of epileptic seizure (134).

III/ Structure of ENaC/Deg members

III-1) Generality on sodium channels

Besides the ENaC/Deg gene family, ion channels are commonly defined as an assembly of proteins inserted in the plasma membrane that form aqueous pores through which ions can flow down their electrochemical gradient. They are classified by the nature of their gating: (i) those activated by a change in membrane potential are called voltage-gated channels and (ii) those activated by an external chemical ligand, called ligand-gated channels. Voltage-gated sodium channels are responsible for action potential creation and propagation. The pore-forming α subunits consist of four homologous repeat domains (I-IV) each comprising six transmembrane segments (S1-S6) for a total of 24 transmembrane segments (Figure 11A). They co-assemble with auxiliary β subunits, each spanning the membrane once and both α and β subunits are highly glycosylated. Ligand-gated channels open in response to specific ligand molecules binding to the extracellular domain of the receptor protein. Ligand binding causes a conformational change in the structure of the channel protein. The pore is formed by a pentameric arrangement of subunits, which are in turn composed of a large extracellular domain (which contains the ligand binding site) and four transmembrane domains (Figure 11B).
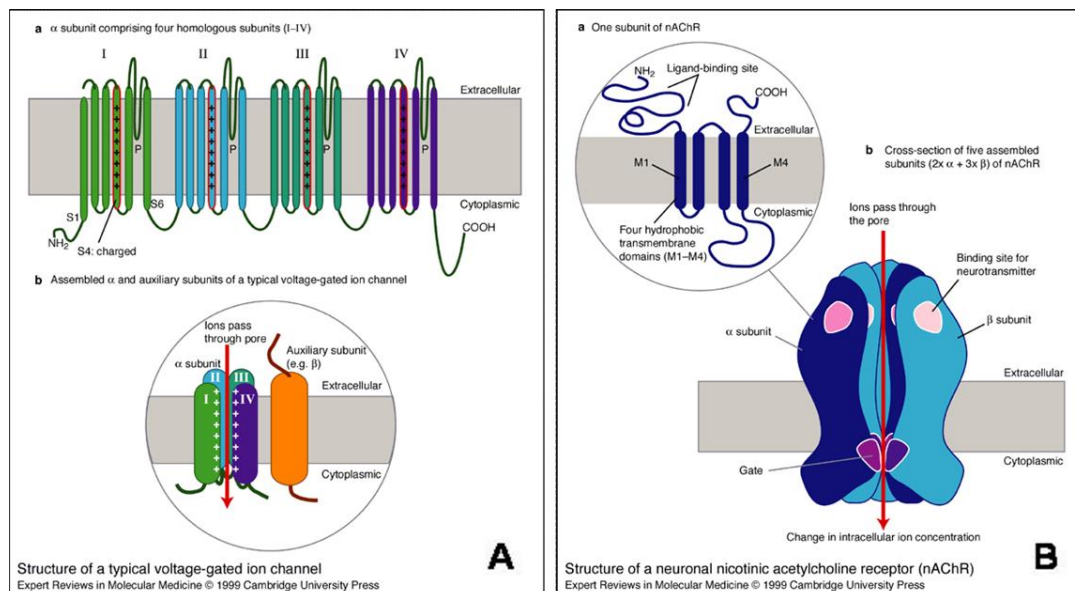
Figure 11: Structure of typical voltage-gated and ligand-gated channels. (**A**) Structure of a typical voltage-gated ion channel composed of (a) α subunit (comprising four subunits I to IV) that forms the aqueous pore (b), assembled with an auxiliary β subunit. (**B**) Structure of the ligand-gated neuronal nicotinic acetylcholine receptor (nAChR). The receptor is pentameric (b) with each subunit containing a ligand binding site and four transmembrane domains. *from Cambridge University Press*

III-2) Structure of an ion channel

The first ion channel to be crystallized was the K^+ channel from *Streptomyces lividans*, the KcsA K^+ channel (34). Bacterial K^+ channel sequence is similar to that of other vertebrate and invertebrate voltage-dependent K^+ channels allowing thus the determination of the general structure of all the potassium channels. As predicted by functional experiments, the K^+ channel is a tetramer presenting a closed gate on the intracellular side. It is composed of four identical subunits that form an inverted teepee with the selectivity filter of the pore in its outer end, and a 10 Å diameter cavity in the centre of the channel with an ion in it (Figure 12A). The lining of the selectivity filter is composed of five amino acids which turn their main chain carbonyls toward the pore axis and their side chains outward. The inner half of the pore is predominantly lined by a side chain of hydrophobic amino acids. It has been observed by electron density maps

that two K^+ ions occupy the short selectivity filter, almost completely dehydrated (Figure 12B). Internal to the selectivity filter, floating in the centre of the 10 Å diameter cavity, is a third K^+ ion, likely surrounded by water molecules (4). This ion is stabilized by two mechanisms: (i) the hydrophobic membrane interior of the large aqueous cavity, and (ii) the partial negative charge of the oriented helices toward the cavity.
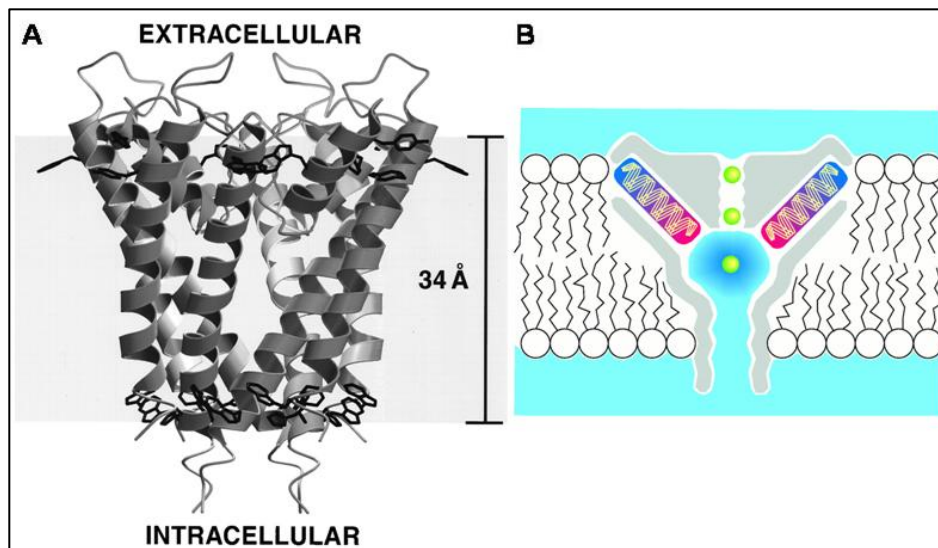
Figure 12: The KcsA K^+ channel. (**A**) Representation of the tetramer as an integral membrane protein. Aromatic amino acids on the membrane-facing surface are displayed in black. (**B**) K^+ ions in the cavity, in the middle of the membrane. *From Doyle et al., Science, 1998 (34)*

III-3) Structure of the epithelial sodium channel

III-3-i) *A tetramer or a trimer?*

ENaC/Deg members share the same channel architecture thought for a long time to be a tetramer but finally described as a trimer in the recent crystallization of chicken ASIC1 (61).

III-3-i-a) *Evidence for a tetrameric channel*

Several studies have shown that FaNaCh (29) and ENaC (37), belonging to the same ENaC/Deg family, were associated in tetrameric complexes. Firsov *et al.* (37) have shown by quantitative analysis of cell surface expression of ENaC that in a functional channel, the number of α subunits is higher than β or γ subunits. Then functional analysis of differential sensitivities to Zn^{2+}, conferred by point mutations in the three ENaC subunits, have allowed the assessment of the two α, one β and one γ stoichiometry as a functional tetrameric conformation for ENaC. This subunit stoichiometry was confirmed by biophysical assays using amiloride-binding site mutated ENaC channels that display significant differences in sensitivity to external MTSEA from the wild-type channel (73). Moreover, a sucrose gradient analysis (33) demonstrated a tetrameric subunit stoichiometry in agreement with the studies above, at least in the intracellular pool of proteins. Recently, single-channel current measurements were performed in *Xenopus laevis* oocytes expressing individual mutations that alter the channel conductance (2). In the case of mutation on the α subunit, coexpression of wild-type and mutated subunits resulted in the appearance of channels with an additional single-channel conductance between those of wild-type and mutant channels. This intermediate single channel conductance suggested the presence of two α subunits in the channel. This was not observed for the mutation in β and γ subunits confirming the number of each subunit to one per channel. Altogether, these results confirmed the tetrameric functional structure of ENaC and the stoichiometry 2α, 1β and 1γ.

However, with a combination of different techniques, the group of D. Stockand suggested that for maximal ENaC activity, each subunit is required and that ENaC at the membrane contains preferentially equal numbers of each type of subunit (118). He therefore suggests a trimer (1α, 1β and 1γ), a hexamer (2α, 2β and 2γ) or a nonamer (3α, 3β and 3γ) as the functional arrangement of ENaC.

III-3-i-b) *Crystallization of a trimeric truncated chicken ASIC*

The crystallization of the chicken form of ASIC 1 (cASIC1) has led to a re-evaluation of ENaC/Deg channels structure (61). As predicted by the amino sequence of the subunits, each subunit has intracellular N- and C-termini, two transmembrane domains and a large extracellular loop. The crystallization of cASIC1 has been performed on a deleted channel, missing the N- and the C-termini and leading to a non-functional channel, called cΔASIC1. Transmembrane domains are α helix coupled to β strands in the large extracellular domains but no continuous pore along the three-fold axis of molecular symmetry is visible for the passage of ions (Figure 13B). Ions may access the ion pore by way of fenestrations near the extracellular membrane surface (Figure 13A). The extracellular domain resembles a forearm with 'wrist', 'thumb', 'finger', 'knuckle', 'β-ball' and 'palm' depending of the α helixes and β sheets configuration as described in the Figure 13C. The 'thumb' domain presents five disulfide bridges forming a straight line from the conserved residue Trp288, in the 'wrist' junction, to the interface 'thumb' / 'finger'. Concerning the transmembrane domains of each subunit, they adopt different conformation with a bent TM2 (Figure 13C) for two of the three subunits and a straight TM2 for the third one (Figure 13A). This asymmetry remains unclear. The proton binding-site was identified in the extracellular domain as multiple close acidic residue pairs, far from the channel region. Its effect on channel gating seems to involve movement of the disulfide-rich 'thumb' domain depending of proton binding / unbinding. This suggests that the movement is transmitted to transmembrane domains by way of primarily non-covalent interactions, mediated by residues at the base of the 'thumb' like the conserved Trp288.
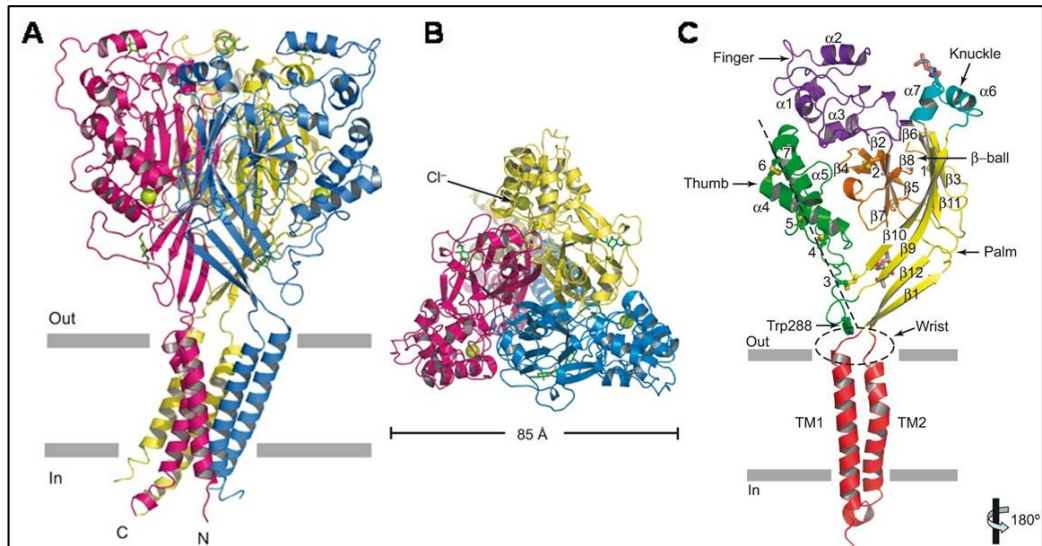
Figure 13: Trimer assembly of cΔASIC1. (**A**) Stereoview of the homotrimeric structure viewed parallel to the membrane plane. Each subunit is in a different colour. (**B**) View of the homotrimeric structure parallel to the molecular three-fold axis from the extracellular side of the membrane. (**C**) Domain organization of a single subunit, locations of disulfide bridges (labelled 1-7). *From Jasti et al., Nature, 2007 (61)*

The pore is defined primarily by residues from the TM2 (Figure 14A), with a negative electrostatic potential that likely contributes to cation selectivity (Figure 14B), although TM1 also lines portions of the pore, especially in the extracellular vestibule. The degenerin site (Figure 14C, Gly432 ('d')) was located at the interface between TM2 and TM1 of adjacent subunits, indicating that introduction of a large residue into this interface may perturb the gating.
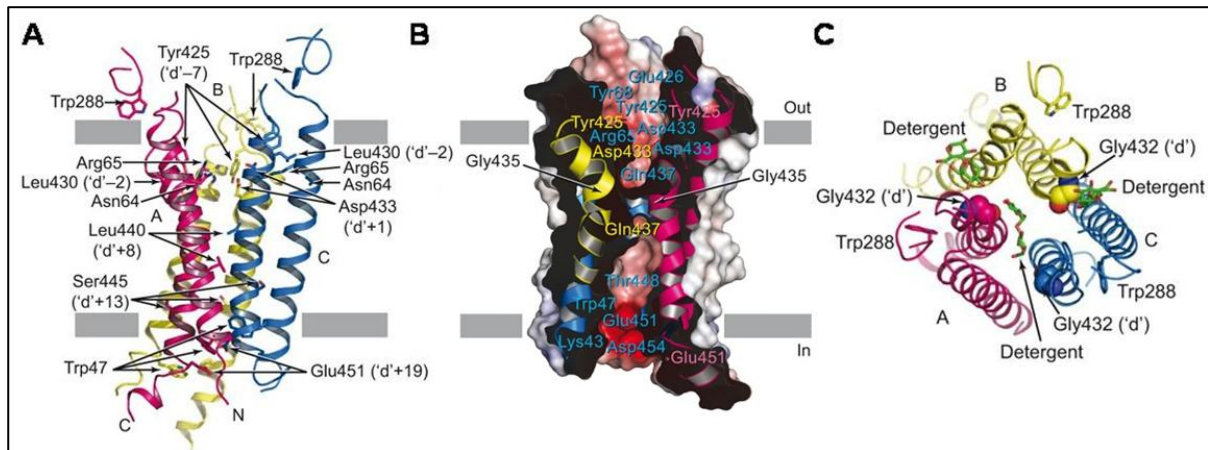
Figure 14: Structure and key residues in the transmembrane domains of cΔASIC1. (A) View of the homotrimeric structure parallel to the membrane plane. Oxygen atoms are red, nitrogen atoms are blue and numbering indicates residues in TM2 relative to the degenerin ('d') position. (**B**) Surface potential representation of the TM region sliced through the pore along the plane of membrane bilayer to show the negative potential along the pore. Contours are from -8 (red) to +8 kT (blue). (**C**) View from the extracellular side, along the pore axis, showing the location of Gly432 ('d'). *From Jasti et al., Nature, 2007 (61)*

The three-dimensional structure was obtained from a non-functional truncated form of cASIC1, missing the N- and C-termini. These parts of the channel are important in the function and structure of the channel as illustrated by physiopathology linked to intracellular deletion of ENaC subunit such as the PHA1 and the Liddle syndrome (*cf. 'Physiopathology of ENaC'*). Thus, we cannot exclude that the absence of the intracellular part leads to invalid observations and interpretations for a functional channel.

III-3-ii) *Structure of the subunit*

The αENaC subunit is a 79 kDa protein composed of 698 amino acids; the βENaC, a 72 kDa protein of 638 amino acids; the γENaC, a 74 kDa protein of 650 amino acids and the

hASIC1a subunit, a 60 kDa protein with 528 amino acids. As we have seen above, each subunit has intracellular N- and C-termini, two transmembrane (TM) domains and a large extracellular loop. We will see below the main sites and domains present in ENaC and ASIC subunits.

III-3-ii-a) *HG domain*

Study of the PHA-1 (*cf. 'Pseudohypoaldosteronism type 1'*) has permitted the identification of a missense mutation βG37S in the N-terminus of the human βENaC subunit leading to a loss of the channel function (44). Amino acids sequence alignments show a high conservation of this residue between human and rat ENaC (hαG70, hβG37, hγG40, rαG95, rβG37 and rγG40). This residue is also conserved in human and chicken ASIC1 (hA1a-G29 and cA1a-G30). It has been shown that the mutation rβG37S, as the homologous mutations in α (rαG95S) and γ (rγG40S) subunits, decreases the channel open probability underlining the potential involvement of this glycine residue in the gating of ENaC. Complementary studies showed on the rat α subunit that a conserved pre-TM1 segment, from T92 to C101, determine the open probability of ENaC and are involved in the channel gating kinetic. Three amino acids, the rat αH94, αG95 and αR98, are the most important in maintaining proper channel gating (45). These three amino acids are flanked by two cysteine residues conserved in two or three ENaC subunits: (i) rαC88, rβC30, rγC33; (ii) rαC101, rβC43.

III-3-ii-b) *Cysteine-Rich Domains (CRD)*

Two CRDs, CRD1 and CRD2, are present in the extracellular loop of ENaC/Deg channels. They are likely involved in the formation of disulfide bonds, thus in the formation of

mature channels (70). Mutation C133Y in the CRD1 of human αENaC has been shown to cause PHA-1 as seen above. Firsov *et al.* (38) have shown that mutation of two cysteines in CRD1 of the α, β and γ subunits (αC158, βC98 and γC100; αC332, βC270 and γC284) and two other cysteines in CRD2 of the α and β subunits (αC458 and βC399; αC472 and βC413) prevents the normal transport of assembled channels from intracellular compartments to the plasma membrane leading to a decrease in the number of ENaC expressed at the cell surface. Recently, it has been shown that half of the cysteines in the extracellular loop of α and γ subunits likely form intrasubunit disulfide bonds. This establishes the tertiary structure that ensures a proper Na^+ self-inhibition (110). In ASIC1a, CRDs are also binding site for its specific blocker PcTX1 (*cf. 'PcTX1' in ASIC part*).

III-3-ii-c) *Degenerin site*

The Degenerin site is a common site of all the ENaC/Deg members localized in the extracellular loop, closed to the TM2 (αS576, βS518 and γS530 in rENaC, G432 in cA1 and G433 in hA1a). Mutation of this site in *C. elegans* degenerins leads to the constitutive activation of the channel and then to neuronal cell swelling and degeneration. The substitution of the corresponding Gly into ASIC1 and ASIC2 also causes constitutive channel activity (129). Mutation of the corresponding Ser in the three human α, β and γ ENaC subunits induces an increase of the sodium current. Moreover, modification of adjacent residues has shown that the current increases by conformational change in the outer vestibule of ENaC (116). Modification of the rβS518 has been shown to alter the gating kinetics of the channel by destabilizing the closed state resulting in shorter closings and by slowing the closing of the channel (67).

III-3-ii-d) *Amiloride binding site*

Amiloride is as a potassium-sparing diuretic. In the nanomolar range, it is the specific blocker of ENaC with a 100 fold lower affinity for ASIC and the other members of ENaC/Deg family (70). The IC_{50}, *i.e.* the concentration of amiloride needed for the half inhibition of ENaC, is closed to 0.1 µM (43). Affinity of channels for amiloride depends on the extracellular pH, the transmembrane voltage and Na^+ concentration. Indeed, amiloride is a weak base that can only block ENaC when charged positively underlining the importance of the extracellular pH. Then, the voltage dependence of channel block is explained by the binding of the cationic form of amiloride to its binding site, located within the transmembrane electric field. Moreover, the interaction between Na^+ and amiloride is competitive, suggesting overlapping binding sites within the external ion permeation pathway (92). Finally, site-directed mutagenesis experiments have proposed that residues αS583, βG525 and γG537 form the amiloride binding site in the three rat ENaC subunits (105) and the residue G440 in hASIC1a.

Evidence of the effect of amiloride on aldosterone-stimulated Na^+ current was provided by patch-clamp experiments in A6 (47) and then in rat CCD cells (93). In rat CCD, the on-rate of amiloride is estimated of about 60 $\mu M^{-1}.sec^{-1}$ and the off-rate of 4 sec^{-1} whereas in the toad bladder, the amiloride on-rate is about 20 $\mu M^{-1}.sec^{-1}$ and the off-rate is about 2-3 sec^{-1}. Concerning the K_D, *i.e.* the constant of dissociation, the estimation in CCD cells coincides with macroscopic results that is 7.10^{-8} M (93). Later studies showed that mutation of the amiloride binding site on α and β subunits led to an increase in the dissociation rate of amiloride with little change in the association rate. They also demonstrate that benzamil, a derivative of amiloride, and triamterene, another ENaC blocker, share a common receptor with amiloride (66).

III-3-ii-e) *Selectivity filter*

ENaC/Deg channels are permeable to monovalent small cations such as H^+, Li^+ and Na^+ but not for larger cations like K^+ and NH_4^+. This ion discrimination shows that the selectivity filter constitutes the narrowest part of the pore and that ions tightly interact with amino acids that line the pore (63; 68; 69; 108). The selectivity filter is a three amino acid sequence G/SxS preceding the second transmembrane domain in ENaC and ASIC (G587, S588 and S589 in rat αENaC). In addition to these residues, two residues within the TM2, αGlu595 and αAsp602, have been showed to have a role in conferring ion selectivity (111). Mutation of residue αS589 in the selectivity filter allows the passage of larger ions such as K^+, Rb^+, Cs^+, NH_4^+ and divalent cations. The larger the substituting amino acid is, the higher is the channel permeability to larger cations suggesting that introduction of large amino acids in the selectivity filter induces an enlargement of the outer pore allowing passage of larger ions. It has been thus proposed that the main chain of the G/SxS residues line the pore lumen, rather than their side chain (63). However, a discrepant study has been published proposing that mutated channel αS589Cβγ is sensitive to external Cd^{2+} block because of the sulfhydryl group accessibility at position α589 to Cd^{2+}. They concluded that wild-type αSer589 hydroxyl groups face the lumen pore and contribute to cation selectivity and coordination of permeating cations (112). These results have led to open debate and investigations presented as the first part of this work (124).

III-3-ii-f) *PY motif*

The PY motif is a proline rich motif (PPPxPxxL) located in the C-terminus part of αβγ ENaC subunits and absent in ASIC. Presence of a proline-rich motif in proteins often indicates their involvement in protein-protein interactions because proline residues are breaker of regular secondary structures such as α helixes and β sheets, often rendering the proline-rich motif on

the surface of protein. Modular domains currently known to recognize proline-rich domains include SH3 and WW domains (76). The protein binding the PY motif has been identified as the human ubiquitin-protein ligase Nedd4. Moreover, studies have shown that Nedd4 binds to the PY motif *via* its WW domains 2, 3 and 4 (predominantly WW3) and that, when co-expressed in Xenopus oocytes, it down-regulates ENaC activity (81). Complementary studies have shown that the interaction specifically occurs between the PY motif of the WW3 domain of the isoform 2 of Nedd4 (40; 55). *Ex vivo*, ENaC is ubiquitinated on lysine residues located in the N-terminus of the α and γ subunits (but not on the β subunit) (120).

Mutation of the PY motif causes Liddle syndrome (*cf. 'Liddle syndrome'*) by increasing the cell surface expression and the open probability (39). Nedd4-2 regulates the Na^+ transport by controlling the relative expression of cleaved and uncleaved ENaC at the cell-surface (71), by rapidly removing cleaved ENaC from the cell surface (62). A recent study reports that Nedd4-2 multi-ubiquitinylates the surface-expressed pool of ENaC and underlines the role of the ubiquitin-proteasome pathway in the regulation of Na^+ transport in the collecting duct (99).
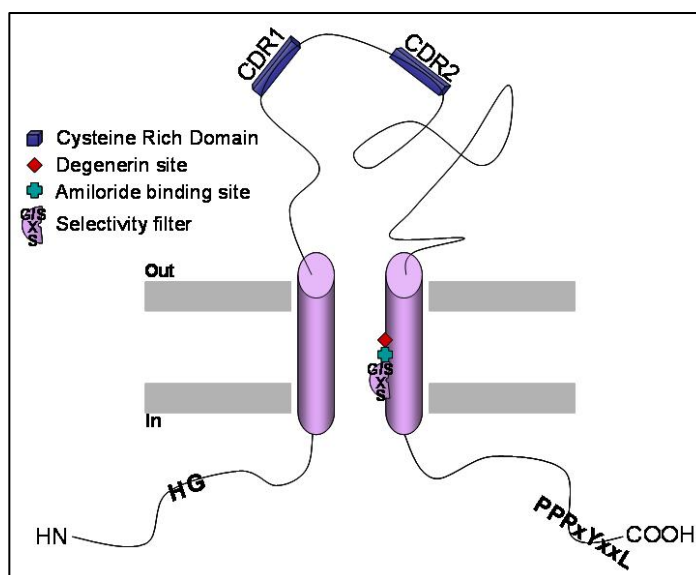
Figure 15: Localization of the main sites and domains conserved among ENaC and ASIC subunits. The N- and C-termini, HG domain and PY motif (PPPxYxxL) are intracellular. Cysteine Rich Domains (CRD) 1 & 2 are extracellular.

III-3-iii) *The internal pore*

Three-dimensional crystal structure of the KcsA K^+ channel provided insights regarding the possible structure of an ionic internal pore but ENaC shares no homology with K^+ channels (34). Investigations on the study of the internal pore in the ENaC/Deg members consist of introduction of cysteines and the study of their accessibility by sulfhydryl reagents. In FaNaC, the ion pore is described as a large aqueous cavity, with a charge selectivity filter in the outer vestibule and the gate close to the interior (96). In ENaC, it has been proposed that the external entry of the pore has been formed by an α helix followed by an extended region that forms the selectivity filter (109). Consequently, it has been suggested the participation of the pore region in ENaC gating. The same group has then proposed, with the identification of β subunit residues lining the pore, that the three ENaC subunits have an asymmetric organization (75). More recently, we have shown in hASIC1a that three residues, Ala22, Ile33 and Phe34, participate in the internal pore (95).

AIM

Before the release of the three-dimensional structure of the chicken ASIC 1, the ion permeation pathway and the molecular mechanism of ion permeation through ENaC/Deg channels were unknown. The first part of my work aimed at the understanding of the pore structure (more specifically of the internal pore located downstream the selectivity filter) that opens to the cytosolic side and at the contribution of the two transmembrane domains (TM1 & TM2). Today the three-dimensional structure of ASIC provides valuable information on the internal pore structure. Nevertheless, our data need to be interpreted in the context of the ASIC1 structure to better understand structure-function relationships of members of the ENaC/ASIC ion channel family. In the second part of my work, we have addressed specific aspects of the cytosolic part of ENaC and ASIC channels that is involved in the modulation of channel activity. We were wondering if the channel inhibition by MTSET results from direct interactions of intracellular ligand with the N-terminal part of ENaC / ASIC and what are the accessible target sites in the N-terminal part for specific ENaC / ASIC inhibition.

I/ Cadmium trapping in an Epithelial Sodium Channel Pore Mutant

The selectivity filter of ENaC is formed by three residues G/SxS present in the three ENaC subunits. Mutation of one of the residues on the αENaC subunit, αSer589, changes the ion selectivity allowing the passage of divalent ions such as Cd^{2+} ions. A study, based on the external Cd^{2+}-mediated inhibition of the mutated αS589Cβγ channel, proposed that this inhibition is the consequence of the interaction of Cd^{2+} ions with the sulfhydryl group of the substituted Cys at position α589. Thus, it was suggested by the authors that the side chain of the

wild-type αSer589 faces the pore lumen (112). We could show that the backbone of the selectivity filter residues line the internal pore and that the Cd^{2+}-mediated inhibition of the mutated αS589Cβγ channel is due to the interaction of Cd^{2+} with a native cysteine located in the TM2 of the γENaC subunit rather than with the substituted cysteine α589. These results have been published in the <u>Journal of Biological Chemistry</u>, *vol. 282, N° 44, pp. 31928-31936, Nov. 2007*. The crystallization of chicken ASIC few months after our publication tends to confirm our selectivity filter residue orientation.

II/ The internal accessibility of the cysteine to sulfhydryl reagents

ENaC has been shown to be inhibited by intracellular methanethiosulfonates (MTS) (64). This study revealed multiple cysteine residues in the N- and C-termini of ENaC subunits responsible for this thiol-mediated inhibition. We have investigated the mechanisms of this inhibition and the identification of the intracellular cysteines target by the MTS. In this part of my work, we set up a new approach based on the Substitution Cysteine Analysis Method (SCAM) coupled to intracellular perfusion of MTSEA-biotin in *Xenopus laevis* oocytes. Generated currents are measured by cut-open voltage-clamp before and after intracellular perfusion of MTSEA-biotin. Then proteins biotinylated by MTSEA-biotin are isolated with pull-down assay, thanks to the specific interaction between biotin and streptavidin beads. Biotinylated proteins are finally separated by SDS-PAGE and analyzed by western-blot with specific antibodies. In this way, we want to identify the cysteine accessible to intracellular MTS reagents and correlate them with cysteines involved in the function of the channel.

Materials and Methods

Biotinylated reagents. We used two sulfhydryl reagents and an amino-reactive reagent.

- N-Biotinylaminoethyl methanethiosulfonate (MTSEA-biotin) was purchased from Toronto Research Chemicals Inc. (Canada). This compound reacts specifically with the sulfhydryl group of cysteine residues to form a disulfide bridge, DTT-sensitive.

- EZ-Link® Maleimide-PEO$_2$-Biotin came from Pierce Biotechnology (USA). This compound with a spacer arm of 29.1 Å reacts specifically with the sulfhydryl group of cysteine to form a DTT-insensitive thioether bond.

- EZ-Link® Sulfo-NHS-SS-Biotin (Sulfosuccinimidyl 2-(biotinamido)-ethyl-1, 3-dithiopropionate) came from Pierce Biotechnology (USA). This thiol-cleavable compound with a spacer arm of 24.3 Å reacts with primary amine-containing molecules.
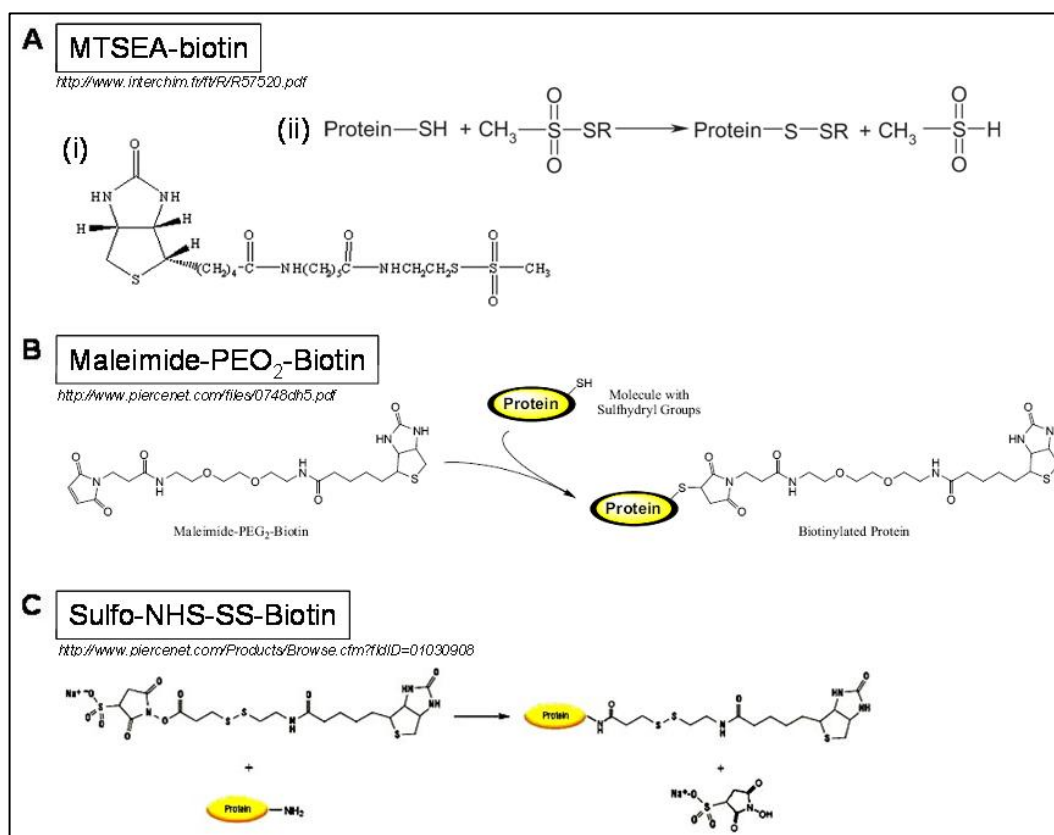
Figure 16: Biotinylated reagents structure and reaction. (**A-ii**) MTSEA-biotin and (**B**) Maleimide-PEO$_2$-Biotin reacts with sulfhydryl groups of protein resulting in the biotinylation of the protein. (**C**) Sulfo-NHS-SS-Biotin reacts with the amine group of protein.

Cross-linkers

- dithio-bis-maleimidoethane (DTME), from Pierce Protein Research Product, Part of Thermo Fischer Scientific, IL, USA. Maleimide ends form stable thioether linkages with sulfhydryl groups on proteins and peptides at pH 6.5-7.5. Between the maleimide ends is a spacer arm of 13.26 Å. The internal disulfide bridge can be cleaved with DTT.

- bis(maleimido)ethane (BMOE), from Pierce Protein Research Product, Part of Thermo Fischer Scientific, IL, USA. BMOE is a homobifunctional maleimide cross-linker that forms stable thio-ether linkages between sulfhydryl groups at pH 6.5-7.5. The spacer arm of 8.0 Å cannot be cleaved by DTT.

- sodium tetrathionate (NaTT), from Sigma-Aldrich Chemie GmbH, Buchs, Switzerland, an oxidizing reagent promoting the formation of disulfide bridges.

Antibodies.

- Polyclonal antibody anti-αENaC targets an epitope located in the N-terminus part of the α subunit and was kindly provided by the group of Bernard Rossier, Department of Pharmacology and Toxicology of Lausanne, CH.

- Polyclonal antibody anti-βENaC targets an epitope located in the C-terminus part of the β subunit and was kindly provided by Johannes Loffing, Institute of Anatomy of Zurich, CH.

- Polyclonal antibody anti-γENaC targets an epitope located in the N-terminus part of the γ subunit and was kindly provided by Johannes Loffing, Institute of Anatomy of Zurich, CH.

- Polyclonal antibody anti-hASIC1 targets a C-terminus epitope of the hASIC1 subunit was from Alomone labs of Jerusalem, Israel.

- Monoclonal antibody anti-Actin, from Sigma-Aldrich Chemie GmbH, Buchs, Switzerland.

Site-directed Mutagenesis. The coding sequences of rat α, β and γENaC are cloned in the pSD5 vector and the coding sequence of human ASIC1a, in the pSDEasy vector. Both plasmids pSD5 and pSDEasy contain the SP6 promoter for the *in vitro* transcription (SP6), a polyA tail for the stabilization of the cRNA (pA), an origin of replication for bacteria amplification (Ori) and a gene coding for the ampicillin resistance (Ampi-R) (Figure 17).
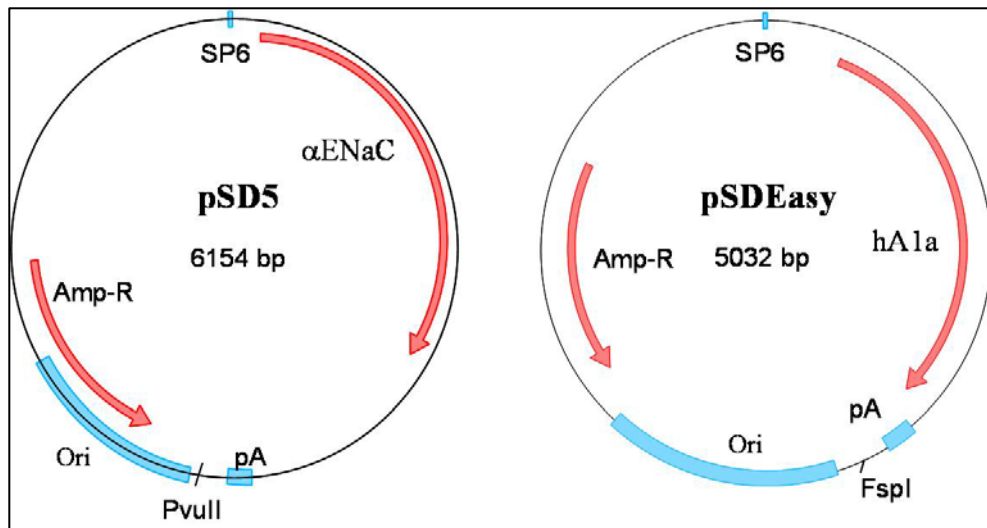
Figure 17: α, β, and γENaC genes are cloned in the pSD5 vector and human ASIC1a gene is cloned in the pSDEasy vector. Coding sequences of ENaC, ASIC1a and ampicillin resistance (Ampi-R) are in red arrow, SP6 is the promoter controlling ENaC and ASIC1a expression, pA is the polyA tail which will be synthesized at the 3' end of the cRNA and Ori is the origin of replication of the vector. *PvuII* and *FspI* are the unique restriction sites used for the linearization of the plasmids before the *in vitro* transcription of, respectively, αENaC and hA1a.

ENaC and hASIC1a mutants were obtained by site-directed mutagenesis using Stratagene's QuickChange® protocol (Figure 18). The mutagenesis was carried out by PCR DNA amplification in a solution containing: 10 ng/µl template DNA, 20 mM dNTP, 100 ng/µl of each the forward and the reverse oligonucleotide primers carrying the intended mutations, 2.5 U of *Pfu* Polymerase (Promega) and its 1X reaction buffer. The double stranded template DNA was denatured at 95 °C and annealed to the oligonucleotide primers.

The *Pfu* Polymerase extended the DNA strands from the mutagenic primers at 68 °C. The methylated DNA template was then specifically digested with the enzyme *DpnI* (1 h, 37 °C) leaving intact the mutated, non-methylated PCR product which was subsequently amplified in *E. Coli* DH5α cells.
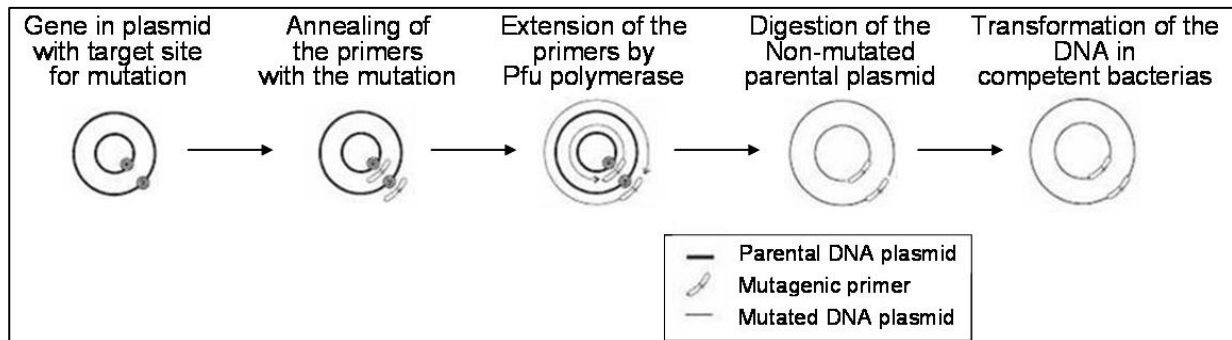
Figure 18: QuikChange® Site-Directed Mutagenesis Protocol.

In the design of the oligonucleotide primers, along with the desired mutations, I introduced a silent mutation resulting in the removal of a restriction site. This allowed us to identify by enzymatic digestion the plasmid containing the desired mutation. After selection of the positive clones, we controlled the presence of the mutations by sequencing (Synergene Biotech GmbH). The region containing the desired mutations was subcloned into the wild-type backbone in order to prevent undesirable mutations or into a previously modified sequence to combine several mutations together.

In vitro *cRNA transcription*. 1 μg of wild-type or mutant α, β, γENaC, or hA1a cDNA-encoding vectors was linearized with an enzyme having a unique restriction site located after the polyA tail, *i.e. PvuII* (α and γ subunits), *BglII* (β subunit) or *FspI* (hA1a). After purification of the linearized plasmid with the QIAQuick Gel Extraction Kit (Qiagen), complementary RNAs of each α, β, γ ENaC or hA1a subunits were synthesized *in vitro* for 1 h at 40 °C in a solution containing: 5 mM 5' RNA 7-methylguanosine cap (Promega), that protects RNA from RNases, 5 mM A/C/UTP, 1 mM GTP (Pharmacia Biotech), 400 ng/μl

BSA (Promega), 52 U RNAse Inhibitor (Promega), 100 mM DTT (Promega), 30 U SP6 RNA Polymerase (Promega) and its reaction buffer 1X. At the end of the transcription, DNA was removed by 1 h incubation with 10 U RNase-free DNase (Promega). RNAs were then purified with the RNEasy® kit of Qiagen and kept at -70 °C.

Expression in* Xenopus laevis *Oocytes. Healthy stage V and VI *Xenopus laevis* oocytes were pressure-injected with either 100 nl of a solution containing equal amounts of α, β and γ ENaC subunits RNAs or 100 nl of hA1a subunit cRNA at a total concentration of 100 ng/μl. For standard experiments, oocytes were kept at 19°C in a low-Na$^+$ modified Barth's saline (MBS) solution: (in mM) 10 NaCl, 0.82 MgSO$_4$, 0.41 CaCl$_2$, 0.33 Ca(NO$_3$)$_2$, 80 NMDG, 2 KCl and 5 HEPES, pH 7.2. MBS solution was supplemented with antibiotics: 10 μg/ml penicillin and 5 μg/ml streptomycin.

Two-Electrode Voltage Clamp. Electrophysiological measurements were made 16-30 hours after injection. Sodium currents were recorded using the two-electrode voltage-clamp (TEV) technique (model TEV-200; Dagan Corp.). TEV measurements were carried out by placing the oocyte in a bath perfused with different solutions and impaled with two electrodes (Figure 19). One electrode measures the membrane potential (Vm) and the second one injects the current necessary to maintain the desired potential that would otherwise be modified by the channel activity. The two electrodes are realized using micropipettes containing a 1 M KCl solution. All electrophysiological experiments were performed at room temperature (22-25 °C). For ENaC, the holding potential was -100 mV. Oocytes were maintained in a recording chamber continuously perfused with a standard bath solution containing in mM, 120 NaCl, 2.5 KCl, 1.8 CaCl$_2$-2H$_2$O and 10 HEPES-NaOH, pH 7.2. The amiloride-sensitive currents, defined as the difference in currents measured before and after addition of 10 μM

amiloride (Sigma-Aldrich) in the bath, were considered as ENaC-mediated macroscopic I_{Na+}. For hASIC1a sodium current measurements, we used a holding potential at -80 mV. The control solution at physiological pH contains in mM, 120 NaCl, 2 MgCl2, 10 HEPES*H$^+$, adjusted at pH 7.4 with N-Methyl-D-Glucosamine (NMDG). The acidic solution for the activation of hA1a contains in mM, 120 NaCl, 2 MgCl2, 10 MES and pH 6.0 is adjusted with NMDG. For each oocyte expressing hA1a, three to four activations were performed at 40 seconds intervals.
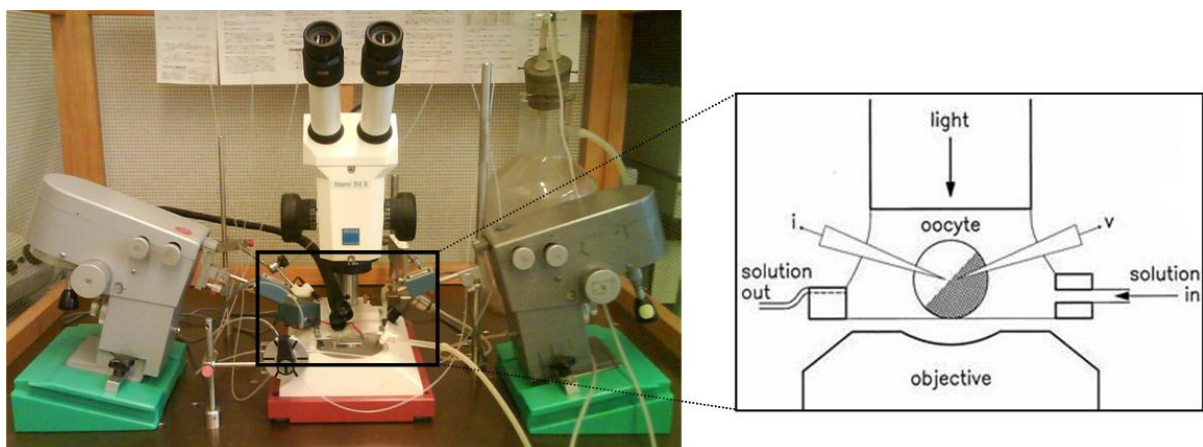
Figure 19: **Two-Electrode Voltage Clamp (TEV) set-up.**

Cut-Open. The cut-open technique allows the recording of macroscopic currents while both the inside and the outside of the oocyte are continuously perfused. *Xenopus* oocytes are placed in an experimental holder divided in three chambers (Figure 20). The superior pole of the oocyte is in contact with the upper chamber and perfused with the extracellular solution. The lower pole is impaled by a microperfusion pipette used as well as microelectrode. The external (upper) and the internal (lower) compartments are electrically isolated by the guard compartment. The voltage clamp was performed using a Dagan cut-open oocyte voltage clamp apparatus (Dagan Corporation, Minneapolis, MN; model CA-1 high performance oocyte clamp). 24 hours after RNA injection, oocytes were perfused intracellularly with either a control or a 1 mM MTSEA-biotin or Maleimide-PEO$_2$-Biotin solution and the sodium

current was measured. In cross-linking experiments, oocytes were perfused with either 1 mM DTME, 10 μM BMOE or 10 or 20 mM NaTT.

To test if the MTSEA-biotin-mediated biotinylation specifically involved cysteines modification, some experiments were performed with oocytes perfused with a solution containing 1 mM MTSEA-biotin with or without 5 mM free cysteines (L-Cysteine*HCl, pH 7.35 with NMDG, Fluka).
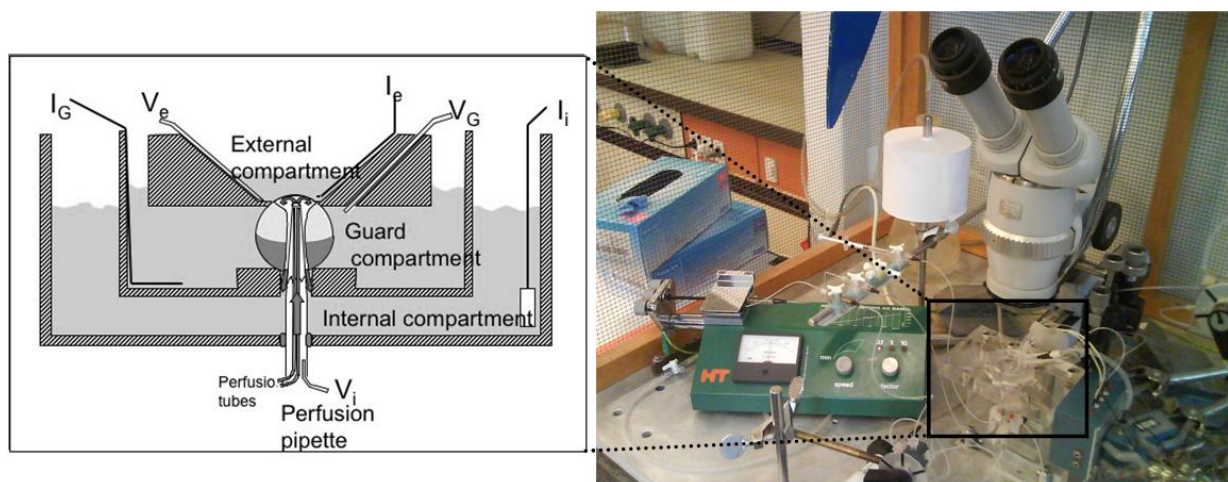
Figure 20: Cut-Open set-up.

Surface biotinylation. 16 - 30 h hours after RNA injection, oocytes were incubated in 1 ml of Biotinylation buffer (10 mM triethanolamine, 150 mM NaCl, 2 mM $CaCl_2$, pH 9.5) containing 1 mg/ml NHS-SS-Biotin for 15 min, at 4 °C. Oocytes were washed twice and then incubated 5 min, at 4 °C, with 2 ml of Quench buffer (192 mM glycine, 25 mM Tris-HCl pH 7.5 in MBS) in order to quench remaining free NHS-SS-Biotin. Finally, oocytes were washed two times with MBS and used for pull-down assays as described below.

Pull-Down assay. From the cut-open experiments, 12 perfused oocytes per condition were lysed with 20 μl of lysis buffer (1 % triton X-100, 500 mM NaCl, 5 mM EDTA, 50 mM Tris-HCl pH 7.5, 1 mM PMSF and 10 μg/ml of each Leupeptin, Pepstatin and Aprotinin) per

oocyte. From surface biotinylation, 40 oocytes per condition were lysed with 20 µl of lysis buffer per oocyte. Oocytes were vortexed and centrifuged for 10 minutes at 13,000g (4 °C). The intermediate phase was delicately withdrawn with a pipette and transferred to a new tube. Protein concentrations in each of the lysates were determined using a Bradford reagent (Bio-Rad Protein Assay Dye Reagent Concentrate) and absorbance at 595 nm was read with a spectrophotometer. Lysates were diluted as required with lysis buffer to obtain the same protein concentration in all samples. A sample of each lysate was kept as a control of "total lysate fraction". The rest of the lysate was incubated overnight (ON) with 40 µl of streptavidin beads (Immunopure Immobilized Streptavidin Gel, Perbio) at 4 °C. After centrifugation (2,500 rpm, 4 °C), a fraction of supernatant was kept to analyze the "unbound fraction". The beads were washed three times with lysis buffer. Sample buffer (25 mM DTT, final) was added to beads, unbound fractions and total lysate fractions. Each fraction was heated for 5 min at 95 °C. In order to separate the eluted protein from the beads, the bead suspension was transferred to a minicolumn fitted with a microporous sieve and the protein was recovered in a new tube by centrifugation.
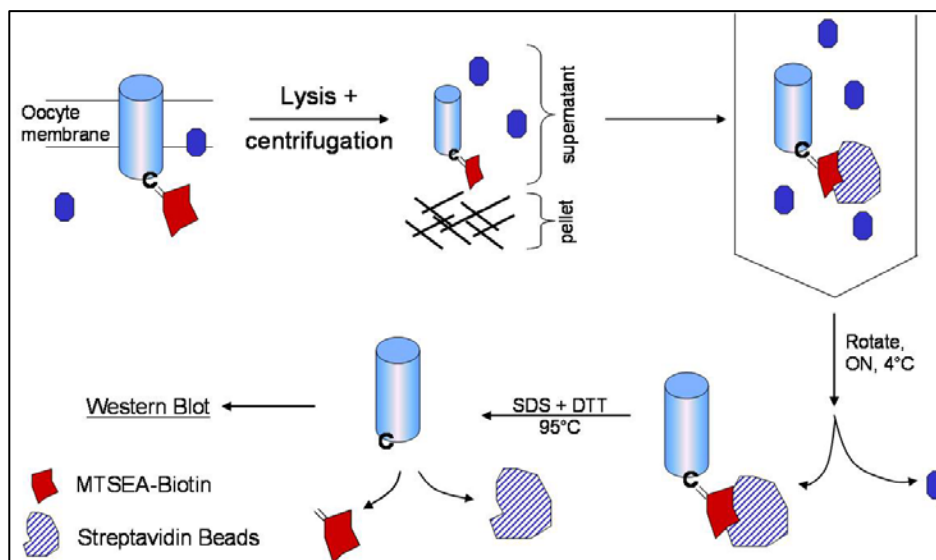
Figure 21: **Principle of the Pull-Down assay.** MTSEA is coupled to biotin in order to keep specifically the proteins bound to the MTSEA *via* the specific interaction biotin-streptavidin.

To test the DTT-sensitivity of MTSEA-biotin-mediated biotinylation of channels subunits, we boiled part of the total lysates at 95 °C in the presence of 2 % SDS and 10 mM DTT for 5 minutes, followed by several minutes in ice, before the streptavidin beads incubation. Another part of total lysates was boiled at 95 °C, for 5 min, in presence of 2 % SDS but without DTT as a control for DTT effect. To be sure that DTT will not disturb the interaction between biotin and streptavidin beads, the lysates were 1/10 diluted with lysis buffer. Thus incubation of proteins with streptavidin beads finally occurred in presence of 0.2 % SDS and 1 mM DTT.

Western-Blot, Infrared detection (Odyssey® Li-Cor®). Proteins were resolved by SDS-Polyacrylamide Gel Electrophoresis (SDS-PAGE), on 5-15% acrylamide gradient minigels. ENaC and ASIC subunits were well resolved by 50-55 minutes migration at 200 V. In order to visualize proteins in the gel before blotting, gels contained 1% Trichloroethanol (Fluka Chemika, Buchs, Switzerland), a molecule which reacts with tryptophan residues when activated by UV light (74). The modified Trp is fluorescent and the conjugated proteins in a gel can be thus visualized under UV light at the same wavelength as that used to trigger the reaction. After UV visualization, proteins were transferred onto nitrocellulose membranes at 100 V, during 3 h. Transferred proteins were visualized by Ponceau Red staining. Membranes were then blocked in a 0.1 % (w/v) casein solution for 1 h in order to reduce non-specific signal and incubated over-night in the presence of specific first antibodies. The day after, membranes were thoroughly washed in TBS, 0.1% Tween , re-blocked in 0.1 % casein solution and incubated for 1 h with the secondary antibody (anti-rabbit IRDye™ 800 CW (LiCor), 1/10000 dilution). After rinsing, membranes were scanned with the Odyssey® Infrared Imaging System.

Data analysis. Results are reported as means ± SEM and represent the average of *n* independent experiments in each of which the average amiloride-sensitive Na$^+$ current I$_{Na+}$ was calculated from measurements carried out with twelve to fourty individual oocytes originating from different frogs.

Molecular modeling. Gouaux's group kindly provided us the pdb file with the coordinates of their crystallized chicken truncated ASIC 1 (cΔASIC1) (61). This file is readable with the Swiss Pdb Viewer software (46), a software utility which also allows browsing of a rotamer library in order to model the structural changes resulting from amino acid replacements introduced in the native sequence. The current side chain is replaced by the "best" rotamer of the new amino acid. The "best" rotamer is the one that totalizes the "lowest" score according to the formula (Nb=Number):

score = (4 x Nb Clash with backbone N CA and C atoms) + (3 x Nb Clash with backbone O atoms) + (2 x Nb Clash with side chains atoms) - Nb H bonds - 4 x Nb SS bonds

Distances between each residue at position 445, called 'd1', 'd2' and 'd3', in each of the three subunits constituting the cΔASIC1 channel were determined with the Swiss Pdb Viewer software. Calculation of area delimited by the three amino acids at position 445, an estimation of the pore diameter at the level of this amino acid, was performed using Heron's formula:

Area = √[s(s-'d1')(s-'d2')(s-'d3')]   with   *s = 1/2 ('d1' x 'd2' x 'd3')*

RESULTS

I / Cadmium trapping in an Epithelial Sodium Channel Pore Mutant.

Armelle-Natsuo TAKEDA, Ivan GAUTSCHI, Miguel X. van BEMMELEN, and Laurent SCHILD.

This study was based on previous findings reporting that the S589C mutation in the selectivity filter of αENaC renders the channel permeant to divalent cations and sensitive to external cadmium (Cd^{2+}) inhibition. We wanted to determine the molecular mechanisms involved in the ion permeation and the structure of the internal pore. We have shown that the external Cd^{2+}-mediated inhibition of the mutated channels αS589Cβγ is not due to the coordination of Cd^{2+} ions with the thiol group of the side chain of α589C as previously proposed (112). Indeed external Cd^{2+} ions also irreversibly inhibited mutated channels αS589Dβγ, αS589Nβγ and αS589Aβγ although it is known that Cd^{2+} has little affinity for Asn and Ala residues. This suggests that the backbone of αSer589 lines the ion pore, rather than its side chain. An example of side chain oriented toward the channel lumen is the amiloride binding site, αSer583. Indeed, mutation αS583C renders the channel sensitive to Cd^{2+} inhibition in a reversible manner, in contrast to mutation αS583N insensitive to Cd^{2+}. Moreover, the Cd^{2+} block of αS589C, -D, and -N βγ mutants is prevented by amiloride showing that the Cd^{2+} binding site is located beyond that of amiloride. We have shown that the native cysteine residue γCys546, in the TM2 of γENaC, is the Cd^{2+} binding site involved in the external Cd^{2+} block of the mutated channel. In conclusion, we propose that the side chain of

αSer589 is not oriented toward the lumen pore and that substitution of the selectivity filter residues with larger amino acid allows the enlargement of the pore, as previously reported (63). Thus Cd^{2+} can go through the ion pore until the γCys546 native residue with which it coordinates leading to the block of the ion conduction pore.

Cadmium Trapping in an Epithelial Sodium Channel Pore Mutant*

Armelle-Natsuo Takeda[1]**, Ivan Gautschi, Miguel X. van Bemmelen, and Laurent Schild**[2]

From the Department of Pharmacology and Toxicology, Faculty of Biology and Medicine, Lausanne University, CH-1005 Lausanne, Switzerland

The putative selectivity filter of the epithelial sodium channel (ENaC) comprises a three-residue sequence G/SXS, but it remains uncertain whether the backbone atoms of this sequence or whether their side chains are lining the pore. It has been reported that the S589C mutation in the selectivity filter of αENaC renders the channel sensitive to block by externally applied Cd^{2+}; this was interpreted as evidence for Cd^{2+} coordination with the thiol group of the side chain of α589C, pointing toward the pore lumen. Because the αS589C mutation alters the monovalent to divalent cation selectivity ratio of ENaC and because internally applied Cd^{2+} blocks wild-type ENaC with high affinity, we hypothesized that the inhibition of αS589C ENaC by Cd^{2+} results rather from the coordination of this cation with native cysteine residues located in the internal pore of ENaC. We show here that Cd^{2+} inhibits not only ENaC αS589C and αS589D but also αS589N mutants and that Ca^{2+} weakly interacts with the S589D mutant. The block of αS589C, -D, and -N mutants is characterized by a slow on-rate, is nearly irreversible, is voltage-dependent, and can be prevented by amiloride. The C546S mutation in the second transmembrane helix of γ subunit in the background of the ENaC αS589C, -D, or -N mutants reduces the sensitivity to block by Cd^{2+} and renders the block rapidly reversible. We conclude therefore that the block by Cd^{2+} of the αS589C, -D, and -N mutants results from the trapping of Cd^{2+} ions in the internal pore of the channel and involves Cys-546 in the second transmembrane helix of the γENaC subunit.

The epithelial sodium channel (ENaC)[3] mediates the Na$^+$ ion influx across the apical membrane of tight epithelia such as the aldosterone-sensitive distal nephron, the distal colon, or the airways epithelium (1). In principal cells of the aldosterone-sensitive distal nephron, the ENaC-mediated influx of Na$^+$ ions constitutes the apical step of the transepithelial Na$^+$ absorption and is regulated by aldosterone (2). The aldosterone-sensitive distal nephron plays an important role in the maintenance of Na$^+$ homeostasis, the regulation of extracellular volume, and blood pressure (3). In the lungs, ENaC together with cystic fibrosis transmembrane conductance regulator controls the height of the airway surface liquid that forms a thin layer coating the airways epithelium, which contributes to the clearance of particles and microbes (4).

Functional ENaC at the cell plasma membrane is a heteromeric protein made of homologous α, β, and γ subunits arranged pseudosymetrically around a central channel pore, presumably in a 2 α, 1 β, and 1 γ configuration (5, 6). Each ENaC subunit is made of two transmembrane helices (TM1 and TM2), a large extracellular loop that represents more than half of the mass of the protein, and intracellular N and C termini. The ENaC subunits belong to the ENaC/degenerin superfamily of ion channels but share no sequence homology with other tetrameric channels also made of two transmembrane domains, such as inward rectifier K$^+$ channels.

In the absence of crystal structures of members of the ENaC/degenerin ion channel family, our understanding of mechanisms and structures involved in the ion permeation is quite limited. The amino acid sequence preceding the second transmembrane domain (TM2) constitutes the outer channel pore (pore region in Fig. 1) where the pore blocker amiloride binds (αSer-583, βGly-525, γGly-537 in rat ENaC sequence, see Fig. 1) (7). Secondary structure predictions conform the TM2 to an α helix (8). The amiloride binding site is located external and upstream to the selectivity filter with an amino-to-carboxyl sense. The conserved three-amino acid sequence G/SXS (587–589 in rat ENaC) that is essential to maintain the high selectivity of ENaC for Na$^+$ over K$^+$ or Ca^{2+} ions is considered therefore a key element of the selectivity filter (9). It has been proposed that the increase in permeability to K$^+$ and NH$_4^+$ resulting from mutations of αSer-589 reflects changes in the geometry of the pore segment comprising the selectivity filter that allow it to accommodate larger cations (10). The molecular basis of the interaction between the permeant Na^{2+} or Li^{2+} ions and oxygen atoms at the binding site is not yet clear. Recent experiments reported that the serine 589 to cysteine substitution in the α subunit (αS589C) confers to ENaC a sensitivity to block by external Cd^{2+} ions, which was interpreted as evidence for an orientation of the side chain of serine 589 toward the lumen of the channel pore (11).

ENaC and the K$^+$ channel KcsA share a similar membrane topology and a heterotetrameric structure made of homologous subunits comprising two transmembrane segments. The

FIGURE 1. **Sequence alignment of the pore region of the α, β, and γ subunits of rat ENaC including the amiloride binding side and the channel selectivity filter, followed by the second transmembrane domain (*TM2*).** According to current prediction models (PredictProtein) (8), the TM2 segment conforms an α helix starting at the conserved Val residue at a position corresponding to 590 in the αENaC sequence, whereas the secondary structure of the pore region is not defined.

conduction pore of ENaC appears to be, however, quite different from that of the members of the K^+ channel superfamily. The amino-terminal portion of the pore region in the KcsA forms an α helix (pore helix) pointing from the outside toward the center of the channel (12). Following this pore helix, the amino acid stretch lining the selectivity filter folds back toward the external surface, exposing binding sites for external blocking ligands such as toxins or triethanolamine (TEA). In ENaC, the pore region points from the outside to the center of the channel with an amino-to-carboxyl sense of, successively, the amiloride binding site, the selectivity filter, and the TM2 (1).

These important differences in the pore organization indicate that the three-dimensional structure of the KcsA K^+ channel does not represent an adequate template to understand ion permeation through ENaC. The pore-lining residues beyond the selectivity filter that constitute the internal channel pore remain to be identified in channels belonging to the ENaC/degenerin family, for which only a few studies have been performed to determine the accessibility of inner pore lining residues. Recent work has shown that, in contrast to the acid-sensing ion channel (ASIC), another member of the ENaC/degenerin family, ENaC is highly sensitive to intracellularly applied sulfhydryl reagents such as Cd^{2+}, Zn^{2+}, or methanethiosulfonates (MTS). Cysteine residues in the N terminus of ENaC contribute to inhibition by MTS reagents (13). Similar inhibition of ASIC by internal sulfhydryl reagents can be reproduced in ASIC mutants in which cysteines have been introduced at the N terminus and in the 5′-start of the TM1 (14). Altogether, these observations suggest that the N terminus and the internal part of TM1 participate in the pore lining of ENaC.

In this study we have revisited the mechanism of channel blockade by external Cd^{2+} in ENaC mutants with amino acid substitutions in the selectivity filter (αS589C) (11). We show that, in order to block ENaC, Cd^{2+} has to bind to distinct sites deep in the channel pore, including a cysteine residue in the TM2 of γENaC subunits.

MATERIALS AND METHODS

Site-directed Mutagenesis, Expression in Xenopus laevis Oocytes, and Electrophysiology—The ENaC constructs used for this study were taken from a previous study (10, 13). Complementary RNAs of each α, β, γ subunit were synthesized *in vitro* with SP6 RNA polymerase from wild-type and mutant α, β, and γENaC cDNA encoding vectors previously linearized with PvuII (α and γ subunits) or BglII (β subunit).

Healthy stage V and VI *X. laevis* oocytes were pressure-injected with 100 nl of a solution containing equal amounts of α, β, and γ ENaC subunits at a total concentration of 100 ng/μl. For standard experiments, oocytes were kept at 19 °C in a low Na^+-modified Barth's saline: in mM, 10 NaCl, 0.82 $MgSO_4$, 0.41 $CaCl_2$, 0.33 $Ca(NO_3)_2$, 80 NMDG, 2 KCl, and 5 HEPES, pH 7.2.

Electrophysiological measurements were made 16–30 h after injection. ENaC current (I_{Na}) was recorded using the two-electrode voltage-clamp technique (model TEV-200; Dagan Corp.). Holding potential was −100 mV. The amiloride-sensitive currents defined as the difference in I measured before and after addition of 10 μM amiloride (Sigma-Aldrich) in the bath were considered ENaC-mediated macroscopic I_{Na}. All electrophysiological experiments were performed at room temperature (22–25 °C). Oocytes were maintained in a recording chamber continuously perfused with a standard bath solution containing in mM, 120 NaCl, 2.5 KCl, 1.8 $CaCl_2$-$2H_2O$, and 10 HEPES-NaOH, pH 7.2. For cadmium block experiments, 0.01, 0.1, 1, or 10 mM Cd^{2+} was freshly added to the perfusion solution. Results are reported as means ± S.E. and represent the mean of n independent experiments in which the average amiloride-sensitive Na^+ current I_{Na} was measured for four to ten individual oocytes originating from different frogs.

Analysis of the Data—Data obtained from the time course of I_{Na} decrease in the presence of external Cd^{2+} were best fitted by the sum of two exponentials. To analyze the voltage dependence curve of the I_{Na} current of the ENaC mutant, the ratio I/I_0 measured in presence (I) of 1 or 3 mM Cd^{2+} to that in the absence of the Cd^{2+} (I_0) is described by the Woodhull equation (15) as shown in Equation 1

$$P_{un} = I/I_0 = K_B(0)\exp(z'FV/RT)/\{[B] + K_B(0)\exp(z'FV/RT)\} \quad \text{(Eq. 1)}$$

where P_{un} is the probability that the binding site of Cd^{2+} is unblocked; $K_B(0)$ is the equilibrium dissociation constant at 0 mV; $[B]$ is the blocker concentration; z' is the slope parameter; F, the Faraday's constant; V, the applied voltage; R, the gas constant; and T, the absolute temperature. Moreover, z' is equal to the product of the actual valence of the blocking ion z and the fraction of the membrane potential (or electrical distance) δ acting on the ion: $z' = z\delta$.

RESULTS

It has recently been reported that serine-to-cysteine substitution at position 589 in αENaC makes the channel inhibitable by external Cd^{2+} (11). The block of ENaC αS589C mutant by Cd^{2+} shows an unusual slow on-rate ($k_{on} > 1000$ $M^{-1}s^{-1}$), as well as a slow and incomplete recovery of ENaC activity after external Cd^{2+} removal. This was interpreted as evidence for Cd^{2+} coordination with the thiol group of the side chain of the cysteine at position α589 (11).

αSer-589 is located in the selectivity filter sequence $G_{587}S_{588}S_{589}$ of rat ENaC (see Fig. 2), and its mutation drastically changes the ion selectivity of the channel (9, 10). We hypothesized that these unusual characteristics of block by Cd^{2+} are due to the trapping of Cd^{2+} ions in the internal pore of the channel, *i.e.* downstream the selectivity filter as far as the channel opening to the cytosol. Two previous observations support this hypothesis. First, the αS589C mutation makes the
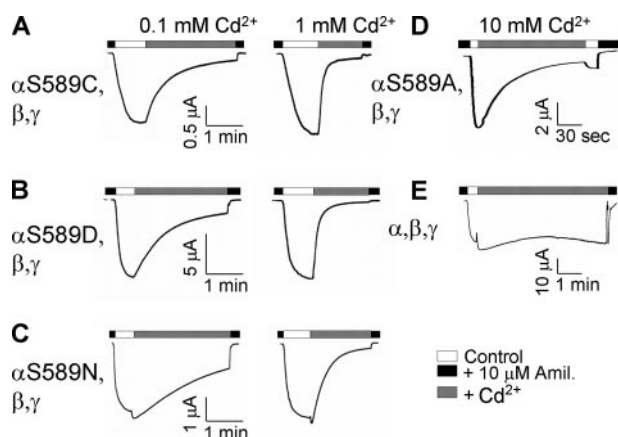
FIGURE 2. **Current inhibition of the αSer-589,β,γ mutants by external Cd²⁺.** Representative tracings of macroscopic ENaC (I_{Na}) currents obtained in oocytes injected with ENaC αS589C,β,γ (*A*); αS589D,β,γ (*B*); αS589N,β,γ (*C*); αS589A,β,γ (*D*); or α,β,γ wild-type (*E*). Removal of amiloride (10 μM) in the bath induced a robust inward Na⁺ current. The addition of 0.1 or 1 mM external Cd²⁺ (*A–C*) decreased I_{Na}, whereas 10 mM Cd²⁺ decreased I_{Na} of the αS589A,β,γ (*D*). The wild-type ENaC (*E*) remained insensitive to 10 mM cadmium.

FIGURE 3. **Inhibition of αS583C,β,γ mutant by external Cd²⁺.** *A*, representative tracings of macroscopic ENaC (I_{Na}) currents recorded in oocytes injected with EnaC α,β,γ, αS583C,β,γ, or αS583N,β,γ at increasing concentrations of Cd²⁺. *B*, dose-dependent inhibition of I_{Na} of the αS583C,β,γ (■) by Cd²⁺ compared with the wild type (○) and the αS583N,β,γ (▲). Fit of the data (■) was obtained by simple Langmuir isotherm and gave a K_D for Cd²⁺ of 0.105 ± 0.0012 mM.

channel permeable to divalent cations such as Ca²⁺ and possibly also to Cd²⁺, which has a smaller ionic radius than the former (9). Second, we have recently reported that, in both inside-out patch and in cut-open oocytes, Cd²⁺ applied at micromolar concentrations to the intracellular side of ENaC blocks the channel; this block was characterized by a slow and partial recovery upon removal of Cd²⁺ (13).

To determine the requirement of a thiol side chain at position α589 for the binding of external Cd²⁺ and the inhibition of ENaC, we tested its effect on different substitution mutants, *e.g.* αS589C, αS589D, αS589N, and αS589A. Cd²⁺ ions are known to bind the sulfhydryl group of cysteine or the fully charged oxygen atoms contributed by glutamate or aspartate side chains; however, Cd²⁺ has little affinity for side chains of asparagine. Fig. 2 shows representative recordings of ENaC-mediated amiloride-sensitive currents (I_{Na}) and their inhibition by external Cd²⁺. Cadmium at 0.1 or 1 mM inhibits the I_{Na} generated by ENaC αS589C, αS589D, and αS589N mutants (Fig. 2, *A–C*). A higher concentration of Cd²⁺ (10 mM) is required to inhibit the αS589A mutant (Fig. 2*D*), whereas wild-type ENaC remains insensitive to inhibition by Cd²⁺ (Fig. 2*E*).

The blockade of ENaC αSer-589 mutants by Cd²⁺ slowly reaches equilibrium. This is particularly evident for low concentrations of Cd²⁺ and for the αS589N mutant, which appears slightly less sensitive to Cd²⁺ than the αS589C and αS589D counterparts. It was difficult to determine the true affinity of the αSer-589 mutants for Cd²⁺ because at low Cd²⁺ concentrations the blockade equilibrium was still not reached after several minutes. At a higher concentration of Cd²⁺ (1 mM) the rate of channel inhibition is faster and the block almost complete after 1 min. This contrasts with the fast kinetics of inhibition of the αS583C ENaC mutant by Cd²⁺ at concentrations varying from 0.01 to 1 mM (IC₅₀ = 0.105 ± 0.0012 mM, $n = 10$): external Cd²⁺ rapidly reduces the current level in a dose-dependent manner without changes in the on-rate of channel blockade (Fig. 3). By contrast to the αS589N, the αS583N

mutant is insensitive to inhibition by external Cd²⁺. There is strong evidence that the side chain of the cysteine at position Ser-583 is oriented toward the channel lumen, allowing Cd²⁺ to bind in the external pore and to block the channel (16, 17). It also shows that Asn does not bind Cd²⁺ at any of the assayed concentrations, and we conclude therefore that the lower sensitivity of the αS589N mutant to Cd²⁺ inhibition probably results from a decreased permeability to this cation as compared with that of the other α589 mutants. Moreover, the discrepancy between the αSer-589 and αSer-583 mutants regarding their sensitivity to Cd²⁺ and the kinetics of block indicate that the mechanism of ENaC inhibition by Cd²⁺ is different for the two mutants.

The on-rate of channel inhibition by Cd²⁺ of the αS589C, -D, -N, and -A mutants is summarized in Fig. 4; the best fit of the data were obtained using the sum of two exponentials, consistent with two components of the ENaC block with a fast and a slow rate constant (Table 1). The data also show that increasing Cd²⁺ concentrations between 0.01 and 1 mM affect predominantly the time required to reach the equilibrium rather than the magnitude of current inhibition. From the extrapolation of the best fit of αSer-589 channel inhibition, we can predict that, at equilibrium, the half-maximal inhibition (IC₅₀) for Cd²⁺ is largely below 0.1 mM for the αS589C, -D, and -N mutants, suggesting a high affinity site for the Cd²⁺ binding site. However, the slow on-rate of the Cd²⁺ block points to the presence of important diffusional constraints in the αSer-589 mutants for Cd²⁺ ions to bind at its blocking site. Interestingly, the conserved αS589A substitution, which only slightly modifies the cation selectivity of the channel compared with the αS589C, -D, and -N mutants, shows the slowest on-rate of Cd²⁺ block.

A αS589C,β,γ

B αS589D,β,γ

C αS589N,β,γ

D αS589A,β,γ
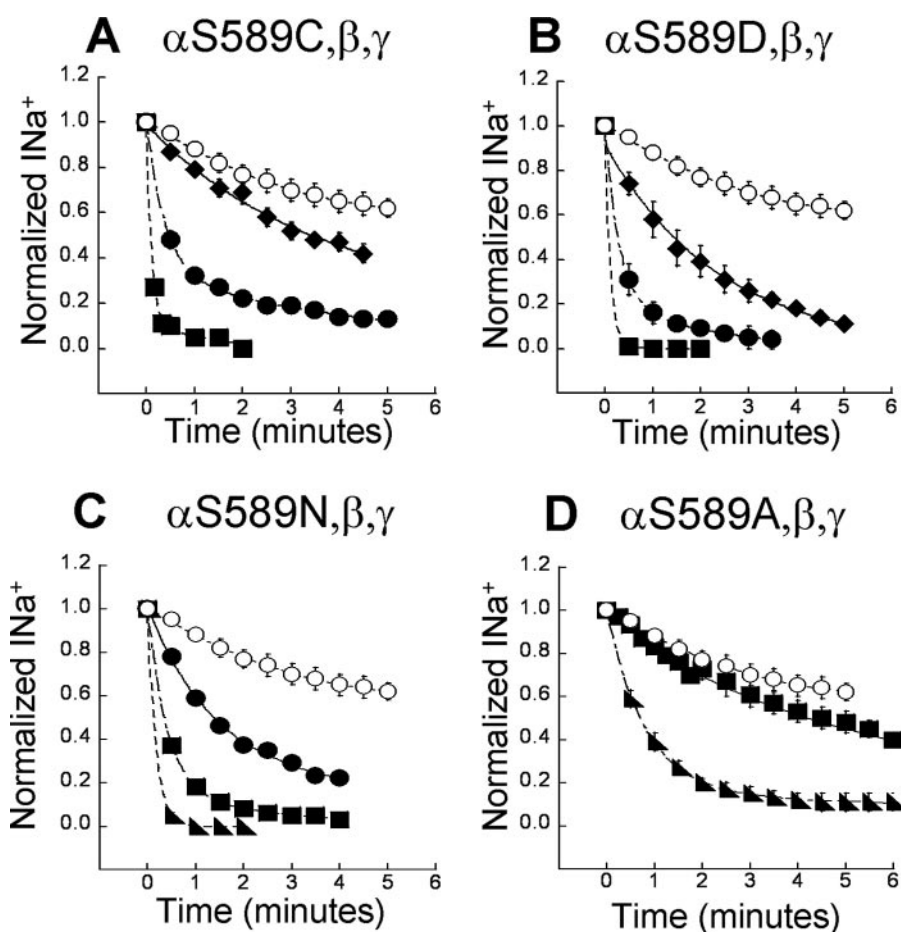
FIGURE 4. **Time course of inhibition of ENaC current (I_{Na}) by Cd^{2+} in oocytes expressing the mutants αS589C,β,γ ($n = 12$) (A), αS589D,β,γ ($n = 6$) (B), αS589N,β,γ ($n = 11$) (C), or αS589A,β,γ ($n = 6$) (D) or expressing ENaC wild-type (*open symbols*).** Inhibition curves were obtained with Cd^{2+} 0.01 mM ($\blacklozenge$), 0.1 mM ($\bullet$), 1 mM ($\blacksquare$), and 10 mM ($\blacktriangle$) for ENaC mutants and concentration up to 1 mM of Cd^{2+} for the wild type. Data were best fitted by the sum of two exponentials, and results are listed in Table 1.

TABLE 1

Rate constants of the inhibition of ENaC mutants by external Cd^{2+}

Rate constants were obtained from data on Figs. 4 and 5. Best fit of the data was obtained with the sum of two exponentials, except for inhibition of S589D and S589C by low (0.01 mM) concentration of Cd^{2+}.

	Rate constants							
	αS589D		αS589C		αS589N		αS589A	
	k_1	k_2	k_1	k_2	k_1	k_2	k_1	k_2
mM				min^{-1}				
[Cd^{2+}]								
0.01	0.419		0.190					
0.1	3.506	0.478	2.166	0.160	0.746	0.097		
1.0	9.181	1.815	10.21	0.927	2.5327	0.394		
10.0					5.924	0.081	1.260	0.066
[Zn^{2+}]								
0.1	6.48	1.39	1.290	0.149	0.782	0.313		
1.0	6.87	0.4	5.950	0.749	2.623	0.608		

We have also tested the ability of Zn^{2+} to block αS589C, -D, and -N ENaC mutants (Fig. 5). We observed that Zn^{2+}, at similar concentrations, shows inhibition curves of I_{Na} that are superimposable to those obtained for Cd^{2+}, indicating similar blocking kinetics for Cd^{2+} and Zn^{2+}. We do not have any sound explanation for the stimulatory effect of external Zn^{2+} (1 mM) on ENaC wild type.

Another particularity of the blockade of the αS589C mutant by Cd^{2+} is the slow and partial recovery from inhibition. We

asked whether differences may exist in the dissociation of Cd^{2+} from its blocking site (off-rate) among the αS589C, αS589D, and αS589N mutants. The tracings in Fig. 6A compare the αS589C, -D, and -N mutants with respect to the recovery from amiloride and Cd^{2+} block. The recovery from the channel inhibition by amiloride is rapid and nearly complete, whereas the recovery from Cd^{2+} blockade is considerably slower and incomplete. The amount of I_{Na} recovered 2 min after removal of external Cd^{2+} was similar for the three αSer-589 mutants (Fig. 6C), indicating that coordination of Cd^{2+} at position α589 is not responsible for its slow dissociation rate. In comparison, the recovery from blockade by Cd^{2+} of the αS583C mutant is rapid and fully reversible (Fig. 6, B and C). These experiments further support our hypothesis that the mechanism of block of the αSer-589 mutants by Cd^{2+} differs from the block of the S583C that involves direct coordination with the sulfhydryl side chain of the cysteine. Residues other than Cys or Asp introduced at position αSer-589 likely participate in the channel inhibition by external Cd^{2+}.

It can be argued that mutations at αSer-589 create a novel binding site that allows inhibition of I_{Na} by Cd^{2+} independently of the diffusion of this cation into the pore. However, if Cd^{2+} has to bind within the pore in order to block the channel, this inhibition should be prevented by the pore blocker amiloride. To test this hypothesis we took advantage of the slow and partial reversibility of ENaC block by Cd^{2+} and measured the recovery of I_{Na} from channel inhibition by Cd^{2+} when amiloride was simultaneously added to the external medium. Fig. 7A shows that the I_{Na} of the αS589C, -D, and -N mutants exposed to 1 mM Cd^{2+} in the presence of amiloride (10 μM) in the bath solution recovered rapidly and almost completely after removal of both blockers. These experiments demonstrate that amiloride prevents the irreversible inhibition of αSer-589 mutants by Cd^{2+}. These results are summarized in Fig. 7B in which it can be seen that the I_{Na} recovered after ENaC inhibition by amiloride and Cd^{2+} was identical to I_{Na} after the same control period. The interpretation of these results is that upon binding to its receptor at the external entrance of the channel pore (see Fig. 1), amiloride prevents the access of Cd^{2+} to its binding site located beyond that of amiloride. We conclude that in the αS589N, as in the αS589C or -D mutants, Cd^{2+} likely binds to cysteine resi-
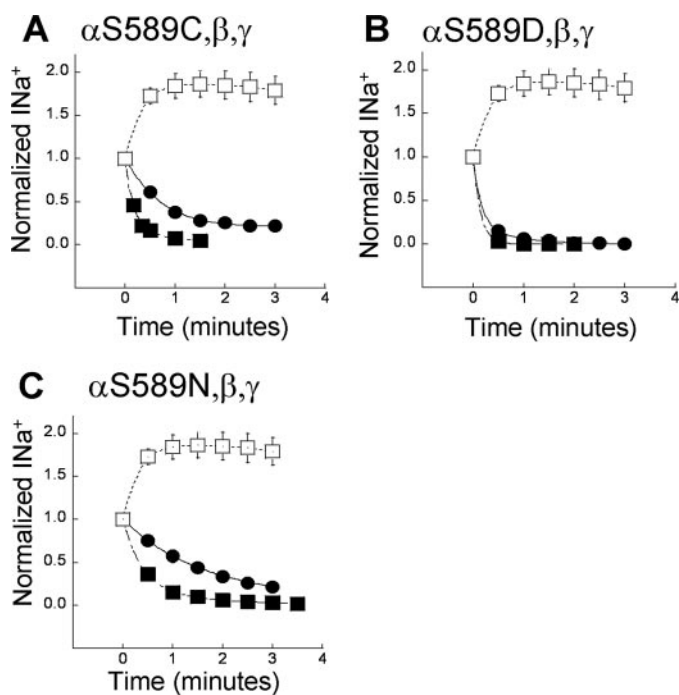
FIGURE 5. **Time course of inhibition of ENaC current (I_{Na}) by Zn^{2+} in oocytes expressing $\alpha S589C,\beta,\gamma$ (A), $\alpha 589D,\beta,\gamma$ (B), or $\alpha S589N,\beta,\gamma$ (C)** (*closed symbols*) compared with oocytes expressing ENaC wild-type (*open symbols*). Inhibition curves were obtained with Zn^{2+} concentrations of 0.1 mM (*circle*) or 1 mM (*square*). Data were best fitted by the sum of two exponentials, and results are given in Table 1. $n = 4$.
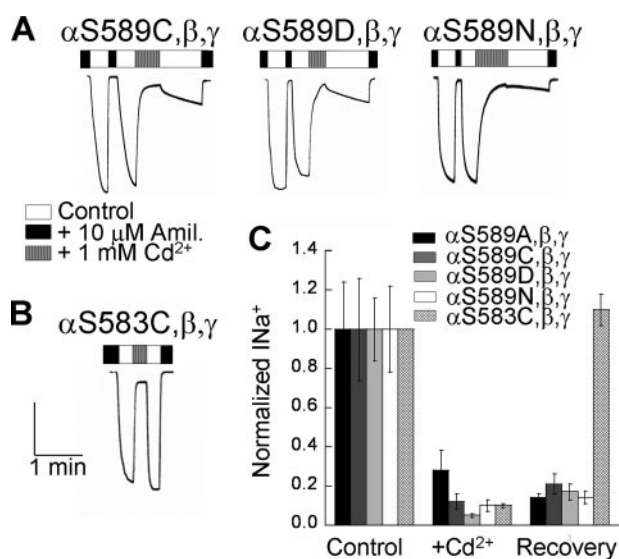

FIGURE 6. **Slow and partial recovery of ENaC currents from Cd^{2+} block.** A, Oocytes were injected with $\alpha S589C,\beta,\gamma$, $\alpha S589D,\beta,\gamma$, or $\alpha S589N,\beta,\gamma$. Removal of amiloride induced a large and reversible I_{Na}. The addition of 1 mM Cd^{2+} inhibited I_{Na} that slowly and partially recovered after Cd^{2+} removal. B, oocytes expressing $\alpha S583C,\beta,\gamma$ show a rapid and complete recovery of I_{Na} after inhibition by 1 mM Cd^{2+}. *Scale*, x-axis, 1 min; y-axis, Cys, 3 μA, Asp, 5 μA, Asn 7 μA (A), 13 μA (B). C, normalized I_{Na} before, during, and 2 min after application of Cd^{2+} (1 mM) in the bath ($n = 20$).

dues within the channel pore at a site downstream or deeper relative to the amiloride binding site.

For positively charged pore blockers binding within the transmembrane pore region, the large electric field across the membrane provides the energy to move the blocker along the channel pore. If Cd^{2+} binds within the transmembrane electric field, we
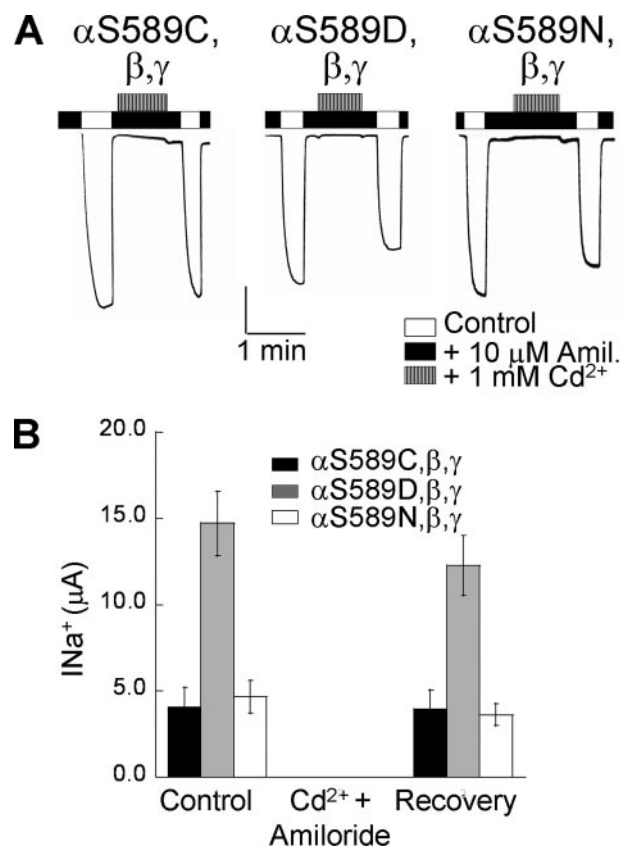
FIGURE 7. **The nearly irreversible I_{Na} inhibition by Cd^{2+} is prevented by amiloride.** A, oocytes expressing $\alpha S589C,\beta,\gamma$, $\alpha S589D,\beta,\gamma$, or $\alpha S589N,\beta,\gamma$, were exposed to external Cd^{2+} (1 mM) in the presence of 10 μM amiloride; I_{Na} completely recovered after removal of Cd^{2+} and amiloride. *Scale*, x-axis, 1 min; y-axis, Cys, 3 μA, Asp, 5 μA, Asn, 3 μA. B, recovery of Cd^{2+} inhibition in the presence of amiloride ($n = 6$).

expect the inhibition of αSer-589 ENaC mutants by Cd^{2+} to be dependent on voltage across the membrane. Fig. 8 shows the I_{Na} inhibition of the $\alpha S589N$ and $\alpha S589C$ mutants by 1 and 3 mM extracellular Cd^{2+} at transmembrane voltages ranging from -120 to 0 mV. Inhibition of both mutants by Cd^{2+}, arbitrarily determined 40 s after application, was clearly dependent on voltage, with a stronger inhibition at negative holding potentials. According to Woodhull's formulation, the slope parameter z' is equal to the product of the actual valence of the blocking ion (2 for Cd^{2+}) and the fraction of the electrical distance, δ, acting on Cd^{2+} at the binding site. The δ values of 0.34 ± 0.05 and 0.42 ± 0.05 calculated for the voltage dependence of Cd^{2+} block of $\alpha S589N$ and $\alpha S589C$, respectively, represent apparent relative distances in the electric field, because they were not determined at equilibrium. Still our data clearly indicate that Cd^{2+} binds to a site within the transmembrane electric field that is indistinguishable for both mutants.

So far, our analysis of the current inhibition of ENaC αSer-589 mutants by Cd^{2+} reveals that this cation binds to a site in the channel pore located deeper than the amiloride binding site and that the contribution of the substituted residue at position $\alpha589$ in coordinating Cd^{2+} ions to block the channel is not essential since the $\alpha S589N$ substitution also confers to the channel a sensitivity to Cd^{2+}. We further investigated this point by probing the $\alpha S589D$ mutant with external Ca^{2+} and looked
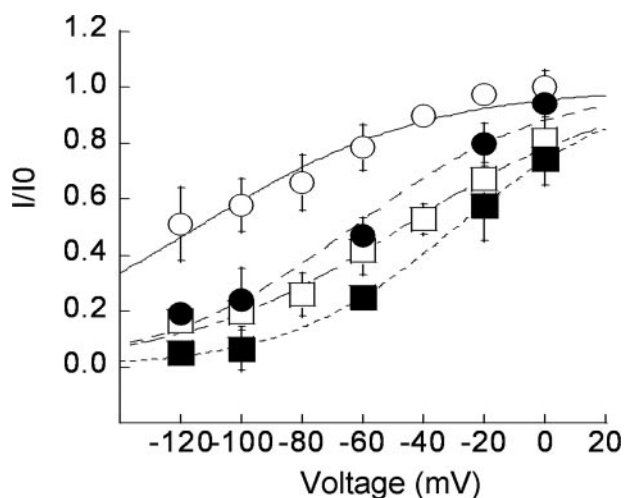
FIGURE 8. **Voltage dependence of Cd^{2+} block in the mutants αS589C,β,γ and αS589N,β,γ.** I_{Na} inhibition is defined as the $I_{Na}(Cd^{2+})/I_{Na}$ (0) ratio measured at holding potentials ranging from -120 mV to 0 mV. $I_{Na}(Cd^{2+})$ is the I_{Na} measured 40 s after the application of either 1 mM (*circle*) or 3 mM (*square*) Cd^{2+}; I_{Na} (0) is defined as I_{Na} in the absence of Cd^{2+}. Data were fitted according to the Woodhull formula (see "Materials and Methods") yielding δ values of 0.34 ± 0.05 and 0.425 ± 0.05 for Cd^{2+} block of the αS589N (*open symbols*, $n = 15$) and αS589C (*closed symbols*, $n = 9$) mutants, respectively.
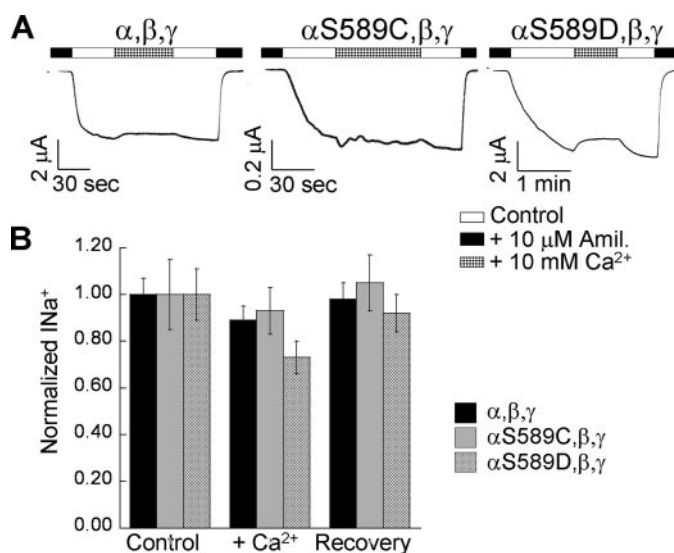
FIGURE 9. **Recovery of ENaC currents from external Ca^{2+}.** *A*, representative recordings of I_{Na} in oocytes expressing $\alpha\beta\gamma$, αS589C,β,γ or αS589D,β,γ ENaC after the addition of 10 mM external Ca^{2+}. *B*, normalized I_{Na} before, during, and after application of 10 mM Ca^{2+} in the bath ($n = 12$).

for binding interactions between Ca^{2+} and the engineered aspartate side. The Ca^{2+} ions have an ionic radius comparable with Cd^{2+} or Zn^{2+}. As shown in Fig. 9, Ca^{2+} at 10 mM in the external medium exerts only a modest inhibition of the αS589D mutant (~25% inhibition of I_{Na}) compared with Cd^{2+} or Zn^{2+} (Figs. 4 and 5). Furthermore, in contrast to Cd^{2+}, the weak block by Ca^{2+} was rapidly and completely reversible.

Taken together, our experimental evidence does not support the participation of the side chain of the amino acids at position αSer-589 in coordinating Cd^{2+}, Zn^{2+}, or Ca^{2+} ions, although such interaction cannot be firmly excluded in the absence of structural data. It seems more likely that the inhibition of the αS589C, -D, or -N substitution mutant by Cd^{2+} or Zn^{2+} is due

to coordination with native cysteines in the internal pore of ENaC that become accessible to Cd^{2+} and Zn^{2+}, due to the αSer-589 mutation in the channel selectivity filter.

There are a large number of cysteines in the α-, β-, and γENaC sequences that represent potential binding sites for Cd^{2+} ions in the internal pore of the channel. We have limited our analysis to conserved regions of the N terminus, the TM1 and TM2 transmembrane segments that involve 13 cysteine residues. We initially planned to substitute all the 13 cysteines, but we quickly realized that we were unable to generate a functional channel in the background of the αS589N mutation when more than 5 substituted cysteines were mutated in α-, β-, or γENaC subunits.

We have performed a first screen with different ENaC mutants in which native cysteines were substituted individually or in pairs in the αS589N mutant background. We have identified γCys-546 as a potential binding site for Cd^{2+}. Recordings in Fig. 10, *A–C*, show the time course of Cd^{2+} inhibition of the S589C, -D, and -N mutants with the substitution of the native cysteine to serine at position Cys-546 in γENaC. When compared with the tracing in Fig. 2, the I_{Na} inhibition by 0.1 mM Cd^{2+} was almost negligible for the αS589C/D,β,γC546S mutants and considerably reduced at 1 mM for the αS589N,β,γC546S. Fig. 10 (*bottom in each panel*) displays the effect of the γC546S mutation on the time course of I_{Na} inhibition by Cd^{2+} of the αS589C, -D, -N mutants. At all the Cd^{2+} concentrations tested, the γC546S substitution decreases the magnitude of the I_{Na} inhibition by Cd^{2+}, but current inhibition persists at high Cd^{2+} concentrations. Such I_{Na} inhibition in the presence of Cd^{2+} is expected for a channel mutant with a permeability to Cd^{2+} ions that is lower than for Na^+ ions since the slower diffusion of Cd^{2+} along the pore will consequently reduce as well that of Na^+.

We asked whether the lower sensitivity of the γC546S mutant to block by Cd^{2+} might be related to a faster dissociation rate from its binding site and tested the recovery of the αS589C,β,γC546S, αS589D,β,γC546S, and αS589N,β,γC546S mutants from Cd^{2+} block at millimolar concentrations. I_{Na} recordings of the αS589C,β,γC546S, αS589D,β,γC546S, and αS589N,β,γC546S mutants in Fig. 11*A* show that, after the Cd^{2+}-dependent decrease in I_{Na}, removal of external Cd^{2+} allowed a fast and almost complete recovery of I_{Na}. These experiments show that the γCys-546 is responsible for the almost irreversible trapping of Cd^{2+} within the pore that leads to the channel block.

DISCUSSION

The ENaC channel is insensitive to block by external Cd^{2+} but is highly sensitive to block by Cd^{2+} applied at micromolar concentrations from the intracellular side of the membrane (13). The cysteine substitution αS589C has two major consequences on channel function; first, it confers a block by externally applied Cd^{2+} or Zn^{2+} ions, and second, it changes the ion selectivity of the channel (11). Mutations at position αSer-589 have been shown to drastically change the ion selectivity of ENaC, allowing divalent cations to pass through the channel. Detectable currents carried by divalent cations such as Sr^{2+} or

A αS589C,β,γC546S

B αS589D,β,γC546S

C αS589N,β,γC546S

□ Control
■ + 10 μM Amil.
▤ + Cd²⁺
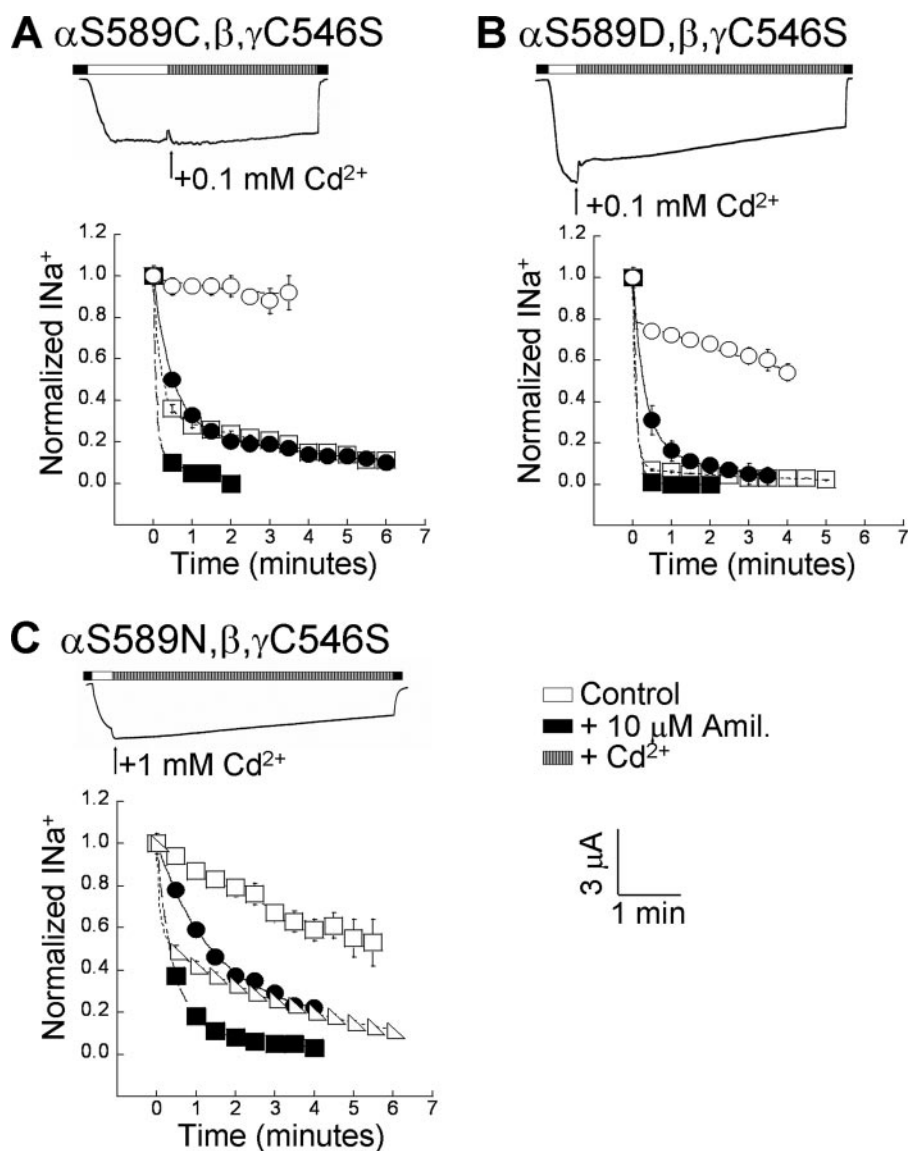
FIGURE 10. **Effect of the ENaC γC546S mutation on the Cd²⁺ block.** Effect of γC546S on the Cd²⁺ block in the background of αS589C (*A*, *n* = 10), αS589D (*B*, *n* = 5), or αS589N (*C*, *n* = 10). *Top*, representative recordings of Cd²⁺ block. *Bottom*, direct comparison of the time course of 0.1 mM (*circle*), 1 mM (*square*), or 10 mM (*triangle*) Cd²⁺ inhibition of αSer-589 mutants alone (*closed symbols*) or together with the γC546S mutation (*open symbols*).

ions with the sulfhydryl group of the α589 cysteine pointing toward the channel pore (11). The contribution of this cysteine site chain in coordinating Cd²⁺ ions seems questionable since alternative αSer-589 substitutions such as αS589N render ENaC equally sensitive to block by Cd²⁺. Therefore, a sulfhydryl group at serine 589 is not necessary for Cd²⁺ block of the αS589C mutant, and it is difficult on this basis to draw any conclusion about the side chain orientation of the residue at αSer-589 relative to the channel pore. The extremely weak inhibition of the αS589D mutant by external Ca²⁺ at concentrations as high as 10 mM further supports the absence of interaction between divalent cations in the channel pore and the side chain residue at position αSer-589. It remains likely that, as for the KcsA K⁺ channel, the selectivity filter of ENaC is lined essentially by the backbone atoms of the G/SXS sequence as has been already proposed (10).

Our observations are consistent with a mechanism for Cd²⁺ blocking of the αS589C mutant that involves a change in the selectivity filter allowing the access for external Cd²⁺ ions to a binding site within the internal pore. The block of αS589C, αS589D, and αS589N by Cd²⁺ is characterized by a slow on-rate and an equally slow and partial recovery from blockade. These blocking kinetics are clearly different from those of αS583C ENaC block by Cd²⁺. This latter mutant with the substitution located in the amiloride binding site at the outer entrance of the channel pore shows a fast and fully reversible current inhibition by submillimolar Cd²⁺ or Zn²⁺ consistent with the accessibility of the cysteine sulfhydryl group at position α583 to permeant ions. The slow on-rate of αS589C block by Cd²⁺ rather suggests the presence of significant diffusional constraints for Cd²⁺ to reach a site within the channel pore where it binds nearly irreversibly and with high affinity. This is illustrated in our experiments by the fact that the concentration of external Cd²⁺ between 10 μM and 1 mM mainly affects the on-rate of block and has relatively little effect on the maximal current inhibition.

Our experimental data provide little evidence for a direct interaction between Cd²⁺ and the sulfhydryl group of the cysteine at position α589. The question remains where does Cd²⁺ bind? The voltage dependence of the channel block by Cd²⁺

Ca²⁺ could be measured through αS589C and αS589D ENaC mutants (9).

The aim of this work was to understand the molecular mechanism of the block of the αSer-589 ENaC mutants by extracellular Cd²⁺ and to identify the amino acid residues coordinating Cd²⁺. We have hypothesized that external Cd²⁺ ions are unable to block wild-type ENaC essentially because the channel is impermeable to divalent cations. Rendering ENaC permeable to divalent cations by mutations at residues in the selectivity filter such as the αSer-589 should make the channel sensitive to block by external Cd²⁺ in a way similar to the ENaC block by internally applied Cd²⁺. This approach could be applied to identify the residues lining the conductive pore and therefore to better understand the structure of ENaC.

It has been recently proposed that the block of the αS589C ENaC mutant by Cd²⁺ results from the coordination of Cd²⁺

FIGURE 11. **The γC546S mutation affects the recovery from Cd²⁺ block.** *A*, recordings of I_{Na} in oocytes expressing αS589C,β,γC546S, αS589D,β,γC546S, or αS589N,β,γC546S after Cd²⁺ exposure (1 or 10 mM) and after Cd²⁺ removal. *B*, summary of I_{Na} recovery after Cd²⁺ removal. (αS589C,β,γC546S, $n = 12$; αS589D,β,γC546S, $n = 8$; or αS589N,β,γC546S, $n = 5$).

indicates that this cation binds within the transmembrane electric field. In addition, we provide strong evidence that Cd²⁺ binds in the channel pore, since amiloride, the classical pore blocker, of ENaC prevents Cd²⁺ from blocking the channel. Thus, Cd²⁺ binds at a site located deeper in the channel pore with respect to the amiloride binding site and likely beyond the selectivity filter since the αSer-589 mutations altering the channel ionic selectivity are required for Cd²⁺ block. The Ser-589 in the αENaC is in close vicinity of the amiloride binding site corresponding to αS583C, and experimental evidence is consistent with αSer-589 participating in the narrowest part of the channel pore at the selectivity filter.

Our experiments support the view that the substitutions at position Ser-589 in the αENaC subunit result in steric modifications of the channel pore that allow externally applied Cd²⁺ to reach a binding site normally inaccessible within the internal pore of ENaC located beyond the selectivity filter. Wild-type ENaC is blocked by micromolar concentrations of Cd²⁺ applied from the intracellular side, and this block shares two important characteristics with the block of αS589C mutant by extracellular Cd²⁺: it displays both an affinity in the micromolar range and is slowly and only partially reversible. The steric modifications resulting from αSer-589 mutations affect the ionic selectivity of ENaC, making the channel more permeable to K⁺ and Ca²⁺. It has not been possible to show that the αSer-589 mutants are permeable to Cd²⁺ or Zn²⁺ ions, since both divalent cations block the channel, but it remains very likely that the steric modifications in the narrowest part of ENaC, due to αSer-589 mutation, allow Cd²⁺ ions to pass the selectivity filter and to bind cysteine residues located along the channel pore. In the case of wild-type ENaC, these binding sites for Cd²⁺ are only accessible from the intracellular side.

The αSer-589 ENaC mutants provide an interesting model to identify the cysteine residues that coordinate Cd²⁺ ions along the ion permeation pathway. Unfortunately, in our search for cysteines interacting with Cd²⁺, we were limited by the low amiloride-sensitive current of the cysteine substitution ENaC mutants performed in the background of the αSer-589 mutations. It was thus difficult to obtain a complete picture of the cysteines lining the internal pore of the channel. However, we identified Cys-546 in the TM2 of the γENaC subunit as a residue that contributes to the channel block by Cd²⁺. First, the γC546S mutation decreases the apparent affinity for Cd²⁺ of a site that is responsible for the fast component of the channel inhibition. Second, the γC546S substitution makes the channel block by Cd²⁺ rapidly reversible. Such increase in the off-rate of Cd²⁺ blocking kinetics represents a strong argument supporting both a direct participation of the γCys-546 in the coordination of Cd²⁺ ion and the orientation of the sulfhydryl group of γCys-546 toward the ion permeation pathway. The γCys-546 residue is likely the first accessible site for external Cd²⁺ ions, and Cd²⁺ binding to this site results in a channel block. The slower component of the Cd²⁺ block seems unaffected by γCys-546 mutation, suggesting the presence of a deeper and less accessible site for binding Cd²⁺ along the internal part of the channel pore. The γCys-546 may not be the only residue involved in the coordination with Cd²⁺ ions. The identification of additional cysteine partners involved in binding interactions with Cd²⁺ ion requires the substitution of these cysteines in the background of the αSer-589 and γCys-546 mutations. Unfortunately, these ENaC constructs did not express measurable amiloride-sensitive currents.

Even though several structural models have been proposed, the structure of the ion channel pore of the members of the ENaC/degenerin family has yet not been elucidated (16, 18). Functional analysis of voltage-dependent blocking of ENaC by impermeant cations supports a funnel-like structure of the external conduction pore of ENaC that can accommodate amiloride in its outer mouth (position 583 in the rat ENaC sequence) and then narrowing down to the selectivity filter (G/SXS sequence, Fig. 1) (19). The primary sequence of this pore region (Ser-583-Ser-589 in rat αENaC, Fig. 1) does not allow reliable secondary structure predictions. However, the second transmembrane domain starting at the conserved Val residue Val-590 conforms to a highly probable α helix (Fig. 1) (8). The side chain orientation of the amino acid residues lining the pore region has clearly been demonstrated for the residues involved in the binding interactions with amiloride, *i.e.* Ser-583 in the αENaC (Fig. 1) and the corresponding glycine residues in the β and γ ENaC subunits (17). The thiol side chains of cysteine substitutions at positions Leu-584, Trp-585, Phe-586, and Ser-588 in the αENaC sequence are not accessible to sulfhydryl reagents such as methanethiosulfonates or Cd²⁺ (16). Similar data were obtained with cysteine substitutions on γENaC. From our data little evidence supports the interaction between Cd²⁺ or Ca²⁺ with the side chain of aspartate or cysteine, respectively, at position α589. We have not analyzed in detail the mechanism of block by Cd²⁺ of the αG587C mutant, but the characteristics of this block are basically similar to that of the

αS589C mutant (11). Thus, from this experimental evidence, the αSer-583 appears to be the only residue in the pore region sequence having its side chain facing the ion conduction pore and interacting with ions present in the pore lumen. Amino acid substitutions of the corresponding glycine in β (Gly-525) and γ (Gly-537) ENaC subunits suggest orientations of these residues similar to Ser-583 in α subunit (17, 20).

The second transmembrane α helix likely starts with residue Val-590, according to model predictions of the αENaC subunit (Fig. 1) (8). The Cys-546 in the γENaC interacts with permeant Cd^{2+} ions in the background of the αSer-589 mutation, providing strong evidence that the thiol side chain is facing the ion conduction pore. It is therefore likely that γCys-546 is accessible to permeant ions after passing successively through the external pore and the selectivity filter. This represents the first evidence for the contribution of the second transmembrane segment to the internal pore lining. A previous cysteine accessibility scan performed on ASIC1a using methanethiosulfonates applied from the intracellular side of the channel revealed that cysteines introduced at several positions corresponding in the γENaC sequence to Val-547, Ile-548, and Ile-550, as well as others located more distally in the TM2, were inaccessible to MTSET, *i.e.* did not interact with internal MTSET to block the channel (14). Thus, according to the presently available experimental evidence, it seems that only the first residues in the proximal part of the TM2 corresponding to position γCys-546 participate in the pore lining. In the KcsA, the distal part of TM2 forms the tip of "inverted tepee" architecture that corresponds to the intracellular end of the conduction pore (12). Recent evidence suggests that the intracellular start of the TM1 and part of the amino terminus of ASIC and ENaC channels participate to the inner pore structure (13, 14). We can therefore conclude that the ion conduction pore of ENaC/ASIC channels does not conform to the general structural feature of the potassium channels.

REFERENCES

1. Kellenberger, S., and Schild, L. (2002) *Physiol. Rev.* **82,** 735–767
2. Loffing, J., Zecevic, M., Feraille, E., Kaissling, B., Asher, C., Rossier, B. C., Firestone, G. L., Pearce, D., and Verrey, F. (2001) *Am. J. Physiol.* **280,** F675–F682
3. Lifton, R. P., Gharavi, A. G., and Geller, D. S. (2001) *Cell* **104,** 545–556
4. Boucher, R. C. (2004) *Eur. Respir. J.* **23,** 146–158
5. Firsov, D., Gautschi, I., Merillat, A. M., Rossier, B. C., and Schild, L. (1998) *EMBO J.* **17,** 344–352
6. Kosari, F., Sheng, S. H., Li, J. Q., Mak, D. D., Foskett, J. K., and Kleyman, T. R. (1998) *J. Biol. Chem.* **273,** 13469–13474
7. Kellenberger, S., Gautschi, I., and Schild, L. (2003) *Mol. Pharmacol.* **64,** 848–856
8. Rost, B., Yachdav, G., and Liu, J. (2004) *Nucleic Acids Res.* **32,** W321–W326
9. Kellenberger, S., Gautschi, I., and Schild, L. (1999) *Proc. Natl. Acad. Sci. U. S. A.* **96,** 4170–4175
10. Kellenberger, S., Auberson, M., Gautschi, I., Schneeberger, E., and Schild, L. (2001) *J. Gen. Physiol.* **118,** 679–692
11. Sheng, S., Perry, C. J., Kashlan, O. B., and Kleyman, T. R. (2005) *J. Biol. Chem.* **280,** 8513–8522
12. Doyle, D. A., Cabral, J. M., Pfuetzner, R. A., Kuo, A. L., Gulbis, J. M., Cohen, S. L., Chait, B. T., and MacKinnon, R. (1998) *Science* **280,** 69–77
13. Kellenberger, S., Gautschi, I., Pfister, Y., and Schild, L. (2005) *J. Biol. Chem.* **280,** 7739–7747
14. Pfister, Y., Gautschi, I., Takeda, A. N., van Bemmelen, M., Kellenberger, S., and Schild, L. (2006) *J. Biol. Chem.* **281,** 11787–11791
15. Ravindran, A., Schild, L., and Moczydlowski, E. (1991) *J. Gen. Physiol.* **97,** 89–115
16. Sheng, S. H., Li, J. Q., Mcnulty, K. A., Kieber-Emmons, T., and Kleyman, T. R. (2001) *J. Biol. Chem.* **276,** 1326–1334
17. Schild, L., Schneeberger, E., Gautschi, I., and Firsov, D. (1997) *J. Gen. Physiol.* **109,** 15–26
18. Li, J., Sheng, S., Perry, C. J., and Kleyman, T. R. (2003) *J. Biol. Chem.* **278,** 13867–13874
19. Palmer, L. G. (1990) *Renal Physiol. Biochem.* **13,** 51–58
20. Snyder, P. M., Olson, D. R., and Bucher, D. B. (1999) *J. Biol. Chem.* **274,** 28484–28490

II / Internal accessibility of the cysteine to sulfhydryl reagents.

Kellenberger *et al* (64) have shown that intracellular methanethiosulfonates (MTS) are able to inhibit ENaC current suggesting the presence of intracellular cysteines which may play an important role in ENaC function. We asked whether intracellular inhibition of ENaC by MTS occurs *via* its direct interaction with ENaC subunits and which cysteines in ENaC subunits are involved in the inhibition. We thus proposed a new approach based on the Substituted Cysteine Accessibility Method (SCAM) which consists of single cysteine substitutions within a target protein coupled with covalent cysteine modification by hydrophilic thiol-reagents. Here, the effect of a sulfhydryl reagent on the sodium current is measured in cut-open oocytes. In addition, a modified SCAM was performed with sulfhydryl reagent coupled to biotin (MTSEA-biotin) in order to isolate the target protein by streptavidin pull-down assay. This new approach permits us to correlate the MTS binding and its effect on the channel activity, and hence to determine the accessibility of the cysteines within the channel and their involvement in the channel function.

II-1) **ENaC**

II-1-i) *Specificity of the method*

We first tested the effect of MTSEA-biotin on ENaC current: results are shown in the Figure 22. We measured the amiloride-sensitive sodium current of oocytes expressing the wild-type ENaC protein with a two-electrode voltage clamp (TEV). Oocytes were first incubated in an external solution containing 10 μM amiloride. Removing amiloride led to an increase of the inward sodium current which was completely inhibited by addition of amiloride. The same oocyte was then incubated for 2 minutes in an external solution containing 1 mM MTSEA-biotin. Removal of amiloride induced an inward sodium current (I_{Na+}) similar to the current without MTSEA-biotin treatment. Thus, external MTSEA-biotin had no effect on the amiloride-

sensitive sodium current generated by the wild-type ENaC channel (Figure 22A). We then performed the same experiment with intracellularly-applied MTSEA-biotin. Oocytes expressing wild-type ENaC were placed in a cut-open chamber, which routinely allows the modification of both the extracellular and intracellular media. As shown before, removal of external amiloride led to an increase of inward sodium current. In this case, perfusion of 0.1 mM intracellular MTSEA-biotin induced a 95 % inhibition of the amiloride-sensitive sodium current generated by the wild-type ENaC channel (Figure 22B). Bar graphs summarize the normalized amiloride-sensitive sodium current obtained before (t=0) and after 2 minutes (t=2') incubation with extracellular MTSEA-biotin (left graph) or perfusion of intracellular MTSEA-biotin (right graph). Results showed that extracellular MTSEA-biotin had no effect on ENaC-mediated sodium current while intracellular MTSEA-biotin inhibited 65 % of the ENaC-mediated sodium current after 2 minutes of perfusion.
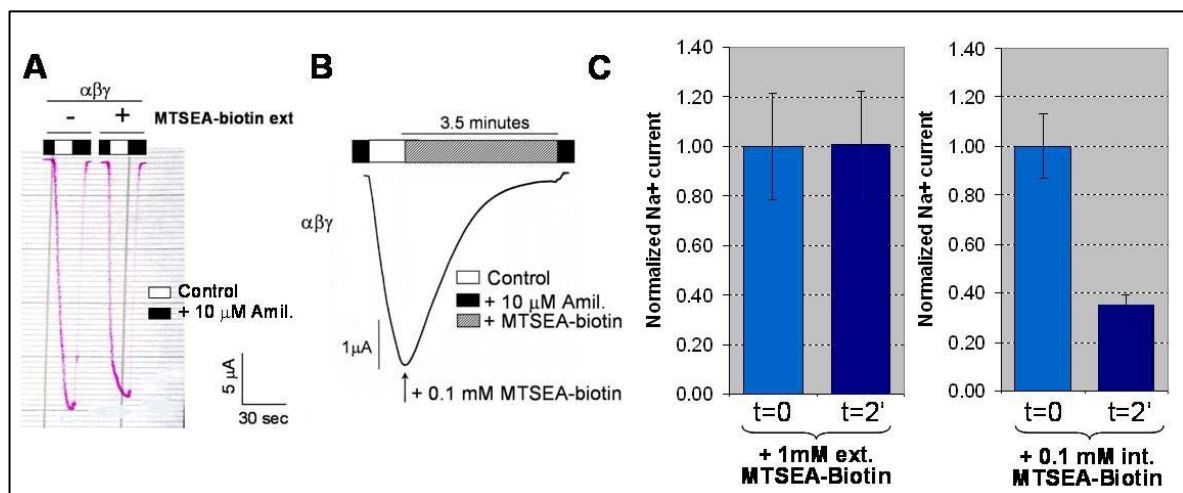
Figure 22: Effect of MTSEA-biotin on the amiloride-sensitive current (I_{Na+}) generated by ENaC wild-type. (**A**) Effect of 1 mM extracellular MTSEA-biotin on wild-type I_{Na+} (n=1). (**B**) Effect of 0.1 mM intracellular MTSEA-biotin on wild-type I_{Na+} (n=1). (**C**) Summary of normalized amiloride-sensitive sodium currents obtained before (t=0) and after 2 minutes (t=2') incubation with 1 mM extracellular MTSEA-biotin (left, n=8 oocytes) or perfusion of 0.1 mM intracellular MTSEA-biotin (right, n=10 oocytes) on oocytes expressing wild-type ENaC. Sodium currents were normalized against the mean current obtained at t=0.

We then studied the biotinylation of ENaC subunits when MTSEA-biotin was applied either extracellularly or intracellularly. Some oocytes were entirely incubated with extracellular and other ones were perfused with intracellular MTSEA-biotin. In both cases, biotinylated proteins were isolated by affinity for streptavidin beads and then separated by SDS-PAGE. The western blots of α and β subunits are shown in figure 23. The left panel shows the total expression of both α and β subunits in the oocyte total lysates. In total lysates of oocytes expressing αβγ, α and β subunits were similarly expressed in all MTSEA-biotin conditions. As a control for the specificity of the antibodies, non-injected oocytes (Non-Inj.) did not show any signal for both α and β subunits. The right panel shows the biotinylated proteins, *i.e.* the proteins bound to MTSEA-biotin. We did not observe any specific signal with anti-α antibody suggesting that extracellular MTSEA-biotin (Ext.) does not biotinylate the extracellular region of the α subunit. In the case of the β subunit, a low intensity signal of biotinylation appeared for oocytes expressing αβγ in the presence or absence of extracellular MTSEA-biotin. This is likely to indicate that there is non-specific binding between the β subunit and the streptavidin beads. In contrast, we observed biotinylated α and β subunits in oocytes expressing αβγ that were perfused with intracellular MTSEA-biotin (Int.). This indicates there is a MTSEA-biotin mediated biotinylation of the cytosolic region of both the α and β subunits of ENaC. The absence of an actin signal in the biotinylated fraction indicates that extracellular MTSEA-biotin did not interact with cytosolic proteins. Altogether, these results showed that the inhibition of ENaC activity by MTSEA-biotin was specifically intracellular and correlated with the binding of MTSEA-biotin on the intracellular part of the two α and β subunits.
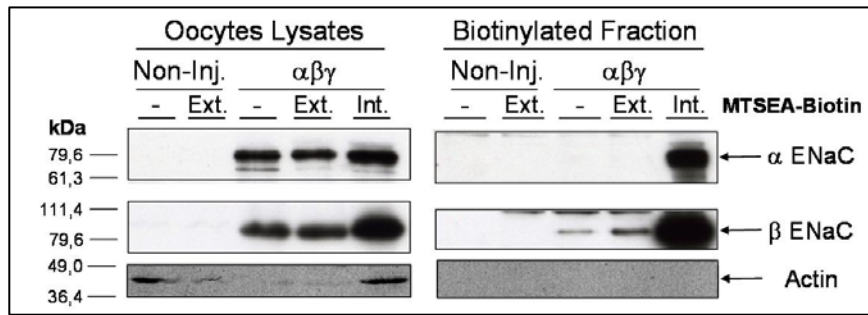
Figure 23: Western Blot analysis of the MTSEA-biotin mediated biotinylation of ENaC α and β subunits (N=2). The left panel shows total protein expression and the right panel shows the biotinylated fraction of these proteins. Oocytes were non-injected (Non-Inj.) or injected with ENaC wild-type channel (αβγ). They were then incubated with 1 mM extracellular MTSEA-biotin (Ext.), perfused with 0.1 mM intracellular MTSEA-biotin (Int.) or non-treated with MTSEA-biotin (-). An actin control was used throughout to show the absence of contaminating cytosolic proteins in the surface biotinylated fraction. (n=12 oocytes per condition)

In order to verify the specificity of interaction between MTSEA-biotin bound to ENaC and streptavidin beads, we perfused oocytes expressing αβγ ENaC with 1 mM intracellular MTSEA, either coupled or not coupled to biotin. Proteins were incubated with streptavidin beads and then separated by SDS-PAGE. The western blot is shown in figure 24. The left panel indicates that, in the total lysates, the three α, β and γ subunits were similarly abundant under all perfusion conditions. In the biotinylated fraction (right panel), we observed that the three α, β and γ subunits were biotinylated when oocytes were perfused with MTSEA-biotin. This signal did not appear when perfused with MTSEA, except for the β subunit, where we observed a residual signal of biotinylation. This confirmed the presence of a non specific binding between the β subunit and streptavidin beads, as we had previously observed. However, overall these results showed that the binding of streptavidin was highly specific to presence of MTSEA-biotin and not just MTSEA alone.
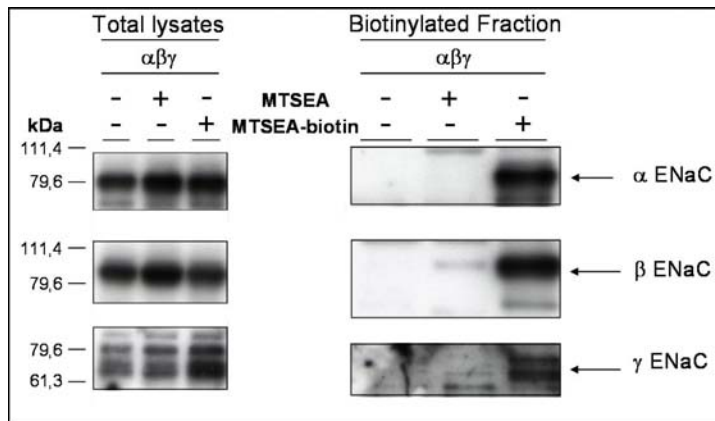
Figure 24: Western Blot analysis of the MTSEA-biotin - streptavidin beads binding specificity. (N=1) Oocytes expressing αβγ ENaC were either non-perfused or perfused with MTSEA alone or MTSEA coupled to biotin. (12 oocytes per condition)

MTS reagents covalently bind to the thiol group of cysteine residues. In order to confirm that the biotinylation by MTSEA-biotin is mediated by interaction with cysteines, we performed experiments where oocytes expressing ENaC wild-type were perfused intracellularly with 1 mM MTSEA-biotin with or without 5 mM free cysteine (Figure 25). As seen previously, perfusion of 1 mM intracellular MTSEA-biotin led to the almost complete inhibition of the amiloride-sensitive ENaC wild-type sodium current (Figure 25A, left panel). Perfusion with 1 mM MTSEA-biotin together with 5 mM of free cysteine prevented the inhibition of ENaC. Several measurements (21 oocytes) showed that the MTSEA-biotin mix with free cysteine did not significantly inhibit the ENaC-mediated sodium current (Figure 25B). In the perfusion solution, it is likely that the free cysteines were modified by MTSEA-biotin even before the perfusion of the mixture into the oocytes expressing ENaC. Thus, the presence of 5 mM free cysteine in the intracellular perfusion mix prevented the inhibitory effect of MTSEA-biotin on the ENaC-mediated amiloride-sensitive sodium current, most likely by competing with the native intracellular ENaC cysteines. This showed that the MTSEA-biotin inhibition was mediated by the interaction of MTSEA-biotin with cysteine.
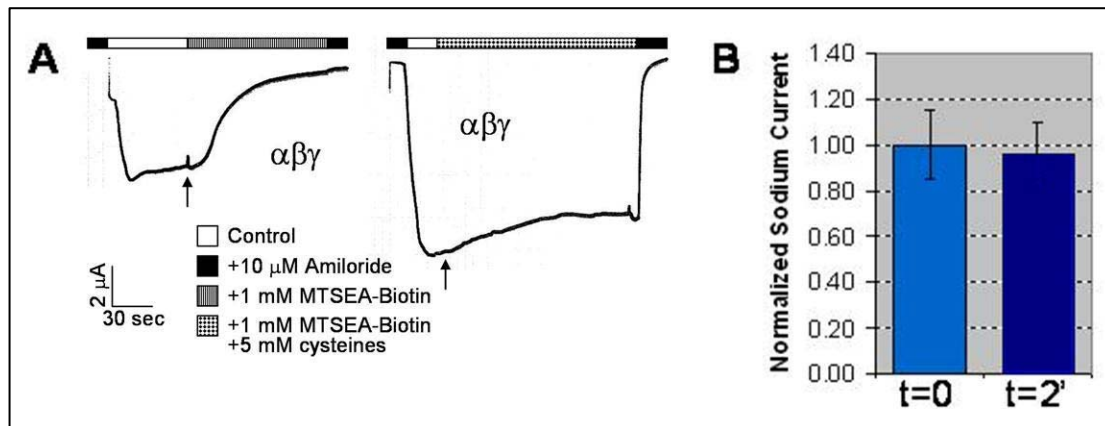
Figure 25: Effect of 5 mM free cysteines on MTSEA-biotin I$_{Na+}$ inhibition. (**A**) Typical sodium current measurement of ENaC wild-type. In the left panel, oocytes were perfused with 1 mM MTSEA-biotin alone while, in the right panel, oocytes were perfused with 1 mM MTSEA-biotin + 5 mM free cysteines. (**B**) Summary of the WT sodium currents obtained before (t=0) and 2 minutes (t=2') after perfusion of 1 mM MTSEA-biotin + 5 mM free cysteines. Sodium currents were normalized with current obtained before the perfusion (n=21 oocytes).

The oocytes expressing αβγ ENaC and perfused with either 1 mM MTSEA-biotin or 1 mM MTSEA-biotin with 5 mM free cysteine were retained and lysed for total protein extraction. These proteins were then incubated with streptavidin beads and separated by SDS-PAGE (Figure26). Total lysates on the left panel indicated that the two α and β subunits were similarly expressed under all perfusion conditions. Non-injected oocytes (Ni) were used as negative control for antibody specificity. In the biotinylated fraction, we did not observe any biotinylated signal for α and β ENaC when oocytes were perfused with 5 mM free cysteine alone. Perfusion of MTSEA-biotin alone induced the specific α and β biotinylated subunits signals as seen above. When free cysteine was added to the MTSEA-biotin perfusion mix, α and β subunits were not biotinylated. This experiment was reproducible across three different batches of oocytes, as shown in the figure 26B. These data indicated that free cysteine prevented the MTSEA-biotin mediated biotinylation of the α and β subunits of ENaC. The loss of inhibition of ENaC-mediated I$_{Na+}$ by MTSEA-biotin in the presence of free cysteine

correlated with an absence of binding of MTSEA-biotin to both the α and β subunits. This confirmed our hypothesis that there was competition between free cysteines and native cysteines of ENaC subunits to bind MTSEA-biotin.
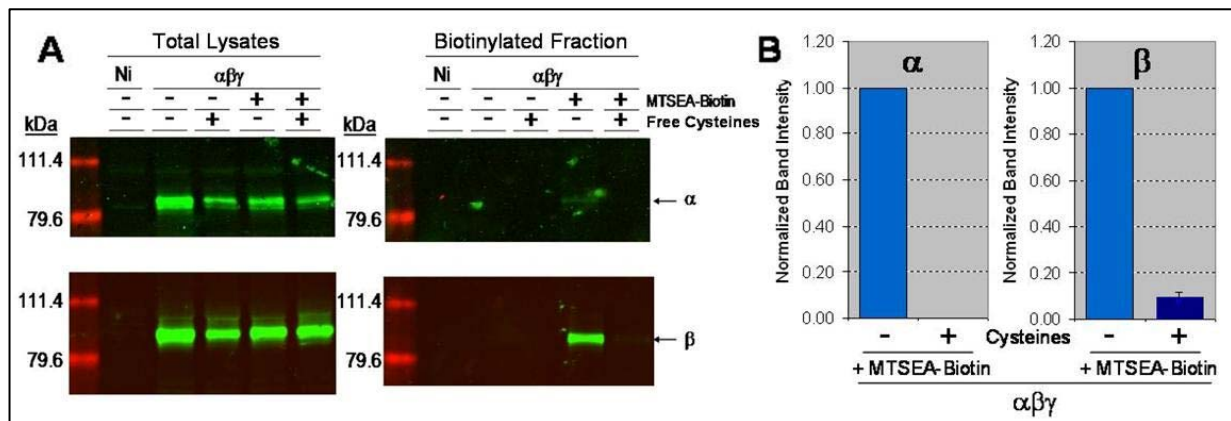
Figure 26: **MTSEA-biotin mediated biotinylation of α and β subunits in presence or absence of 5 mM free cysteines.** (**A**) LiCor® western blot analysis of the biotinylation of the α and β subunits of ENaC. Oocytes expressing αβγ ENaC were intracellularly perfused with 1mM MTSEA-biotin with or without 5 mM free cysteine (n=12 oocytes per condition). (**B**) The signal of biotinylated α and β subunits was quantified with the Odyssey® software. For each α and β subunit, two conditions of perfusion are presented: (i) perfusion with MTSEA-biotin alone (light blue, -) and (ii) perfusion with MTSEA-biotin and free cysteine (dark blue, +) (n=3 batches of oocytes per condition). The band intensity was normalized with the signal obtained when oocytes were perfused with MTSEA-biotin alone.

In summary, extracellular MTSEA-biotin had no effect on ENaC activity and did not bind to the α or β subunits, whereas intracellular perfusion of MTSEA-biotin led to the inhibition of the channel through direct interaction with both the α and β subunits. The inhibition of ENaC activity by intracellular MTSEA-biotin, as its binding to α and β subunits, was a result of the direct interaction between MTSEA-biotin and cysteine residues. This assay will enable the isolation of specific cysteine residues that are important for channel function.

In order to determine which intracellular cysteines in the α and β ENaC subunits are modified by MTSEA-biotin, a series of site-directed cysteine substitutions were performed on the N- and C-termini of each ENaC subunit. Figure 27 shows the localization of the native cysteines on the three α, β and γ ENaC subunits that can be potentially accessible to intracellular MTSEA-biotin, *i.e.* cysteines located in the N- and C-termini and in the transmembrane domains (TM1 & TM2) of the subunits. Some cysteines are conserved between the subunits: αC88, βC30 and γC33; αC101 and βC43; and βC534 and γC546.
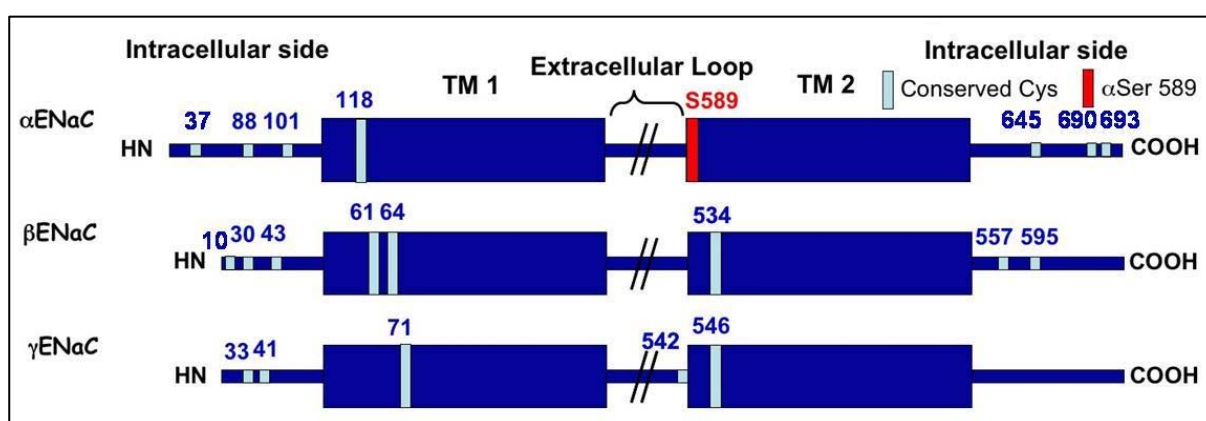
Figure 27: Schematic representation of the three α, β and γ ENaC subunits with the putative native cysteines accessible to intracellularly-applied MTSEA-biotin. HN and COOH represent respectively the amino- and the carboxyl-termini of the subunits; TM1 & TM2 are two transmembrane domains; and the extracellular loop is not represented here. The conserved intracellular native cysteines are in light blue and the selectivity filter αSer589 has been indicated in red.

We first substituted all the intracellular cysteines in the N- and C-termini of αβγ ENaC subunits and tested the functionality of this "Int_ΔCys" mutant of ENaC in TEV (Figure 28). All the cysteines were mutated either by site-directed substitution or by deletion. Deletion was performed on the C-terminus of the α subunit either on Arg618 (R618Stop) or Pro646 (P646Stop). Compared to oocytes expressing αβγ ENaC (left panel), the Int_ΔCys mutant

channel (rαC37S-C88A-C101A-R618Stop, βC10G-C30A-C43A-C61S-C64S-C557S-C595S, γC33A-C41A-C71S, right panel) did not present any inward sodium current when amiloride was removed.
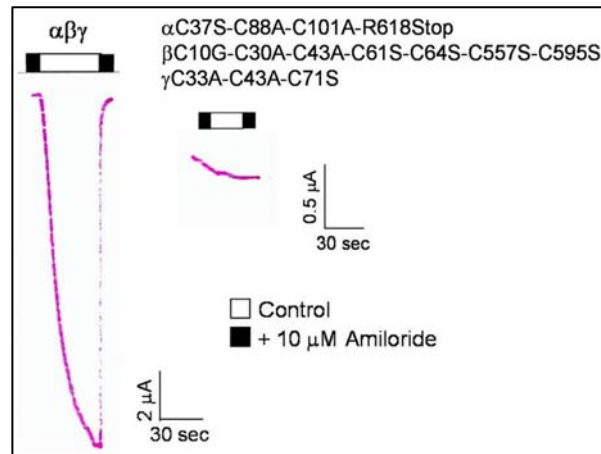
Figure 28: Functional test of ENaC wild-type and Int_ΔCys mutant: αC37S-C88A-C101A-R618Stop, βC10G-C30A-C43A-C61S-C64S-C557S-C595S, γC33A-C41A-C71S. Representative inward sodium current generated by ENaC wild-type was measured by TEV experiments.

The absence of amiloride-sensitive sodium current observed for the Int_ΔCys mutant channel can be potentially explained either by an insensitivity of the channel to amiloride, a channel loss of function, or a decrease in the surface expression or in the protein synthesis. We first checked at the surface expression of the Int_ΔCys mutant channel by a surface biotinylation with 1 mM extracellular Sulfo-NHS-SS-Biotin (see methods) performed on oocytes expressing either the wild-type or the Int_ΔCys mutant channel (Figure 29).
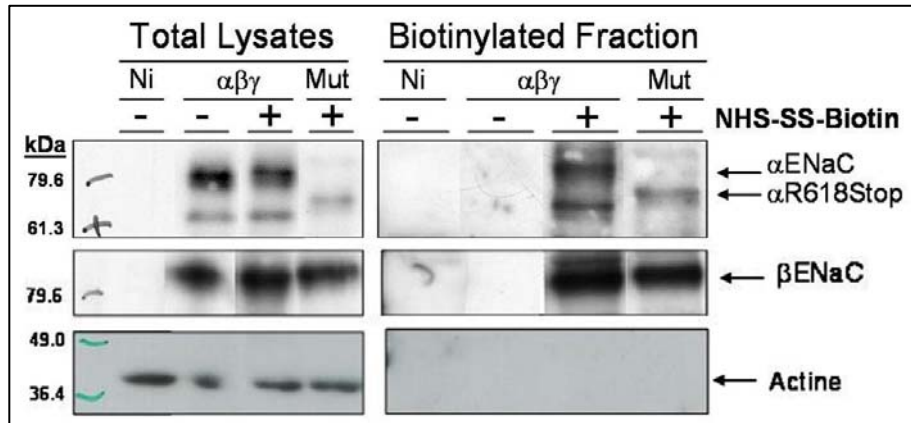
Figure 29: Study of the ENaC Int_ΔCys mutated α and β subunits surface expression. Surface NHS-SS-biotinylation of oocytes injected with ENaC wild-type or Int_ΔCys mutant (αC37S-C88A-C101A-R618Stop, βC10G-C30A-C43A-C61S-C64S-C557S-C595S, γC33A-C41A-C71S, 'Mut'). (n=40 oocytes per condition)

In the total lysates (Figure 29, left panel), we observed two bands for the α wild-type subunit, the full-length α subunit (95 kDa), and a lower signal around 70 kDa that likely corresponded to the amino fragment of the α subunit obtained after proteolysis by serine protease (proteolytic sites located in the pre-M2 domain (101)). Oocytes expressing the Int_ΔCys mutant channel (Mut) showed a signal for the α mutated subunit that had a lower apparent molecular weight than the full-length α subunit and also a 80 % lower signal of abundance compared with the wild-type α subunit. The lower apparent molecular weight was potentially due to the deletion of the C-terminal region of the α subunit in the Int_ΔCys mutant channel (αR618Stop). The lower signal intensity of the α mutated subunit underlines a weaker total expression of the α subunit. It is likely that deletion of the C-terminus led to the instability of the RNA or that mutation of all the native cysteines in the α subunit led to a decrease in the synthesis of the α mutated subunit and/or to its rapid degradation. In the biotinylated fraction of proteins (Figure 29, right panel), *i.e.* proteins expressed at the plasmatic membrane, oocytes expressing wild-type ENaC and incubated with extracellular NHS-SS-Biotin presented two bands of biotinylated α subunit, the full-length and the likely proteolysed subunit outlined

above. Oocytes not treated with extracellular NHS-SS-Biotin were used as a negative control for specific biotinylated signal. Oocytes expressing the Int_ΔCys mutant channel (Mut) and incubated with extracellular NHS-SS-Biotin also contained a biotinylated α subunit, as observed in the total lysates, with the similar lower apparent molecular weight due to the C-terminus deletion and 40 % lower signal of abundance compared with the biotinylated wild-type α subunit. It seems that a major fraction of the mutated α subunits present in the total lysates was expressed at the surface membrane. With respect to the β subunit, the wild-type β subunit and the Int_ΔCys β subunit were expressed equally in the total lysates (left panel). In the biotinylated fraction, oocytes incubated with extracellular NHS-SS-Biotin also showed a similar specific signal of biotinylated wild-type and Int_ΔCys β subunits. Neither the total protein expression nor the surface expression of the β subunit seemed to be influenced by the substitution of the intracellular cysteines in the β subunit. The actin (42kDa) control allowed the possible presence of cytosolic proteins in the biotinylated fraction to be excluded.

To investigate whether substitutions of the intracellular cysteines in ENaC subunits are able to abolish the binding of MTSEA-biotin to α and β subunits, we performed internal perfusion of MTSEA-biotin in oocytes expressing αβγ ENaC or the Int_ΔCys mutant channel rαC37S-C88A-C101A-C118S-P646Stop, βC10G-C30A-C43A-C61S-C64S-C534S-C557S-C595S, γC33A-C41A-C71S (Mutant). In this experiment, we used the αPro646 deletion instead of αArg618, since it showed a higher level of expression. The Int_ΔCys mutant channels, either with mutation αR618Stop or αP646Stop, were not functional. After intracellular perfusion of MTSEA-biotin, oocytes expressing the wild-type or the Int_ΔCys mutant channel were retained and, as before, proteins were incubated with streptavidin beads and the ENaC subunits were studied by western blot (Figure 30). Results showed that, in the total lysates, the wild-type and

the Int_ΔCys (Mutant, containing the αPro646 deletion) α subunits were similarly expressed in contrast to the decreased expression of the mutated subunit containing the mutation αArg618Stop. It is likely the 28 C-terminal amino acids of the α subunit were necessary for the efficient expression of the α mutated subunit. The deletion of the C-terminus αP646Stop led to a decrease in the apparent molecular weight of the α mutated subunit. The expression of the wild-type and Int_ΔCys mutated (Mutant) β subunits were similar irrespective of the mutation. Analysis of the biotinylated fraction (right panel) showed there was a strong decrease in expression of the mutated α and β subunits, 90 % and 80 % respectively, compared with the wild-type subunits.
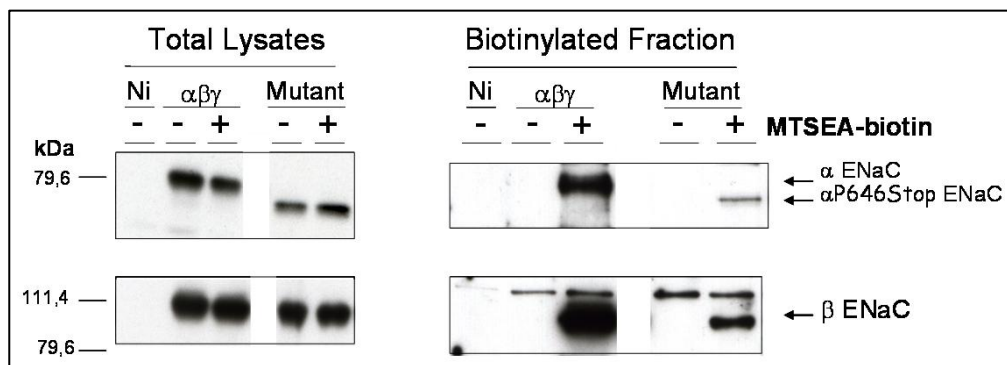
Figure 30: Western Blot analysis of oocytes injected with ENaC wt or Int_ΔCys mutant (αC37S-C88A-C101A-C118S-C645S-P646Stop, βC10G-C30A-C43A-C61S-C64S-C534S-C557S-C595S, γC33A-C41A-C71S, 'Mutant') and perfused with 1 mM intracellular MTSEA-biotin. (n=12 oocytes per condition)

However, despite the substitution of all the putative accessible intracellular cysteines, a small but detectable signal of biotinylated α and β subunits remained. This could be explained by: (i) a non-specific binding of MTSEA-biotin to the subunits, (ii) an indirect binding of MTSEA-biotin to the subunits *via* an accessory protein, (iii) a cysteine located in the extracellular loop but accessible only intracellularly, or (iv) the presence of unbound MTSEA-

biotin during the lysis that modified cysteines not normally accessible when subunits are assembled.

To test the first hypothesis, we performed an intracellular biotinylation with MTSEA-biotin in presence or absence of dithiothreitol (DTT), a reducing agent that disrupts disulfide bonds. We anticipated that addition of DTT would remove the remaining biotinylation of the Int_ΔCys mutant of ENaC (rαC37S-C88A-C101A-C118S-C645S-C690S-C693S, βC10G-C30A-C43A-C61S-C64S-C534S-C557S-C595S, γC33A-C41A-C71S-C542S-C546S). Oocytes perfused with MTSEA-biotin were lysed and proteins were treated or not treated with 10 mM DTT before incubation with streptavidin beads (*cf. Methods 'Pull-Down Assay'*). Biotinylated proteins were then analyzed on western blot (figure 31A). The total lysates (left panel) showed that both α and β subunits, wild-type and Int_ΔCys, were similarly expressed. The biotinylated fraction (right panel) confirmed there was a decrease in biotinylated α and β mutated subunits, compared with wild-type, when all the intracellular cysteines were removed. Quantification of the band intensity of biotinylated subunits showed that removal of all intracellular cysteines on the α subunit led to 70 % decrease of subunit biotinylation and a more pronounced 90 % decrease in subunit biotinylation when all cysteines were removed from the β subunit (Figure 31B, light blue bars). When DTT was added to perfused wild-type oocyte lysates, both α and β antibodies still showed the presence of WT biotinylated subunits, 5 % and 10 % of the DTT-untreated lysates respectively (Figure 31B, $\alpha\beta\gamma$). This DTT-insensitive signal suggests there is perhaps some non-specific biotinylation of the wild-type subunits. When DTT was added to perfused Int_ΔCys mutant channel, we did not observe any detectable signal of biotinylated α and β mutated subunits (Figure 31B, Int_ΔCys). This suggests that a part of the MTSEA-biotin-mediated α and β mutated ENaC subunits biotinylation is DTT-sensitive and thus, linked to cysteine residues.
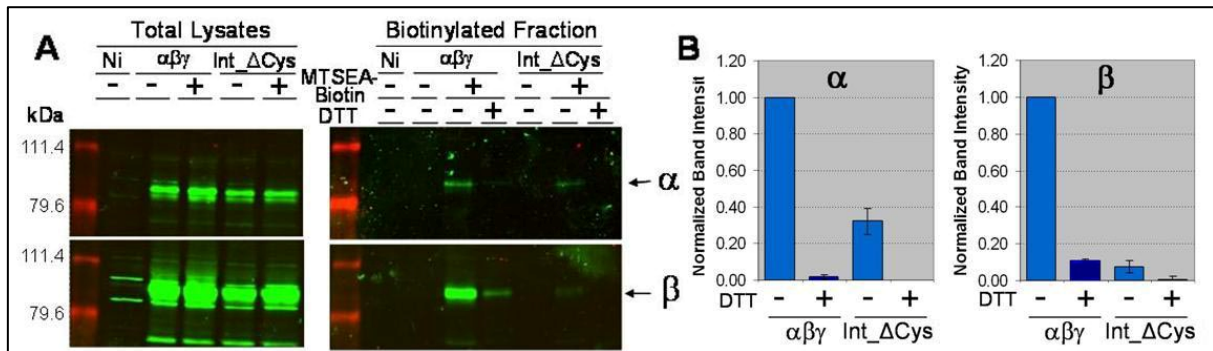
Figure 31: **Study of the DTT-sensitivity of MTSEA-biotin mediated biotinylation of α and β subunits.** (**A**) Western Blot analysis of oocytes injected with ENaC wt or Int_ΔCys mutant (αC37S-C88A-C101A-C118S-C645S-C690S-C693S, βC10G-C30A-C43A-C61S-C64S-C534S-C557S-C595S, γC33A-C41A-C71S-C542S-C546S) and perfused with intracellular MTSEA-biotin. Pull-down assays were performed in presence or not of DTT. (n=12 oocytes per condition) (**B**) For each α and β subunits, we quantified the specific signal of biotinylation obtained for the wild-type channel (αβγ) and the Int_ΔCys mutant channel perfused with MTSEA-biotin and incubated with streptavidin beads with (dark blue, +) or without (light blue, -) DTT. Band intensity was normalized against the intensity obtained for wild-type channel perfused with MTSEA-biotin and incubated with streptavidin beads without DTT. (N=3 Western Blots)

We have shown that the binding of MTSEA-biotin to ENaC subunits occurs effectively *via* disulfide bond with cysteines residues. The Maleimide-PEO$_2$-Biotin is a DTT-insensitive reagent that forms thioether bonds with reduced thiol group of cysteines. We were wondering if ENaC would react in the same way for the two reagents. We performed intracellular perfusion of 1 mM Maleimide-PEO$_2$-Biotin in oocytes expressing either αβγ ENaC or the Int_ΔCys mutant. The effect of Maleimide-PEO$_2$-Biotin on the amiloride-sensitive sodium current is shown in Figure 32. Removal of amiloride led to an increase of the inward sodium current. Then intracellular perfusion of 1 mM Maleimide-PEO$_2$-Biotin induced a 50% inhibition of ENaC activity 2 minutes after the beginning of the perfusion (Figure 32A). The bar graph of the figure 32B shows the sodium current obtained before (t=0) and 2 minutes after (t=2') perfusion of Maleimide-PEO$_2$-Biotin in oocytes expressing αβγ ENaC. Similar to intracellular MTSEA-

biotin (*cf. Figure 22*), we observed that intracellular Maleimide-PEO$_2$-Biotin was able to inhibit ENaC-mediated sodium current.
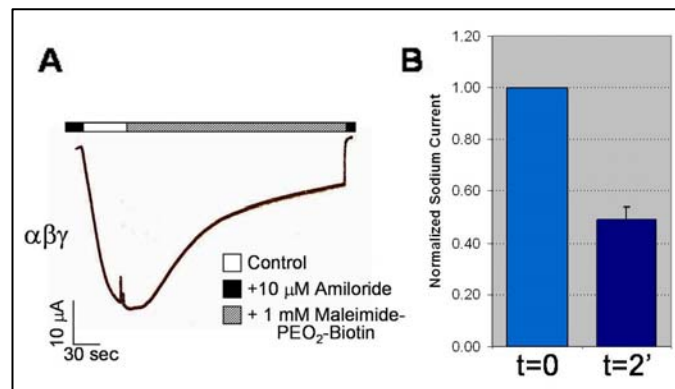
Figure 32: Effect of 1 mM intracellular Maleimide-PEO$_2$-Biotin on ENaC amiloride-sensitive current. (**A**) Effect of 1 mM Maleimide-PEO$_2$-Biotin on wild-type ENaC I$_{Na+}$. (**B**) Bar graph representation of the sodium current obtained before (t=0) and 2 minutes after (t=2') perfusion of 1 mM intracellular Maleimide-PEO$_2$-Biotin. Amiloride-sensitive sodium currents were normalized against current obtained before the perfusion. (n=14 oocytes)

Oocytes perfused with intracellular Maleimide-PEO$_2$-Biotin were analyzed by immunoblotting. The total lysates in the Figure 33A (left panel) showed that wild-type and mutated α and β subunits had similar expression in all conditions of perfusion. In the biotinylated fraction, when intracellular cysteines were substituted (Int_ΔCys), the observed biotinylated α subunit signal was 90 % less intense than the wild-type α subunit. In the case of the β subunit, there was 70 % less Int_ΔCys biotinylated β subunit than wild-type biotinylated β subunit. Specific biotinylated signals were quantified and shown in Figure 33B. As for MTSEA-biotin, there remained a residual biotinylation signal of α and β subunits despite substitution of all the intracellular cysteines on α, β and γ subunits.
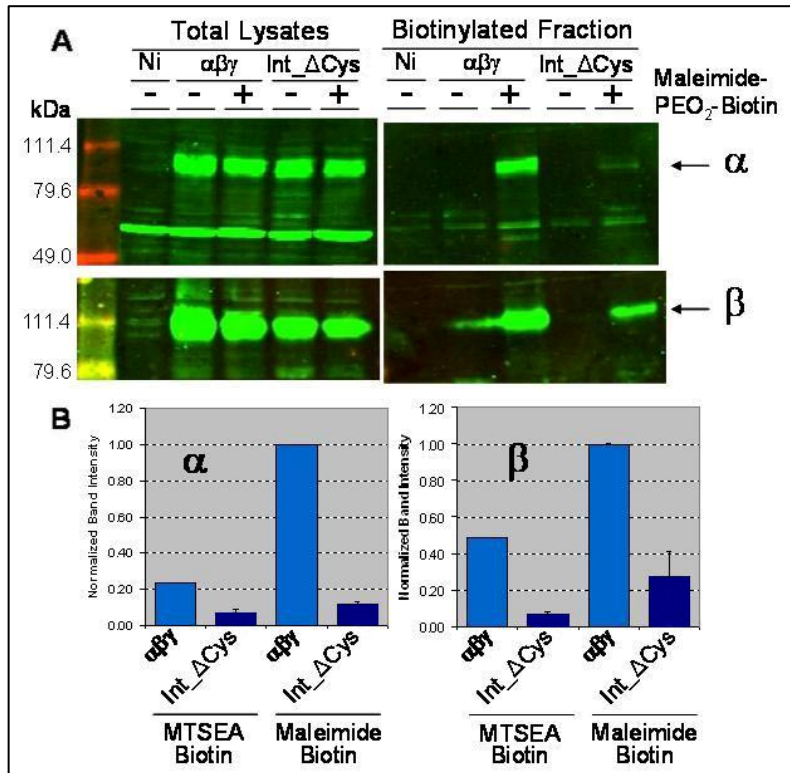
Figure 33: Maleimide-PEO$_2$-Biotin mediated biotinylation of α and β subunits. (**A**) Western Blot analysis of wild-type or Int_ΔCys α and β subunits (αC37S-C88A-C101A-C118S-C645S-C690S-C693S, βC10G-C30A-C43A-C61S-C64S-C534S-C557S-C595S, γC33A-C41A-C71S-C542S-C546S) biotinylated by Maleimide-PEO$_2$-Biotin (n=12 oocytes per condition). (**B**) Bar graph representation of the specific signal quantification for both α and β subunits on oocytes expressing either the wild-type or Int_ΔCys mutant channel and perfused with 1 mM intracellular MTSEA-biotin or Maleimide-PEO$_2$-Biotin. Band intensities were normalized against the intensity obtained for αβγ Maleimide-PEO$_2$-Biotin perfused oocytes. (N=3 Western Blots)

We wanted to determine which of the intracellular cysteines of ENaC subunits were modified by MTSEA-biotin. The three subunits of ENaC contain 20 native cysteine residues that are potentially accessible from the intracellular side (*cf. Figure 27*). We first focused on the cysteines in the N- and the C-termini. We performed a series of cysteine substitutions on the α, β and γ subunits to obtain two mutants: (i) a cysteine-substituted channel mutant in the N-terminus of the three subunits: αC37S-C88A-C101A, βC10G-C30A-C43A, γC33A-C41A; (ii) and a cysteine-substituted channel mutant in the C-terminus of the three subunits: αC645S-

C690S-C693S, βC557S-C595S, γC542S-C546S. As shown in the figure 34, substitutions of the cysteines in the N-terminus of the three subunits (Nter_ΔCys) resulted in an 80 % loss of sodium current compared with the wild-type sodium current. Meanwhile, substitutions in the C-terminus (Cter_ΔCys) caused a 95 % loss of sodium current compared with the wild-type sodium current.
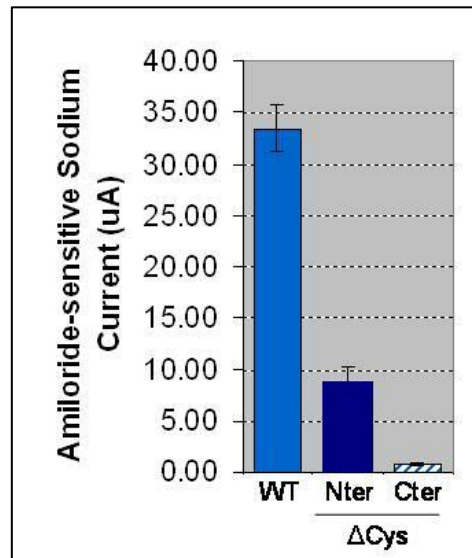
Figure 34: Functional test of the N-terminus and C-terminus ΔCys mutated channels of ENaC. Graphic representation of the amiloride-sensitive sodium current measured by TEV clamp of oocytes expressing ENaC wild-type (WT), N-terminus cysteine-less mutant (αC37S-C88A-C101A, βC10G-C30A-C43A, γC33A-C41A, Nter_ΔCys) and the C-terminus cysteine-less mutant (αC645S-C690S-C693S, βC557S-C595S, γC542S-C546S, Cter_ΔCys) channels. (WT, n=60 oocytes; Nter_ΔCys, n=40 oocytes, Cter_ΔCys, n=10 oocytes)

Oocytes expressing either wild-type ENaC, or the Nter_ΔCys (αC37S-C88A-C101A, βC10G-C30A-C43A, γC33A-C41A) or the Cter_ΔCys (αC645S-C690S-C693S, βC557S-C595S, γC542S-C546S) mutant channels were perfused with 1 mM intracellular MTSEA-biotin. Taking into account the fact that with the cut-open oocyte method the current flowing across only a small fraction (about 10 %) of the oocyte membrane is measured, the level of INa^+ expressed by the N-terminus and the C-terminus cysteine-less mutant channels were too low to

detect in cut-open experiments. Biotinylated proteins isolated from oocytes perfused with MTSEA-biotin were incubated with streptavidin beads. The MTSEA-biotin mediated biotinylation of both mutated α and β subunits was then analyzed on western blot. Since we observed the same pattern of expression for both α and β subunits (data not shown), we focused on the β subunit (Figure 35). As a first step, we performed perfusion of MTSEA-biotin with or without 5 mM free cysteine in oocytes expressing either the ENaC wild-type or the Nter_ΔCys mutant channel (αC37S-C88A-C101A, βC10G-C30A-C43A, γC33A-C41A, Figure 35A). In total lysates (Figure 35A, left panel), the wild-type and the mutated β subunit were expressed at a similar level. In the biotinylated fraction (Figure 35A, right panel), the biotinylated Nter_ΔCys mutated β subunit had 80 % lower signal than the biotinylated wild-type β subunit when oocytes were perfused with MTSEA-biotin alone. Addition of 5 mM free cysteine in the perfusion with MTSEA-biotin led to 90 % decrease of MTSEA-biotin mediated biotinylation of both wild-type and mutated β subunits. There was no detectable signal of biotinylated β subunit when protein lysates were incubated with streptavidin beads in presence of DTT.
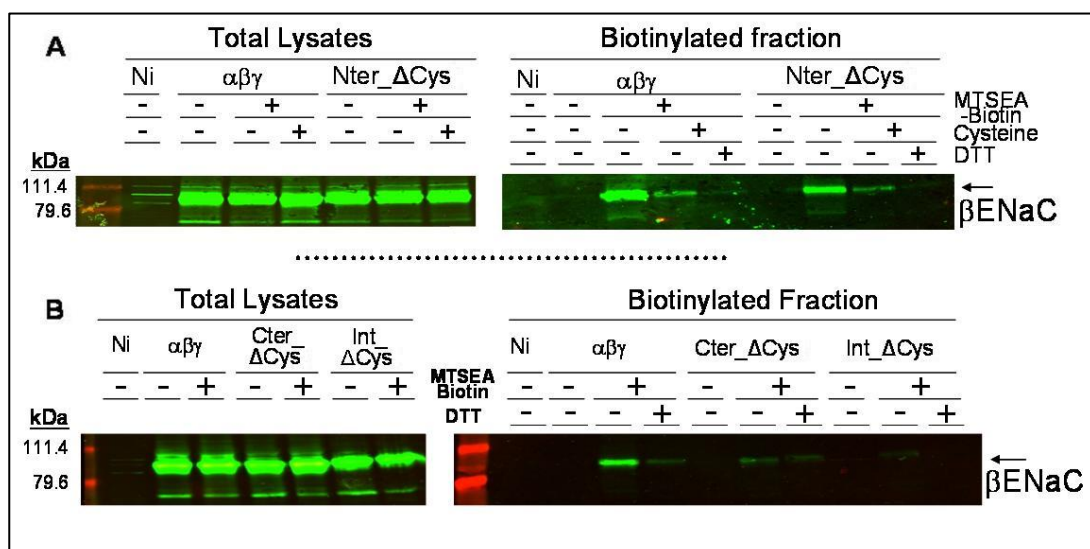
Figure 35: MTSEA-biotin mediated biotinylation of Nter_ΔCys and Cter_ΔCys β subunits. (A) Oocytes expressing either ENaC wild-type or the Nter_ΔCys mutant (αC37S-C88A-C101A, βC10G-C30A-C43A, γC33A-C41A) were perfused with MTSEA-biotin with or without free cysteine and treated or not treated with DTT. (B) Oocytes expressing either

ENaC wild-type, or the Cter_ΔCys mutant (αC645S-C690S-C693S, βC557S-C595S, γC542S-C546S) or the Int_ΔCys mutant (αC37S-C88A-C101A-C118S-C645S-C690S-C693S, βC10G-C30A-C43A-C61S-C64S-C534S-C557S-C595S, γC33A-C41A-C71S-C542S-C546S) were perfused with MTSEA-biotin and treated or not treated with DTT. (n=12 oocytes per condition)

As the second step (Figure 35B), we perfused intracellular MTSEA-biotin in oocytes expressing the wild-type (αβγ), the Cter_ΔCys (αC645S-C690S-C693S, βC557S-C595S, γC542S-C546S) or the Int_ΔCys mutant channel (αC37S-C88A-C101A-C118S-C645S-C690S-C693S, βC10G-C30A-C43A-C61S-C64S-C534S-C557S-C595S, γC33A-C41A-C71S-C542S-C546S). In the total lysates control (left panel), we were able to demonstrate that the β subunit was expressed at a similar level in all conditions. In the biotinylated fraction (right panel), we observed a 80 % and 95 % decrease, respectively, in the biotinylated Cter_ΔCys β subunit and Int_ΔCys β subunit signals compared with the biotinylated wild-type β subunit. A residual biotinylated signal remained for the β wild-type and Cter_ΔCys subunits, even when lysates were treated with DTT. The residual signal almost disappeared in the Int_ΔCys mutated subunit. The graph as part of Figure 36 showed the quantification of the specific signal obtained from different experiments with the anti-β antibody for MTSEA-biotin-mediated β subunit biotinylation. Results showed that substitutions of cysteines in either the N-terminus or the C-terminus led to an average of 50 % decrease of MTSEA-biotin-mediated mutated β subunit biotinylation. Thus, cysteines in the N-terminal and C-terminal regions of ENaC contributed to MTSEA-biotin binding. Furthermore, cysteines in the N-terminal region of the β subunit are likely to be accessible to intracellular MTSEA-biotin to a similar degree as the cysteines in the C-terminal region of the β subunit. Removal of all the intracellular cysteines of the β subunit led to an 80 % decrease of the MTSEA-biotin mediated β subunit biotinylation. Highlighted on the graph is the DTT-insensitive signal of MTSEA-biotin mediated β subunit biotinylation (striped

bars) underlying the presence of a low non-specific biotinylation of the β subunit by MTSEA-biotin.
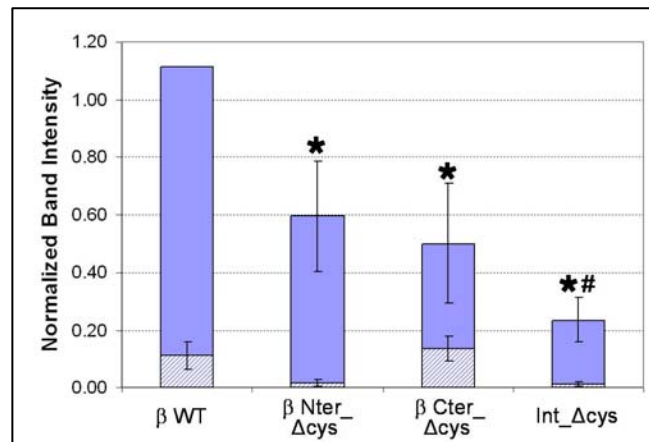
Figure 36: Normalized band intensity of the MTSEA-biotin-mediated β subunit biotinylation. Oocytes were injected with wild-type (β WT, N=11) or Nter_ΔCys mutated (αC37S-C88A-C101A, βC10G-C30A-C43A, γC33A-C41A, N=3), Cter_ΔCys mutated (αC645S-C690S-C693S, βC557S-C595S, γ, N=2) or Int_ΔCys mutated (αC37S-C88A-C101A-C118S-C645S-C690S-C693S, βC10G-C30A-C43A-C61S-C64S-C534S-C557S-C595S, γC33A-C41A-C71S-C542S-C546S, N=7) ENaC subunits and perfused with MTSEA-biotin. Band intensities of biotinylated β subunit were quantified and normalized against the specific intensity obtained for β WT subunit. Empty bars correspond to signal obtained with protein lysates pulled down without DTT (specific signal), striped bars correspond to protein lysates pulled down in presence of DTT (non-specific signal). ✱, $p < 0.001$ compared to βWT, #, $p < 0.05$ compared to β Nter_ΔCys.

Altogether, our data showed that (i) MTSEA-biotin binds to cysteine residues in the N- and the C-termini of ENaC. Substitution of these cysteines leads to channels almost non functional. These residues are thus accessible and important for the channel function. (ii) It is likely that ENaC inhibition is due to direct interaction of MTSEA-biotin with cysteine residues in the N- and C-termini. (iii) The residual biotinylation of the Int_ΔCys mutated subunits is non-specific and might be due to an indirect interaction with cysteines in an ENaC-associated protein.

II-1-iii) *Cross-linking experiments*

In order to identify potential ENaC associated proteins, we performed in cut-open oocytes cross-linking experiments with two different bismaleimide cross-linkers and an oxidizing reagent (*see details in 'Methods'*). Oocytes expressing ENaC wild-type channel were perfused with 1 mM intracellular DTME and amiloride-sensitive sodium current measurement is presented on Figure 37A. A typical recording of ENaC current showed that perfusion of 1 mM DTME resulted in a 60 % inhibition of the sodium current 2 minutes after the beginning of the perfusion (t=2', right panel). When oocytes were perfused with 20 μM BMOE (figure 37B), we observed a 20 % inhibition of ENaC current (t=2', right panel). Formation of disulfide bonds with 10 mM NaTT induced a 70 % inhibition of ENaC current (Figure 37C).
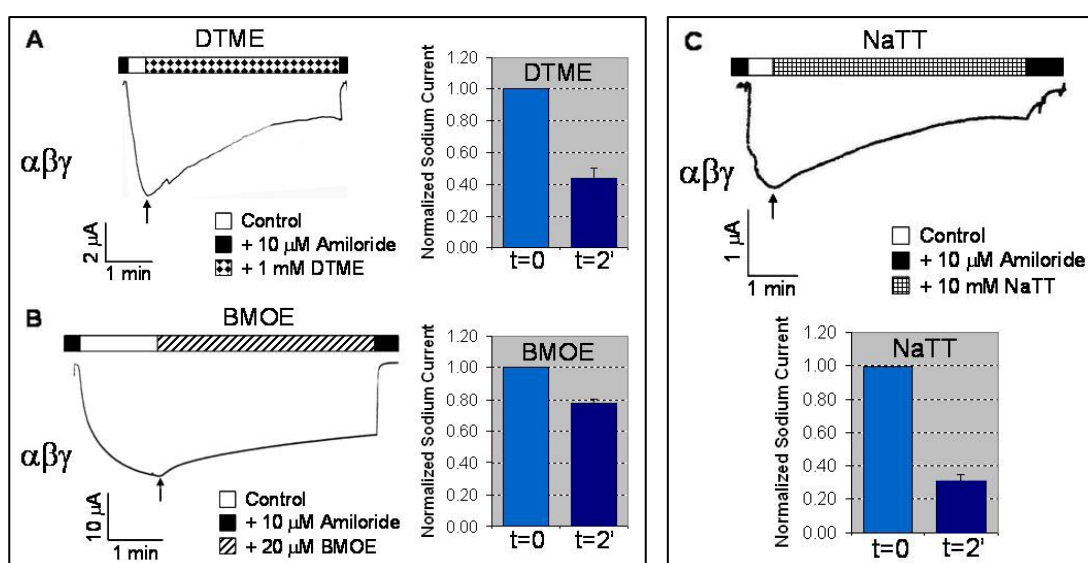
Figure 37: Effect of DTME, BMOE and NaTT cross-linkers on ENaC-mediated sodium current. (**A**) Oocytes expressing ENaC wild-type were perfused with 1 mM DTME. (**B**) Oocytes expressing ENaC wild-type were perfused with 10 μM BMOE. (**C**) Oocytes expressing ENaC wild-type were perfused with 10 mM NaTT. Bar graphs are amiloride-sensitive current normalized with sodium current measured before the perfusion of DTME, BMOE or NaTT. (DTME, n=6 oocytes; BMOE, n=6 oocytes, NaTT, n=6 oocytes)

Oocytes expressing the ENaC wild-type channel and perfused with BMOE were lysed and proteins were separated by SDS-PAGE (Figure 38). Non-injected oocytes (Ni) were used as a negative control for the specificity of the α and β antibodies. Using the α subunit antibody showed only the specific detection of the full-length α subunit and, above all, no difference between oocytes perfused with BMOE and oocytes not perfused with BMOE. In the case of the β antibody, oocytes perfused with BMOE presented specific β subunit full-length signal and a smear of proteins. We could not distinguish another particular band in β detection. Western blot analysis of oocytes perfused with DTME lead to similar pattern (data not shown).
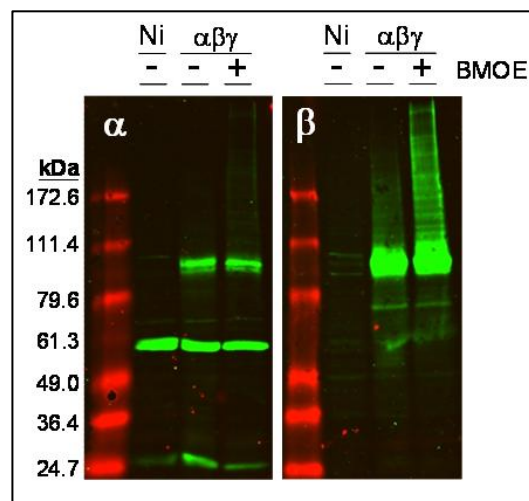
Figure 38: Western Blot analysis of oocytes perfused with intracellular BMOE cross-linker. Specific α subunit detection is show in the left panel and specific β subunit detection in the right panel (n=12 oocytes per condition).

Western blot analysis of oocytes perfused with either 10 mM or 20 mM intracellular NaTT showed a smear of protein's appearance besides the full-length subunit signal (95 kDa) for both α and β subunits. This smear disappeared in the presence of DTT, confirming the involvement of protein interactions *via* disulfide bridges.
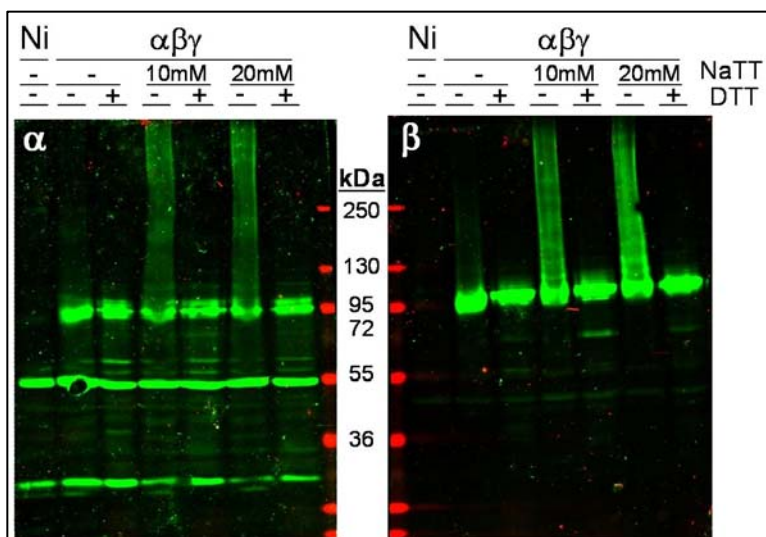
Figure 39: Western Blot analysis of oocytes perfused with intracellular NaTT. Specific antibody detection of the α subunit is show on the left panel and specific β subunit detection on the right panel. (n=12 oocytes per condition)

Taken together, these results suggest that both α and β subunits likely interact with other proteins *via* DTT-sensitive interactions. However, our cross-linking experiments did not allow the determination of the involvement of a specific protein or protein complex with one or two subunits of ENaC.

II-2) **ASIC**

We wanted to compare ENaC with ASIC, another member of ENaC/degenerin family, with respect to the accessibility of the intracellular cysteines to MTSEA reagent and to their role on ASIC activity. Protein sequence alignment of the three αβγ subunits of ENaC with the human and the chicken ASIC1 (Annexe) showed there was 20% homology between ENaC and ASIC1 (70). In hA1a, putative intracellularly-accessible cysteines are located in the first transmembrane domain (TM1): C49, C59 and C61; and in the C-terminus, C466, C471, C497 and C528.
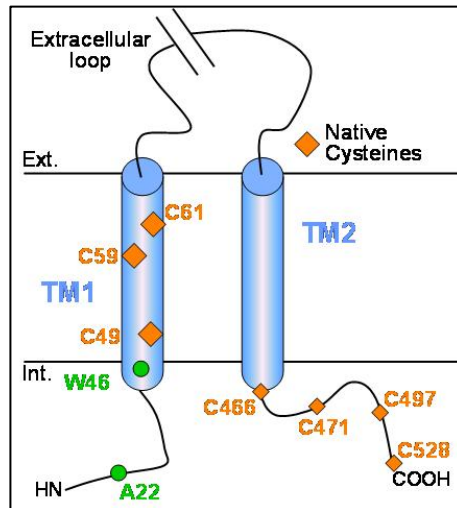
Figure 40: Schematic representation and localization of the putative intracellular cysteines of hA1a. Native cysteines are indicated with an orange diamond. In green are indicated the first and the last amino acids of the hA1a N-terminus that were substituted in cysteine for the cysteine screen.

II-2-i) *MTSEA-biotin effect on hA1a channels*

hA1a is activated by protons with external pH below 6.9 (128) (Figure 41A). A typical sodium current mediated by hA1a wild-type (hA1a-wt) is shown in figure 41B. The base line was obtained at pH 7.4. Acidification of the external medium (↓, pH 6.0) on oocytes expressing hA1a-wt led to an increase of inward sodium current, which was detected using the TEV. For all experiments, two to three acidifications of the medium, at intervals of 40 seconds, were performed on each oocyte (Figure 41B). Compared to the wild-type channel, the channel mutated in the C-terminal cysteines, hA1a-C466A-C471A-C497A-C528Stop (Cter_ΔCys), generates about 50% of the wild-type sodium current (Figure 41C).
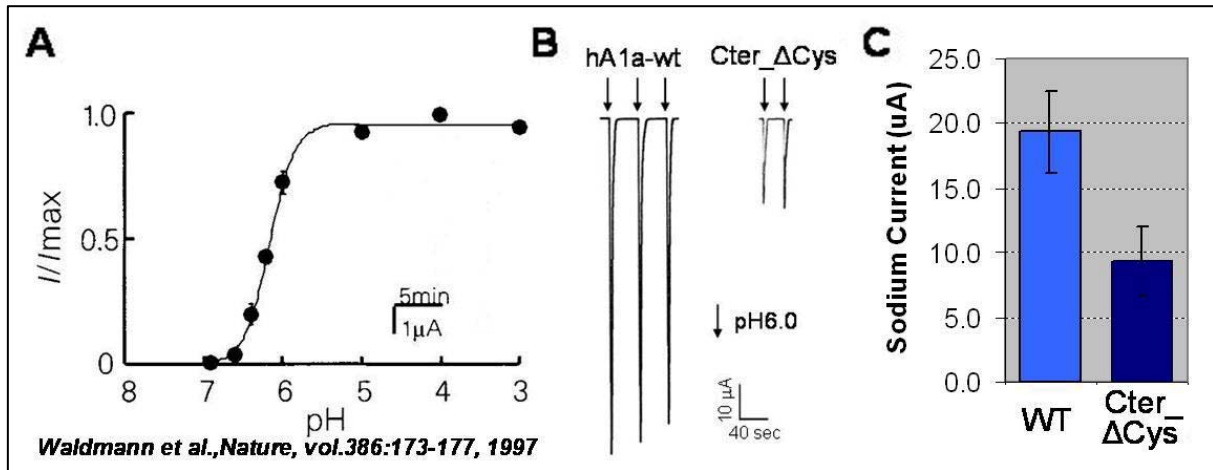
Figure 41: hA1a channel pH activation (**A**) Dose-response curve of hA1a-wt for the extracellular pH from Waldmann *et al.* (128) (**B**) Representative sodium currents of the wild-type (hA1a-wt) and C-terminal cysteines mutant (Cter_ΔCys) hA1a, measured by TEV. Application of acidic pH is indicated with an arrow (↓). (**C**) Mean sodium current obtained for oocytes expressing hA1a-wt or Cter_ΔCys. (wt, N=26; Cter_ΔCys, N=5)

Oocytes expressing hA1a-wt or Cter_ΔCys channel were perfused with 1 mM intracellular MTSEA-biotin and Figure 42A (left panel) shows that acidification of the pH during the intracellular MTSEA-biotin perfusion inhibited only 5 % (p=0.0082) of the hA1a wild-type (hA1a-WT) mediated sodium current. When oocytes expressing the Cter_ΔCys channel were perfused with intracellular MTSEA-biotin, we observed a 20 % increase (p=0.0178) in the amplitude of sodium current generated by the Cter_ΔCys channel. Quantification of the sodium currents obtained before (t=0) and 2 minutes after (t=2') perfusion of MTSEA-biotin are shown in the Figure 42B.
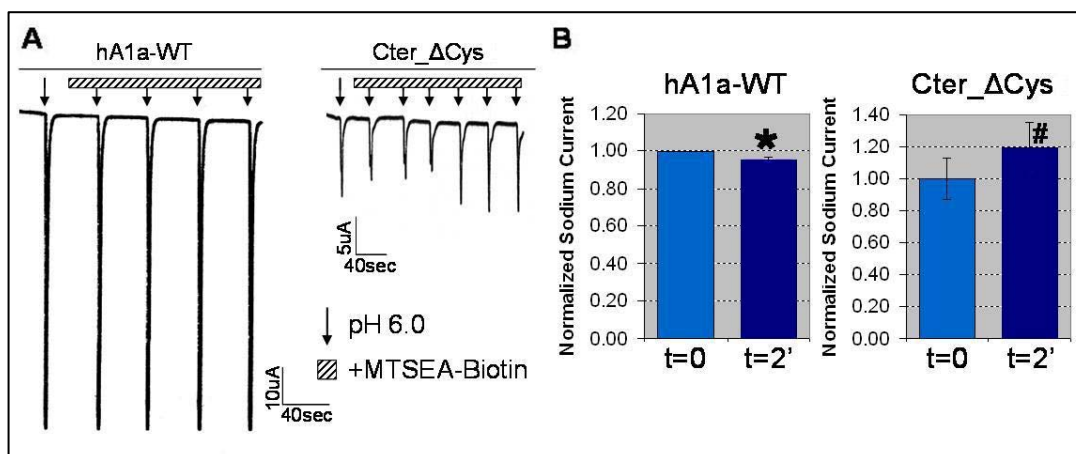
Figure 42: Effect of MTSEA-biotin on hA1a-wt and Cter_ΔCys sodium currents. (**A**) Representative sodium current of hA1a-wt and Cter_ΔCys channels in presence of 1 mM intracellular MTSEA-biotin. The time of application of acidic pH is indicated with an arrow (↓). (**B**) Bar graph representation of the sodium current obtained before (t=0) and 2 minutes after (t=2') perfusion of 1 mM intracellular MTSEA-biotin. Sodium currents were normalized with current obtained before the perfusion (WT, N=6; Cter_ΔCys, N=43). ✱, $p < 0.01$ and #, $p < 0.05$ compared to t=0 respective sodium current.

Oocytes expressing hA1a-WT or Cter_ΔCys channel and perfused with intracellular MTSEA-biotin for current measurements were then lysed and proteins were incubated with streptavidin beads and analyzed by western blot with specific antibody against the hA1 subunit (Figure 43A). Total protein lysates (left panel) showed that hA1a wild-type and Cter_ΔCys subunits were similarly expressed. The biotinylated fraction (right panel) showed a specific biotinylated hA1 wild-type signal when oocytes were perfused with intracellular MTSEA-biotin. Thus, the accessibility of the C-terminus cysteines of hA1a correlated with the accessibility of the C-terminus cysteines of ENaC. However, modification of cysteine residues on hA1a C-terminus does not change ASIC activity (*see figure 42*). When cysteines in the C-terminus of hA1a are substituted (Cter_ΔCys), we observe a 90 % loss of MTSEA-biotin mediated biotinylation of hA1 subunit. Average quantification of biotinylated hA1a for three experiments is shown figure 43B. However, biotinylated subunits were still present despite the C-terminus cysteines substitutions. This remaining biotinylation was DTT-sensitive, suggesting

the involvement of other cysteines possibly in the TM1 that are potentially accessible with intracellular sulfhydryl reagents or non-specific binding. Thus, MTSEA-biotin binds to cysteine residues in the C-terminus of hA1a but do not inhibit the channel.
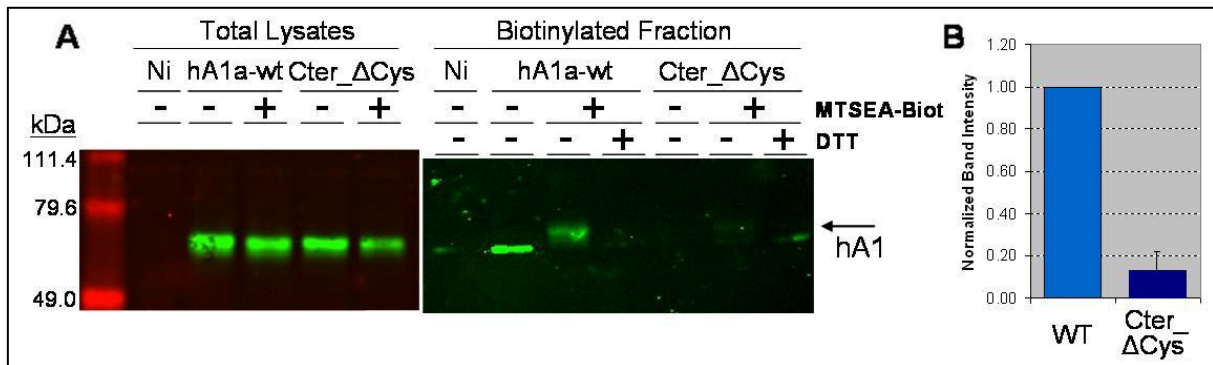
Figure 43: **MTSEA-biotin mediated biotinylation of hA1a-wt and Cter_ΔCys subunits. (A)** Western blots anti-hA1 on oocytes expressing either hA1a-wt or Cter_ΔCys and perfused or not perfused with 1 mM MTSEA-biotin. Pull-down assays on perfused oocytes were performed with or without DTT. (n=12 oocytes per condition) **(B)** Mean band intensities of MTSEA-biotin mediated biotinylation of hA1a-WT and Cter_ΔCys subunits were quantified with Odyssey[®] software. Band intensities were normalized against the wild-type signal. (N=3)

As for ENaC, we tested the effect of Maleimide-PEO$_2$-Biotin on hA1a channel mediated sodium current. Oocytes expressing hA1a wild-type or Cter_ΔCys channel were perfused with 1 mM intracellular Maleimide-PEO$_2$-Biotin (Figure 44) and sodium currents were measured by cut-open. Perfusion of intracellular Maleimide-PEO$_2$-Biotin did not have a great influence on hA1a wild-type current (Figure 44A). Average quantification of sodium current generated after 2 min of intracellular Maleimide-PEO$_2$-Biotin perfusion showed a significant 20 % inhibition of hA1a current (Figure 44B). In contrast, Cter_ΔCys mediated sodium current was not significantly inhibited by Maleimide-PEO$_2$-Biotin (Figure 44B).
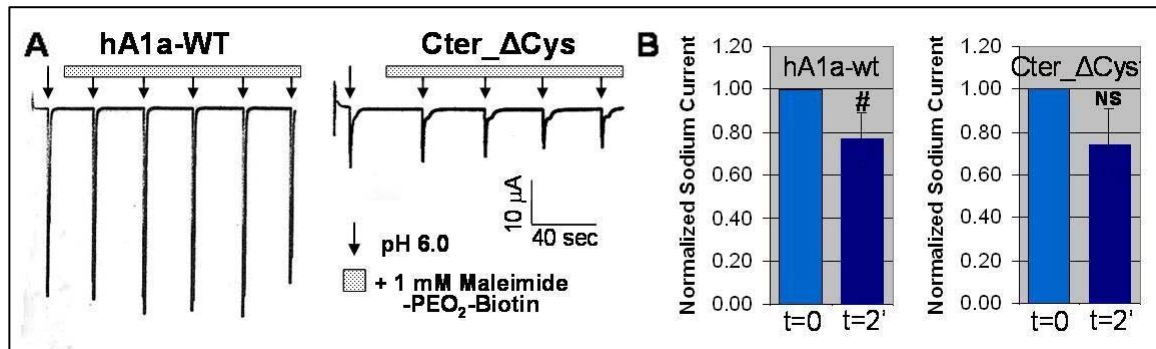
Figure 44: **Effect of Maleimide-PEO$_2$-Biotin on hA1a-wt and Cter_ΔCys currents.** (**A**) Oocytes expressing hA1a wild-type (hA1a-WT) or Cter_ΔCys channel were continuously perfused with 1 mM intracellular Maleimide-PEO$_2$-Biotin and activated with pH 6.0 external solution (↓). (**B**) Bar graphs sum sodium currents generated by the wild-type (hA1a-WT) and the Cter_ΔCys channel and measured before (t=0) and after 2 minutes (t=2') perfusion with Maleimide-PEO$_2$-biotin. (hA1a-WT, N=5; Cter_ΔCys, N=4) #, $p<0.05$ compared to t=0; NS, $p>0.05$ compared to t=0.

Oocytes perfused with Maleimide-PEO$_2$-Biotin were lysed and proteins were incubated with streptavidin beads. The western blot is shown on Figure 45. Total protein lysates (left panel) showed that wild-type and Cter_ΔCys hA1a subunits were similarly expressed in all conditions. In the biotinylated fraction (right panel), oocytes expressing the wild-type channel (hA1a-WT) presented a specific biotinylated full-length hA1 subunit signal. When oocytes expressing the Cter_ΔCys were perfused with Maleimide-PEO$_2$-Biotin, the specific hA1 signal was 80 % weaker than that of the wild-type subunit. These results confirm data obtained with MTSEA-biotin (*cf. Figure 43*).
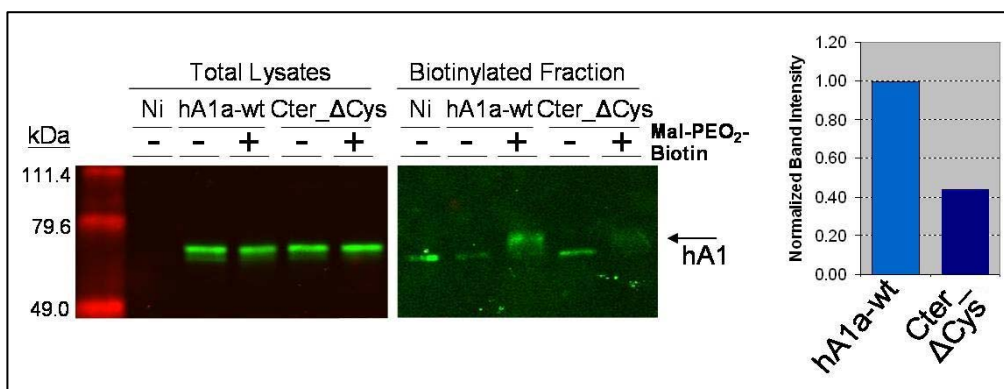
Figure 45: Binding of Maleimide-PEO$_2$-Biotin to hA1a-wt and Cter_ΔCys subunits. Western blots anti-hA1 on oocytes expressing either hA1a-wt or Cter_ΔCys and perfused or not perfused with 1 mM intracellular Maleimide-PEO$_2$-Biotin. Average quantification of MTSEA-biotin mediated biotinylation of hA1a-WT and Cter_ΔCys subunits. Band intensities were normalized with the wild-type signal. (n=12 oocytes per condition)

Similar to ENaC, cysteines located in the C-terminal region of hA1a are accessible to MTSEA-biotin, and also to Maleimide-PEO$_2$-Biotin. However, although direct modification of C-terminal cysteines in ENaC inhibits the channel, the modification of cysteines in the C-terminal part of hA1a does not change ASIC activity. For both channels, substitution of all potential intracellular cysteines did not prevent the biotinylation of the subunits. Since in hA1a, in contrast to ENaC, this residual binding was DTT-sensitive, it would seem that other cysteines residues are involved and potentially those in TM1 are also accessible to MTSEA-biotin.

II-2ii) *N-terminus cysteine-screen substitution*

We have tested whether our biotinylation assay could be used to identify accessible residues to intracellular ligands. The figure 46 shows a sequence alignment of a part of the N-terminus of the three ENaC subunits, α, β, γ, with the chicken and the human ASIC1 subunits. It has been previously shown that substitution of the HG motif or of the residue histidine at position 32 in hA1a lead to non-functional channels (★ Figure 46; (45)). Functional analysis of a series of cysteine substitutions in the N-terminus of hA1a showed that substitutions of the

amino acids Thr26, Ser35, Glu37 and Trp46 in cysteine lead to a complete loss of function of the mutated channel (✖ Figure 46; (95)). Among the functional mutated channels, five distinctive hA1a mutants generated sodium currents that were inhibited by intracellular MTSET (✓ Figure 46, (95)): A22C, I33C, F34C, R38C and R43C. We focused particularly on the sensitivity of the A22C mutant, since the residue hA1a-Ala22 corresponds to a strongly conserved cysteine residue in all three ENaC subunits (rαC88, rβC30 and rγC33). We used these cysteine-substituted mutants, from hA1a-A22C to hA1a-W46C (● Figure 46), to study the MTSEA-biotin intracellular accessibility.

Figure 46: Sequence alignment of the amino terminus and the beginning of the TM1 of the three αβγ ENaC subunits and chicken and human ASIC1 subunits. All marks are explained in the text.

We subcloned each N-terminal cysteine substitution in the background of the C-terminal cysteine-less: hA1a-C466A-C471A-C497A-C528Stop (Cter_ΔCys) and measured their activity on intact oocytes in TEV clamp experiments (Figure 47).

Figure 47: Inward sodium currents of hA1a mutants. Summary of the sodium currents generated by the cysteine-substituted mutant channels in the background Cter_ΔCys. Each mutated channel is annotated as the corresponding N-terminus cysteine substitution, *i.e.* "A22C" means "hA1a-A22C-C466A-C471A-C497A-C528Stop". Dark blue bars indicate sodium current closed to hA1a wild-type (WT) current and striped blue bars, sodium currents closed to zero. (n=4 oocytes per mutated channel; *, p<0.05; **, p<0.01; ***, p<0.001 Student t-test compared to WT current)

In accordance with a previous study (95), the three mutants T26C, E37C and W46C in the background Cter_ΔCys generated almost no sodium current (Figure 47, striped blue bars), despite having a total protein abundance similar to that of the wild-type subunit expression (data not show). Six mutated channels (L39C, S40C, L41C, K42C, A44C and L45C in the background Cter_ΔCys) generated sodium currents that were of either equal or higher intensity to the wild-type channel (dark blue bars). The other mutated channels generated various decreases in the intensity of the sodium current but were still functional allowing testing the effect of intracellular MTSEA-biotin. We first performed the experiments on the mutated channel hA1a-A22C-C466A-C471A-C497A-C528Stop (A22C). Figure 48A shows the effect of intracellular MTSEA-biotin on current generated by the mutant A22C in the background

Cter_ΔCys. Acidification of external medium led to the generation of inward sodium current that was 60 % inhibited after 2 min of perfusion with 1 mM intracellular MTSEA-biotin. Oocytes expressing hA1a wild-type (hA1a-WT), the Cter_ΔCys or the mutated hA1a-A22C-C466A-C471A-C497A-C528Stop (A22C) channel and perfused with 1 mM intracellular MTSEA-biotin were used in pull-down assays to analyzed the binding of MTSEA-biotin on hA1a subunits. In the western blot, the biotinylated fraction showed a specific signal corresponding to the biotinylated hA1a wild-type subunit (figure 48B). When cysteines in the C-terminus were substituted (Cter_ΔCys), we observed a 90 % signal decrease of the biotinylated subunit as previously shown. Addition of the A22C mutation in the background Cter_ΔCys induced a 50 % recovery of the subunit biotinylation signal. Thus, we can conclude that A22C is accessible to intracellular MTSEA-biotin and nicely correlated with inhibition of ASIC activity. This validates our biotinylation assay to identify accessible amino acids in the N-terminal part of ASIC.

Figure 48: Effect of intracellular MTSEA-biotin on the mutant hA1a-A22C-C466A-C471A-C497A-C528Stop. (**A**) Representative sodium current generated by the mutated channel hA1a-A22C-C466A-C471A-C497A-C528Stop in presence of 1 mM intracellular MTSEA-biotin. (n=26 oocytes) (**B**) Western Blot analysis of the effect of MTSEA-biotin on the hA1a-A22C-C466A-C471A-C497A-C528Stop (A22C) subunit compared with the wild-type (hA1a WT) and the Cter_ΔCys subunits. (Western Blot: 12 oocytes per condition; Graph: hA1a, N=3; Cter_ΔCys, N=6; A22C, N=7)

We thus obtained three controls for the binding of MTSEA-biotin: (i) MTSEA-biotin biotinylates the hA1a wild-type subunit (WT) but has no effect on the WT sodium current; (ii) MTSEA-biotin does not biotinylate the Cter_ΔCys subunit and has no effect on the Cter_ΔCys sodium current; (iii) MTSEA-biotin biotinylates the mutated subunit hA1a-A22C-C466A-C471A-C497A-C528Stop ('A22C') and inhibits the generated sodium current. This allows us to identify intracellular accessible sites to MTS reagents and functional domains in the N- and the C-termini of hA1a involved in the MTS intracellular inhibition of the channel.

We extended this experiment to include the other N-terminal cysteine-substituted mutants (from S23C to W46C) generated in the Cter_ΔCys background. Mutant channels were perfused with intracellular MTSEA-biotin using the cut-open technique. These oocytes were kept for determination of biotinylation of hA1a channel mutants. For each channel mutant, the sodium current obtained 2 minutes after addition of 1 mM intracellular MTSEA-biotin was normalized to the current obtained before addition of MTSEA-biotin. Mutated channels T26C, E37C and W46C in the background of Cter_ΔCys were considered non-functional (NF) since they do not generated usable sodium currents for the study of the electrophysiological effects of MTSEA-biotin (*cf. Figure 47*). However they were also perfused and retained for analysis by western blot. Data showed that some mutated channels were not inhibited by MTSEA-biotin after 2 minutes of perfusion (Figure 49, dark blue bars). These included the wild-type (WT) and the C-terminus cysteine-less channels (Cter_ΔCys), as previously shown, as well as the L27C, L30C, S35C, Y36C, S40C and A44C in the background Cter_ΔCys mutants. Student's t-test performed on the other channels (light blue bars) indicated that only seven mutated channels were significantly inhibited by 2 minutes of intracellular MTSEA-biotin perfusion. Six of the mutated channels lost approximately half of their current after two minutes of perfusion: the hA1a-A22C (p=0.0001): 60 % of inhibition; hA1a-F34C (p=1.14.10^{-5}), hA1a-R38C (p=0.0045), hA1a-

K42C (p=0.0013), hA1a-R43C (p=0.0326), hA1a-L45C (p=0.0002): 50 % of inhibition. The mutant hA1a-I33C in the background Cter_ΔCys (I33C) was 95% inhibited by intracellular MTSEA-biotin treatment (p=$6.5.10^{-10}$). The residue Ile 33 is highly conserved among both ENaC and ASIC protein sequences and would therefore seem to play an important role in the function of these channels.
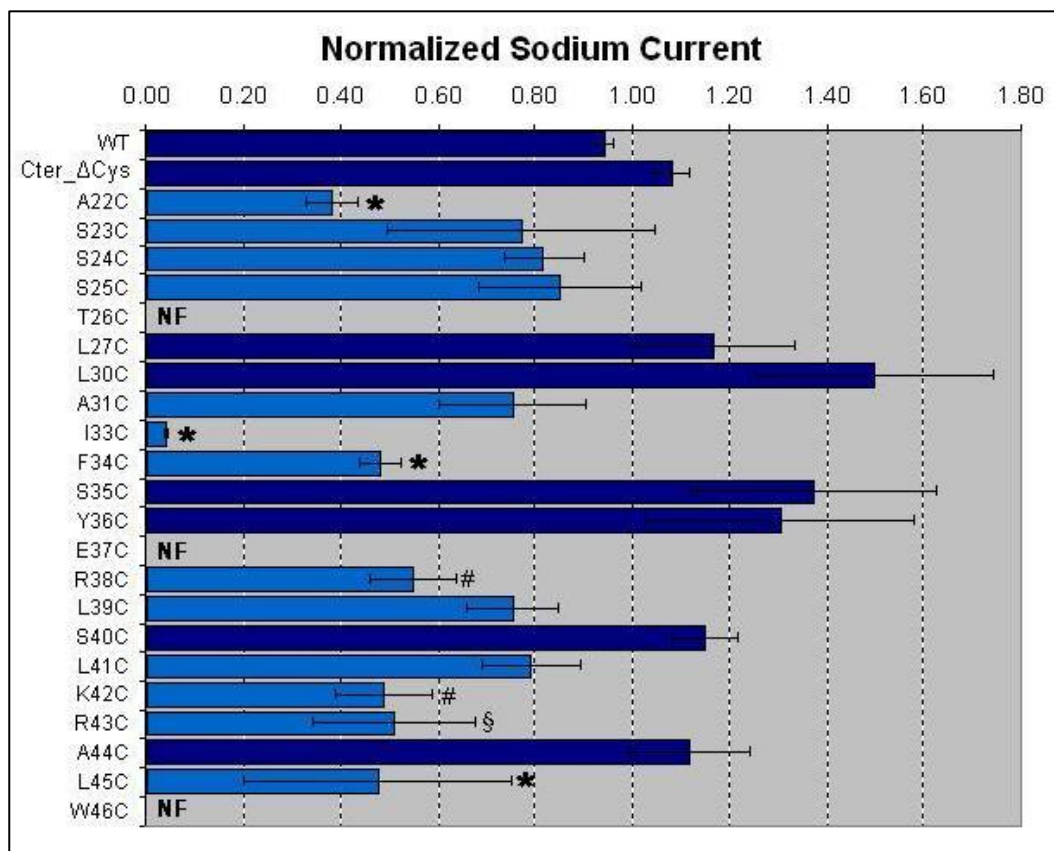
Figure 49: Normalized sodium current measured 2 minutes after addition of 1 mM intracellular MTSEA-biotin for each N-terminus cysteine-substituted in the background Cter_ΔCys channel. Each mutated channel is annotated as the corresponding N-terminus cysteine substitution in a Cter_ΔCys background, *i.e.* A22C means hA1a-A22C-C466A-C471A-C497A-C528Stop. Sodium currents were normalized with current obtained before the addition of intracellular MTSEA-biotin. Dark blue bars indicated MTSEA-biotin non-sensitive currents and light blue bars, sensitive currents. ×, non-functional channel. ✱, p<0.001; #, p<0.01; §, p<0.05 Student test compared to hA1a-WT sodium current obtained 2 min after MTSEA-biotin perfusion. (6 < n < 12 oocytes per mutated channel)

We have analyzed the biotinylation of hA1a mutants with cysteine substitutions at position A22 to E37, L39, L41 and R43. Specific hA1 biotinylation signals were obtained by immunoblotting and quantified using the signal obtained for the hA1a wild-type subunit for normalization. On the left of the table are the results from figure 50, *i.e.* the percentage of the sodium current inhibition for each mutant 2 minutes after addition of 1 mM intracellular MTSEA-biotin. Except for the WT, the Cter_ΔCys, the mutant A22C and the mutant R43C, one western blot was performed per mutated channel (12 oocytes per western blot). As seen before, removal of the four cysteines in the C-terminus (Cter_ΔCys) led to 90 % loss of the MTSEA-biotin mediated biotinylation of the mutated subunit compared with the wild-type. As shown in the previous section, the introduction of a cysteine in the N-terminus at position A22 increased the biotinylated signal compared with Cter_ΔCys, that is, the signal was returned to 50 % of the wild-type signal (Figure 50, highlighted in green). A partial restoration of signal was observed for all substitutions from position S23 to E37, where signal of biotinylated subunit was at least as intense as the mutant A22C. Of particular interest were the mutations S23C, S24C, L30C, A31C, F34C and S35C Cter_ΔCys that showed a full restoration of wild-type biotinylation signal, or even a strong elevation of this signal (Figure 50, highlighted in pink). Mutations L39C, L41C and R43C had no restorative effect and presented a biotinylated signal similar to that observed for the Cter_ΔCys mutant. Because the 10 % residual biotinylation has been shown to be DTT-sensitive, we considered that the lower range of values was due to a residual biotinylation (highlighted in orange), likely due to biotinylation of TM1 cysteines.

Taken together, these results show that cysteines substituted at the N-terminus from position A22 to E37 are accessible to MTSEA-biotin. According to the percentage of current inhibition induced by 2 minutes perfusion of MTSEA-biotin, we can distinguish four main groups:

1.   Mutated channels that are biotinylated by MTSEA-biotin but for which MTSEA-biotin has no effect on the sodium current;

2.   Mutated channels that are biotinylated by MTSEA-biotin and for which MTSEA-biotin inhibits significantly the sodium current. This is the case of the mutated channels hA1a-A22C, hA1a-I33C and hA1a-F34C. Thus, these amino acids are intracellularly accessible to MTSEA-biotin and seem to be important in the regulation of the channel;

3.   Two mutated channels, hA1a-L39C and hA1a-L41C, are not inhibited by MTSEA-biotin and this absence of inhibition is likely due to the inaccessibility of these amino acids to MTSEA-biotin.

4.   The mutated channel hA1a-R43C presents an unexpected pattern: its sodium current is inhibited by MTSEA-biotin but the subunit is not biotinylated ($p < 0.01$, compared to hA1a-A22C biotinylation). Previous studies have shown that the mutant hA1a-R43C, in the background C-terminus wild-type, is inhibited by intracellular MTSET (95). In contrast to hA1a-A22C and I33C, the residue R43C is located in the pore of hA1a and its inhibition by intracellular MTSET is state-dependent. This mean that when the channel is in a closed state, the TM1 undergoes conformational changes associated with channel gating and this reduces the accessibility of R43C to internal MTSET. Thus, MTSEA-biotin can only modified channels activated at the surface membrane explaining the inhibition of the current, but perfusion of MTSEA-biotin involves the biotinylation of non-activated channels in cytosolic vesicles that are much more numerous than membrane expressed channels.
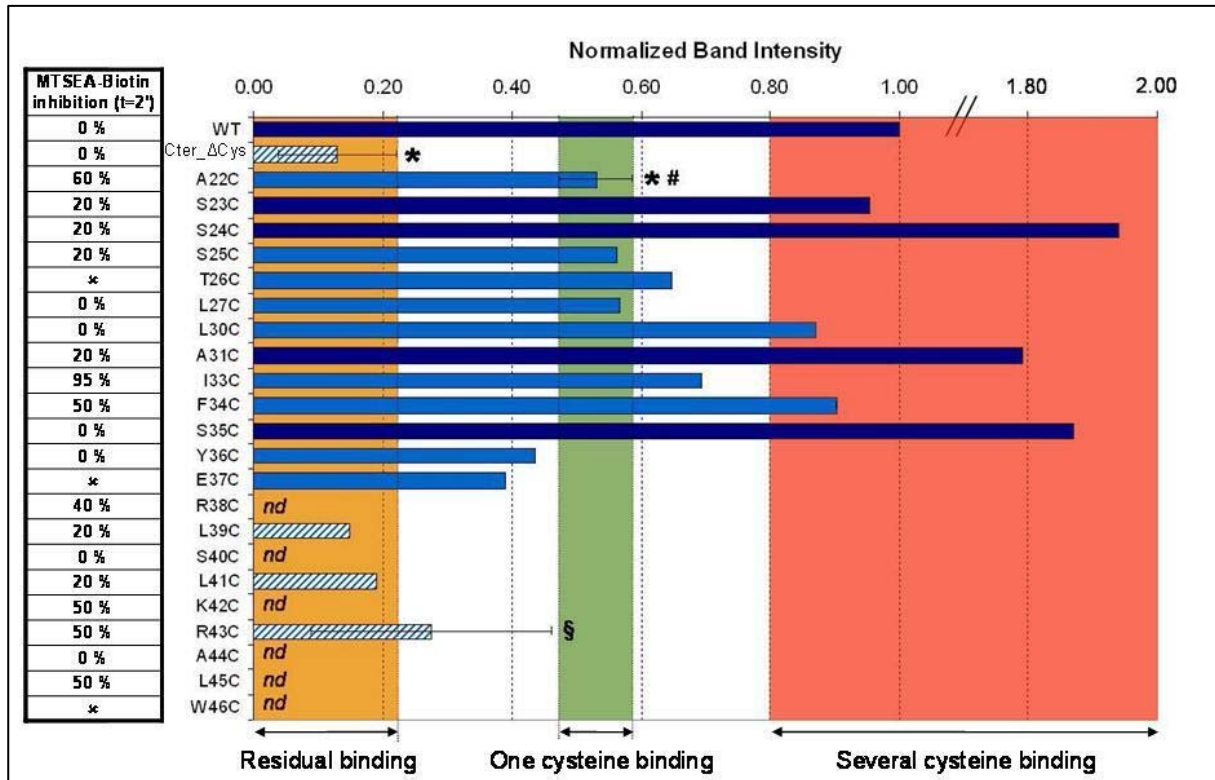
Figure 50: MTSEA-biotin binding to hA1a cysteine-substituted subunits. Each mutated channel is denoted by the corresponding N-terminus cysteine substitution in a Cter_ΔCys background, *i.e.* A22C means "hA1a-A22C-C466A-C471A-C497A-C528Stop". For each channel, the quantification of the specific hA1 signal was normalized with the biotinylated wild-type subunit (WT) signal. Dark blue bars indicate signal intensity at least as strong as the WT; light blue bars, decreased signal intensity. On the left are the reported levels of current inhibition by MTSEA-biotin for each mutant, taken from the figure 49. *nd*, non-determined. ✱, #, §: p<0.01, Student's t-test respectively compared to WT, Cter_ΔCys or A22C values. (WT, N=3; Cter_ΔCys, N=6, A22C, N=6; R43C, N=2; each western blot was performed with 12 oocytes per mutated channel)

We have seen that the wild-type and the Cter_ΔCys hA1a channels activity are insensitive to MTSEA-biotin although MTSEA-biotin binds to both wild-type and Cter_ΔCys subunits. Introduction of cysteine at different positions in the N-terminus allowed the identification of amino acids that are accessible to intracellular MTSEA-biotin and hence potentially involved in the function of the channel. From these results, we mainly have showed that: (i) Residues Ala22 to Glu37 in the N-terminal part of hA1a are accessible to MTSEA-biotin; (ii) Ala22, Ile33 and

Phe34 are accessible to MTSEA-biotin and have an important role in the regulation of ASIC; (iii) Leu39 and Leu41 are not accessible to MTSEA-biotin. Moreover, we confirmed the state-dependent accessibility of the residue Arg43 that we have already shown in a previous article (95). However, although there has been considerable replication with oocyte numbers, these results quantification of biotinylation results are based on single western blots. As such, our data must be considered preliminary and require further replication. To further expand this data set, we have created a mutant channel construct substituted at the TM1 and C-terminus cysteines: hA1a-C49S-C59S-C61S-C466A-C471A-C497A-C528Stop. We plan to performed MTSEA-biotinylation and cross-linking experiments on these channels generated in the TM1 + Cter_ΔCys background which would remove the residual biotinylation of the C-terminus cysteine-less mutated subunit. Such data would further isolate the functional importance of specific residues within the hA1a sequence.

DISCUSSION

I / Cadmium trapping in an Epithelial Sodium channel Pore Mutant.

The selectivity filter of ENaC constitutes the narrowest part of the pore and allows only the passage of the small monovalent cations Na^+ and Li^+. It is composed by three conserved amino acids, G/SxS, and is present in each of the three subunits. Mutation of the residue αSer589 leads to the loss of the channel selectivity and allows other mono- and divalent cations to pass through the channel (63). Sheng *et al.* have reported that the Cd^{2+}-sensitivity of the mutated channel αS589C$\beta\gamma$ was due to the orientation of the side chain of the substituted cysteine toward the channel pore (112). In this study, we have shown that a cysteine at position α589 (S589C) is not necessary to obtain a block by external Cd^{2+}. Indeed, its substitution with an aspartate (S589D), asparagine (S589N) or alanine (S589A) leads also to an almost irreversible inhibition of the channel by external Cd^{2+} although Asn and Ala have no affinity for Cd^{2+} ions. Thus, this contradicts the conclusion of the αSer589 side chain being oriented toward the channel pore.

The crystallization of a truncated, non-functional form of chicken ASIC1 (cΔASIC1) by Jasti *et al.* was published few weeks after publication of our work (61). They kindly provided us the pdb file of the three-dimensional view of the protein (46). In this model, the selectivity filter G/SxS is located in the middle of the membrane closer to the intracellular side rather than to the extracellular side as previously proposed (69) (Ser445, Figure 51A-box). Analysis of the conserved amino acid Ser445 on the cASIC1, corresponding to αS589 on rat ENaC, shows that the side chain of the serine faces the first transmembrane domain of the same subunit rather than the pore lumen channel (Figure 51B), thus corroborating our results as well as those from

Kellenberger *et al.* who proposed in a previous study (63) the orientation of the side chain of αS589 toward the subunit-subunit interface.
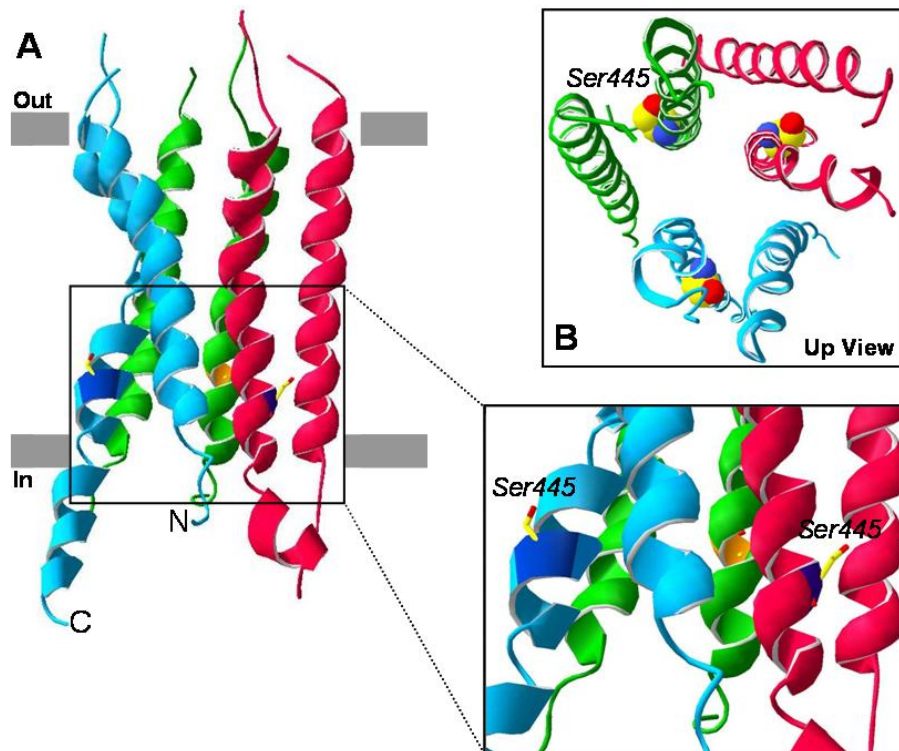
Figure 51: Orientation of the selectivity filter's residue Ser445 in the transmembrane domains of the cΔASIC1. (**A**) View parallel to the membrane plane. The box shows a zoom on the residues Ser445. (**B**) View from the extracellular side, along the pore axis. Each subunit is in a different colour forming the hypothetic trimer. Carbon atoms are yellow; oxygen atoms are red and nitrogen atoms are blue. *Obtained with the Swiss Pdb Viewer software*

In this same study, Kellenberger *et al.* suggested that substitution of αS589 by larger residues increases the pore diameter by adding extra volume at the subunit-subunit interface. We used the Swiss Pdb Viewer software (46) to model the effect of amino acid substitutions on the protein structure on the base of cASIC1 crystal (Figure 52). Substitutions of the Ser445 in Cys, Asp or Asn do not seem to render the side chain of the residue at position 445 more accessible to molecules in the ion pore. Measurements of the distance between each residue at position 445 ('d1', 'd2' and 'd3' on figure 52) do not indicate a real difference in distance

separating the different substituted amino acids (<u>Ser445</u>: d1=15 Å, d2=17.82 Å, d3=19.74 Å; <u>Ser445Cys</u>: d1=14.52 Å, d2=19.2 Å, d3=18.78 Å; <u>Ser445Asp</u>: d1=17.94 Å, d2=19.43 Å, d3=19.41 Å; <u>Ser445Asn</u>: d1=14.21 Å, d2=18.77 Å, d3=20.56 Å). Using Heron's formula (*cf. Methods 'Molecular Modelling'*), I calculated the area between three α445 residues (grey zone delimited by 'd1', 'd2' and 'd3' on figure 52): the three Ser445 form a pore area of 128 Å; the three Ser448Cys, 127.3 Å; the three Ser448Asp, 154 Å; and the three Ser448Asn, 129 Å. Except for the Asp substitution, mutation of the residues participating in the selectivity filter does not seem to change the pore diameter in this model. It remains to be determined whether these same calculations performed on a model of functional channel leads to the same results.
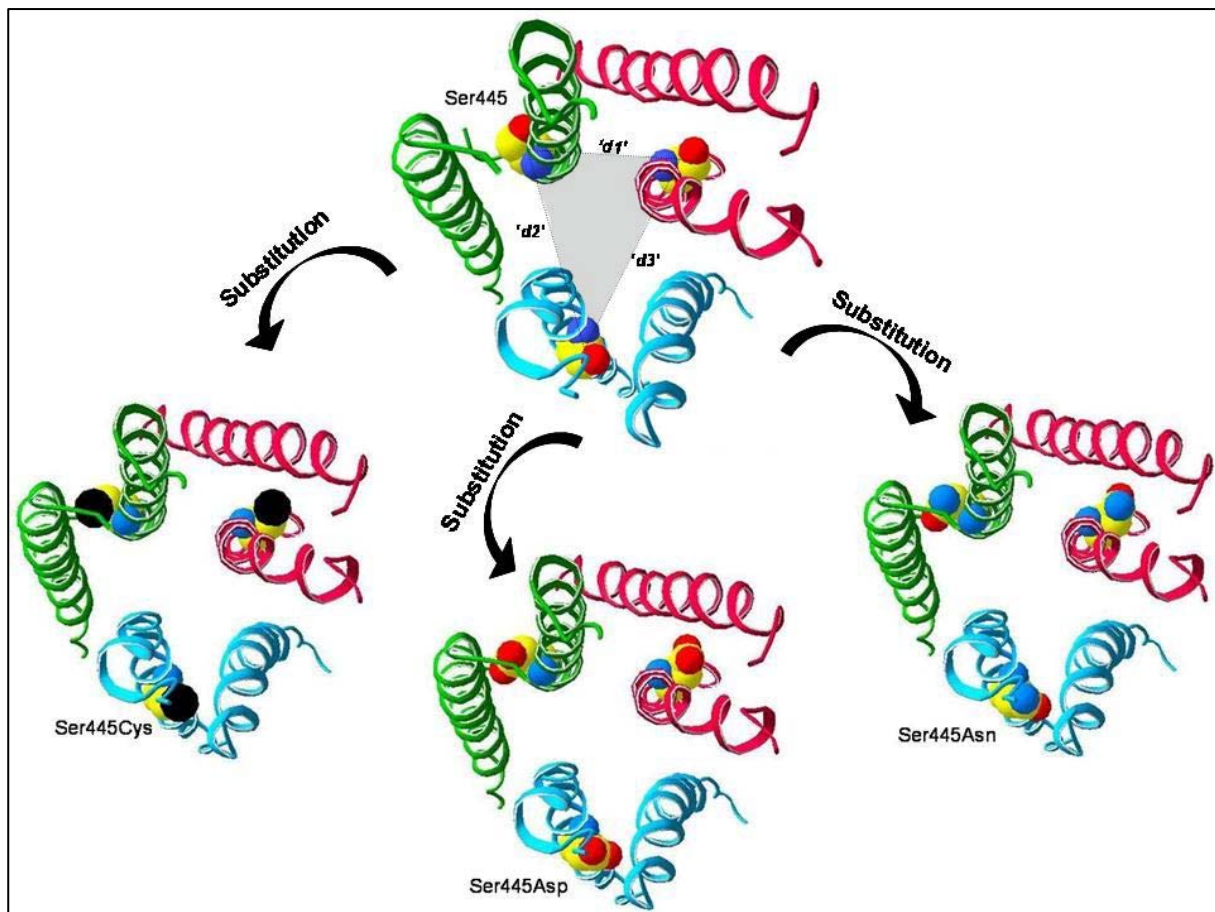
Figure 52: Hypothetic orientations of the selectivity filter's residue Ser445 substitutions in the transmembrane domains of the cΔASIC1. View from the extracellular side, along the pore axis. Each subunit is in a different colour forming the hypothetic trimer. Carbon atoms are yellow; oxygen atoms are red, sulfhydryl atoms are black and nitrogen atoms are blue. 'd1', 'd2'

and 'd3' represent the distances between each residue at position 445. The gray zone corresponds to the area calculated with Heron's formula. Distances and area are only indicated on the Ser445 but were also calculated for Ser445Cys, Ser445Asp and Ser445Asn. *Obtained with the Swiss Pdb Viewer software*

We have shown that Cd^{2+} mediated inhibition of ENaC channel carrying substitutions of the αS589C in either Cys, Asp or Asn, occurs *via* coordination of the metal cation with a native cysteine located downstream the amiloride binding site. This binding displays a high affinity and is irreversible under our experimental conditions. We have identified the Cys546, located in the second transmembrane domain of the γ subunit, as one of the native cysteines involved in the external Cd^{2+} block. There are likely other cysteines involved in this block but it was not possible to identify them since addition of mutations in the αS589C,β,γC546S background renders the channel non-functional.

I verified the orientation of cA1-T448, the residue in cASIC which corresponds to γCys546 according to our alignment (*cf. Annexe*). The lateral chain of Thr448 faces rather the first TM of the same subunit than the pore lumen (Figure 53, left panel). It lies however in the vicinity of the pore lumen and is possibly close to the cation diffusion pathway being therefore a potential binding site for Cd^{2+} entering through the channel. Indeed, a Pdb Viewer model of the T448C substitution in cΔASIC shows that the T448C side chain is quite accessible to ions going through the pore. This orientation might match with our results.
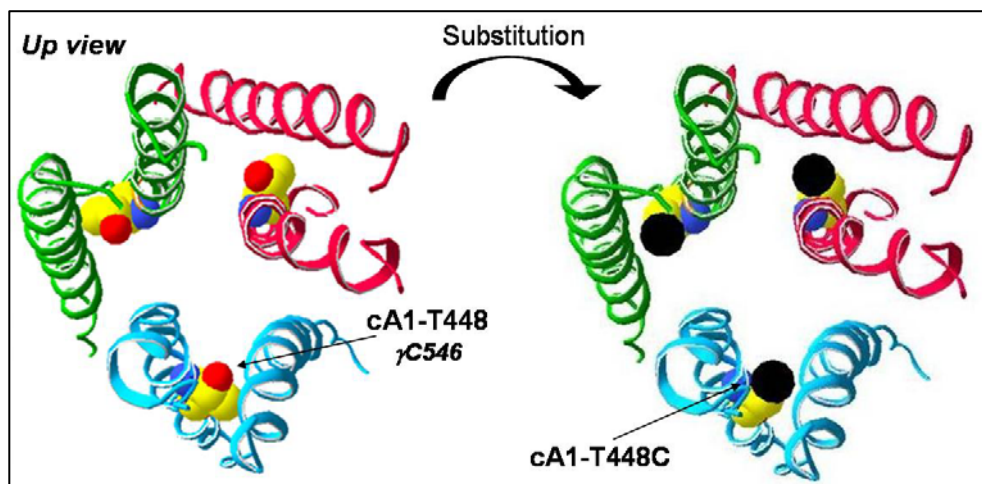
Figure 53: Hypothetic orientation of the residue Thr448 in the transmembrane domains of the chicken ASIC1 and theoretical effect of the cT448C substitution. View from the extracellular side, along the pore axis. Each subunit is in a different colour forming the hypothetic trimer. Carbon atoms are yellow; oxygen atoms are red, nitrogen atoms are blue and sulfhydryl atoms are black. *Obtained with the Swiss Pdb Viewer software*

II / Internal accessibility of the cysteine to sulfhydryl reagents.

Kellenberger *et al* (64) have shown at the channel level that ENaC is rapidly and reversibly inhibited by intracellular thiol reactive reagents such as methanethiosulfonates (MTS), Cd^{2+}, Zn^{2+}, and Copper(II)-phenantroline, *via* an effect on the channel gating. Thus, they have shown that intracellular cysteines in the N- and C-termini of the channel are likely involved in this thiol-mediated inhibition of ENaC. We asked ourselves whether the MTS inhibition of ENaC occurs *via* a direct interaction of the sulfhydryl reagents with ENaC cysteines or if an accessory protein is involved. In order to determine the cysteines involved in inhibition by intracellularly applied MTS, we used a SCAM-derived approach comprising systematic cysteine substitution within the protein of interest and the study of their modification by a MTSEA reagent coupled to biotin. This latter compound allowed us to isolate by affinity for streptavidin beads the subunit specifically target by the sulfhydryl reagent.

II-1) **ENaC**

We first showed that ENaC inhibition and biotinylation by intracellularly applied MTSEA-biotin did not result from diffusion of the reagent and reaction with cysteine residues exposed to the extracellular space. Indeed, extracellularly-applied MTSEA-biotin did not have any effect on the sodium current and it did not allow the biotinylation of any of the ENaC subunits. Inhibition and biotinylation of ENaC by MTSEA-biotin were prevented by addition of free cysteines in the perfusion suggesting that they occurred specifically *via* cysteine residue modification. In order to determine which cysteines were modified by intracellular MTSEA-biotin, we mutated all cysteines which are potentially accessible from the intracellular side, *i.e.* a total of 20 cysteines localized in the N- and C-termini and the 2 transmembrane domains of the three ENaC subunits. Removing cysteines either in the N-terminus or in the C-terminus led to non functional channels, and resulted in a decrease in the extent of protein biotinylation as compared to the wild-type channel. This underlines both the important functional role of cysteines located in the N- and C-termini and their accessibility to the intracellular space. The Int_ΔCys mutant channel, which has all the intracellular cysteines substituted, was not functional, but was still expressed at the cell surface. The rate of biotinylation of the Int_ΔCys mutated α and β subunits, compared to its wild-type counterpart, was reduced by respectively 70 % and 90 %. Thus, it is likely that the direct binding of MTSEA-biotin to N- and C-termini cysteines of ENaC was responsible for the inhibition of the channel current. However, the residual DTT-insensitive signal of biotinylation of both Int_ΔCys mutated α and β subunits suggested the presence of a non-specific interaction between MTSEA-biotin and ENaC. Cross-linking experiments showed that bismaleimide cross-linkers inhibited ENaC current and bound to subunits but did not provide any information on the nature of the potential accessory protein(s). We plan to complete our results using other cross-linkers with different arm lengths and other properties, for example the DPDPB, a homobifunctional sulfhydryl-specific cross-

linking reagent that contains two dithiopyridyl groups separated by a 19.9 Å arm and two cleavable disulfide bonds.

II-2) **ASIC**

We then looked at the effect of MTSEA-biotin on hASIC1a. The wild-type channel was biotinylated by MTSEA-biotin but, in contrast to ENaC, was not inhibited by this reagent. Substitution of the cysteines of hA1a that are potentially accessible from the intracellular side, *i.e.* in the C-terminus, did not disrupt channel activity. Similarly to what was observed with ENaC, MTSEA-biotin-mediated labelling of the mutated channel was decreased by ~90 % as compared to the wild-type subunit, with a residual biotinylation signal typically remaining incorporated to the protein. Thus, while the cysteines at the C-terminus of both ENaC and ASIC were accessible to intracellular MTSEA-biotin, only those of ENaC seemed to be crucial for the channel function.

In the case of hA1a, the residual signal of biotinylation is DTT-sensitive which indicated that one or more of the cysteines, possibly those located in the TM1 of hA1a, was accessible and susceptible to modification by MTSEA reagents. I have taken advantage of the fact that this residual biotinylation was only weakly detected by Western blot analysis, to study the accessibility of N-terminal cysteine substitutions in the C-terminus cysteine-less (Cter_ΔCys) background. Addition of a cysteine in the N-terminus at position A22 in the Cter_ΔCys mutant led to a recovery of MTSEA-biotin mediated biotinylation of the subunit and rendered the mutated channel sensitive to MTSEA-biotin inhibition. This indicated that the Ala22 residue was accessible to intracellular MTSEA-biotin and that it may be involved in channel regulation. Since Ala22 aligns with a conserved cysteine in the N-termini of all three ENaC subunits (αC88, βC30, γC33), these results confirmed the accessibility of the cysteines located in the N-terminus of ENaC and their importance in the function of the channel.

Perfusion experiments with hA1a mutants carrying cysteine substitutions allowed the identification of the region comprising Ala22 to Glu37 as being accessible to intracellularly applied MTSEA-biotin. However, only a few of these substitutions rendered the mutated channel sensitive to inhibition by MTSEA-biotin: besides the already mentioned A22C, I33C and F34C Cter_ΔCys hA1a mutants are significantly inhibited by MTSEA-biotin. We can conclude that residues Ala22, Ile33 and Phe34 were intracellularly accessible and may be important for the regulation of the channel. These results confirm the MTSET sensitivity of the corresponding A22C, I33C and F34C mutants in the C-terminus wild-type background observed by Pfister *et al.* (95). The PredictProtein Server (102) predicts two potential α helix encompassing residues L30 to F34 and residues S40 to Y68 (corresponding to the putative first TM) as shown in figure 54 ('H'=Helix predictions in 'PROF_sec' line). The predicted α helix formed by amino acids L30 to F34 has a low reliability (1 to 2 in 'Rel_sec', figure 54). Our results showed a clear accessibility of these amino acids by MTSEA-biotin when substituted in cysteine. Altogether, this suggests that the formation of a α helix at this position is unlikely. the presence of an α-helix with amino acids R43 to W46 has a high reliability (5 to 7 in 'Rel_sec', Figure 54) as indicated in 'SUB_sec' line in the figure 54, where we only show the prediction with average accuracy superior to 82 %. These amino acids involved in the formation of a α-helix are likely involved in the TM domain. This can explain the absence of accessibility of cysteine substituted residues L39C, L41C and R43C to MTSEA-biotin.

Figure 54: Prediction of the secondary structure of hA1a. Here are only presented the first 80 amino acids. <u>AA</u>, amino acids; <u>OBS_sec</u>, observed secondary structure (H=Helix, E=Extended (sheet)); <u>PROF_sec</u>, "Profil network prediction Heidelberg" (PROF) predicted

secondary structure; <u>Rel_sec</u>: reliability index for PROF_sec prediction (0=low to 9=high); <u>SUB_sec</u>: subset of the PROF_sec prediction for all residues with an expected average accuracy > 82 %, L=loop.

One unexpected result was obtained with the R43C mutant. MTSET accessibility experiments previously performed by Pfister *et al.* (95) had shown that the R43C residue lines the pore and is accessible to MTSET only when the channel is activated, likely when the first transmembrane domain undergoes conformational changes during channel activation. In our experiments, although intracellular MTSEA-biotin did indeed inhibit the sodium current generated by the mutated channel R43C in the Cter_ΔCys background, this effect was not mirrored by an increase in biotin incorporation as compared to its non-substituted counterpart. This result underlines a limit of our new approach. We hypothesized that inhibition of current was the consequence of conjugation of MTSEA-biotin to the subunit at the R43C position. Perfusion of intracellular MTSEA-biotin leads to the biotinylation of the cytosolic pool of proteins, including proteins in vesicles, and of proteins expressed at the cell surface (Figure 55). The channels expressed at the surface membrane are the only channels activated and represent only a fraction of the total biotinylated protein. Because the residue R43C is only accessible when channel is activated, the channels expressed at the cell membrane are the only mutated channels biotinylated by MTSEA-biotin. Thus, biotinylated proteins observed in western blot analysis represent intracellular proteins rather than proteins expressed at the cell surface, *i.e.* non-activated proteins rather than activated proteins.
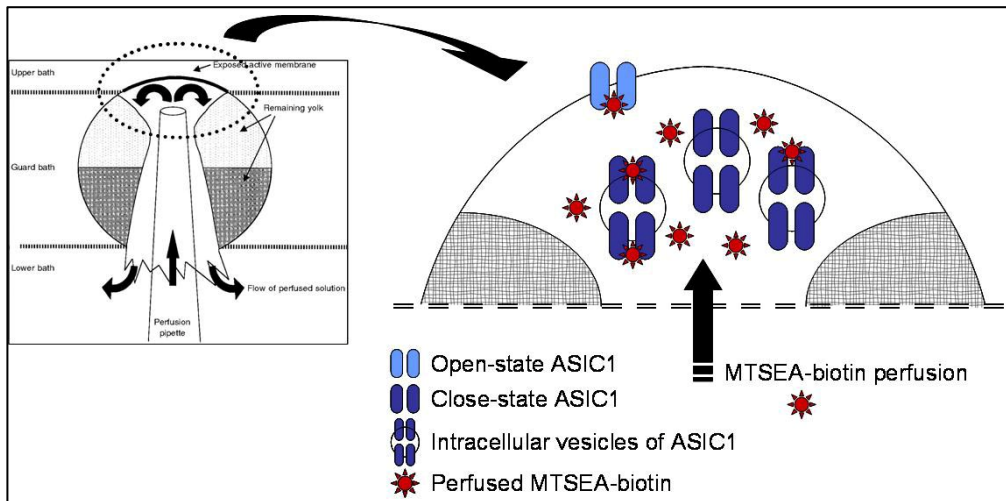
Figure 55: Schematic representation of MTSEA-biotin intracellular perfusion. With the cut-open oocyte method MTSEA-biotin is perfused only in a small fraction (about 10 %) of the oocyte (left panel). In the perfused part of the oocyte, proportion of channels at the surface membrane is much lower than in intracellular vesicles (right panel). In the case of ASIC, activated channels are only at the surface membrane. Thus, the MTSEA-biotin-mediated biotinylation of channels reflects principally intracellular inactivated channels.

A number of substitutions at Cter_ΔCys hA1a N-terminus remain to be analyzed in terms of their accessibility to MTSEA-biotin, namely R38C, S40C, K42C, A44C, L45C and W46C. This will be part of a future work.

Because cysteines located at the TM1 of hA1a are potentially accessible to MTSEA-biotin, I have generated a new mutant channel in which the cysteines in the TM1 and in the C-terminus have been substituted by serine, alanine, or a stop codon: hA1a-C49S-C59S-C61S-C466A-C471A-C497A-C528Stop. In this TM1+C-ter_ΔCys channel, we performed a cysteine screen of the N-terminus, from position A22 to W46. Measurement of the sodium currents generated by these mutants showed that they are all at least partially functional (data not shown). Currents are however not high enough for cut-open experiments but perfusion of intracellular MTSEA-biotin should indicate whether the cysteines at the TM1 are indeed responsible for the residual biotinylation observed with the Cter_ΔCys mutant.

Since the truncated form of cASIC1 used by Jasti *et al.* to generate the crystal structure lacks both N- and C-termini, it is not possible to model the mutations introduced in hASIC1a at these regions. In hASIC1a, the residues corresponding to the pre-TM1 and which have been tested in our study (hA1a-Leu41 to hA1a-Trp46) are however visible in the crystal structure of cASIC1, namely cA1-Leu42 to cA1-Try47.
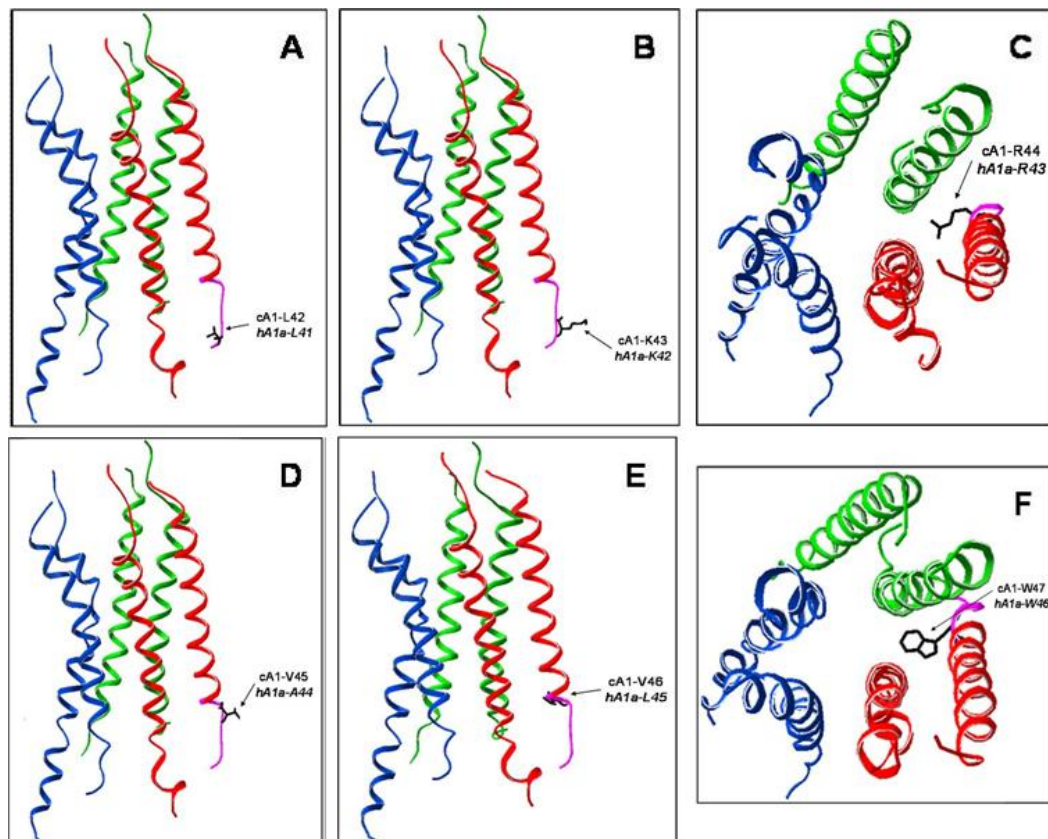
Figure 55: Orientation of the side chain of six N-terminal residues in the chicken ASIC1 crystal structure. (**A**,**B**,**D**,**E**) View of the transmembrane domains of three subunits parallel to the membrane plane showing in black either the cA1-L42 (**A**), the cA1-K43 (**B**), the cA1-V45 (**D**) or the cA1-V46 (**E**) residue (**C**,**F**) View from the extracellular side, along the pore axis, showing in black either the cA1-R44 (**C**) or the cA1-W47 (**F**) residue. Each of the subunits of the trimer is in a different colour. Each residue is represented on only one subunit for the sake of clarity and the corresponding name in the human ASIC1a is indicated in italic. The part of the subunit studied here is in pink.

It is therefore interesting to assess in how far our results are compatible with the localization and orientation of the residues in this stretch relative to the pore. Leucine 41 and Lysine 42 in human A1a are conserved in chicken A1 and their side chains do not seem to disturb the passage of ions. However, our data showed that hA1a-K42C is significantly inhibited by MTSEA-biotin. This suggests thus that the residue ha1a-K42 lines the ion pore, in contrast with the cΔASIC1 model. The orientation towards the lumen of the pore of cA1-R44, agrees with the results obtained with the Cys substitution of the corresponding hA1a-R43. cA1-V45 and cA1-V46 are not conserved between chicken and human ASIC. Substitution of cA1-Val45 in Ala does not change the accessibility but substitution of cA1a-Val46 in Leu (not shown) which introduces a longer side chain that looks more accessible, corroborates with the MTSEA-biotin inhibition observed for the mutated hA1a-L45C. The residue cA1-W47 corresponding to the hA1a-W46, is located in the ion pathway and its side chain points toward the pore. Substitution of this residue in cysteine leads to a non-functional channel underlining the crucial role of the hA1a-W46 in the channel function.

In conclusion, this new approach which takes advantage of the fact that substitution of native intracellular cysteines is not deleterious for the channel function, allows us to identify the residues that are accessible to an intracellular reagent and that are relevant for the function of the channel. We have shown that cysteine residues in the N- and C-termini of ENaC are accessible to intracellular sulfhydryl reagents and are important for ENaC function. We have also shown that cysteines in the C-terminus of hA1a are not essential for the function of hA1a and that a number of amino acids at the N-terminus (A22 to E37) are accessible, some of which being important as well for the activity of the channel. However, this approach is only applicable to those mutants for which the accessibility of the target residue does not change with the conformational changes that accompany the activation and inactivation of the channel,

as it has been shown in the case of the hA1a-R43C substitution. For this particular channel, it should be possible to isolate the activated membrane pool of channels by a set of PEGylation and biotinylation: if oocytes are extracellularly labelled with poly(ethylene glycol) and intracellularly biotinylated with DTT-sensitive MTSEA-biotin, we would increase the molecular weight of channels expressed at the surface membrane. Then, biotinylated proteins will be isolated by affinity for streptavidin beads. And after separation of proteins by SDS-PAGE, it should be possible to differentiate by a shift in the apparent molecular weight intracellularly biotinylated proteins that had been extracellularly PEGylated. In this way, we should isolate intracellularly accessible activated proteins.

Sequence alignment of rat α, β and γ ENaC and human and chicken ASIC. Gene ID: rat αENaC, 25122; rat βENaC, 24767; rat γENaC, 24768; human ASIC, 41; chicken ASIC, 426883. The sequences were aligned with TCOFFEE Regular server of the Swiss Institute of Bioinformatics. Transmembrane domains TM1 and TM2 are indicated in blue cylinder; conserved cysteine residues in ENaC are surrounded by a light blue frame (☐); conserved cysteine residues in ASIC are surrounded by an orange frame (☐); conserved domains (HG domain, Degenerin site (DEG), Amiloride binding site (Amil.), Selectivity filter and PY motif) are surrounded by a red frame (☐); and amino acids substituted in cysteine in the N-terminus part of hA1a are surrounded by green frame (☐).

```
rat_alphaENaC    MLDHTRAPELNIDLDLHASNSPKGSMKGNQFKEQDPCPPQPMQGLGKGDKREEQGLGPEP   60
rat_betaENaC     MP-VKK-YLLK-------------------------------------CLHRLQ--KGPG-   19
rat_gammaENaC    MAPGEK-IKAK-------------------------------------IKKNLPVRGPQA   22
human_ASIC1      ME-LKA-EEEE-------------------------------------------VGGVQP   15
chicken_ASIC1    MMDLKV-DEEE-------------------------------------------VDSGQP   16
                 *          :

                                                    HG                    TM1
                                                   domain
rat_alphaENaC    SAPRQPTEEEEALIEFHRSYRELFQFCNNTTIHGAIRLVCSKHNRMKTAFWAVLWLCTF   120
rat_betaENaC     ----------------YTYKELLVWYCNNTNTHGPKRIICE--GPKKKAMWFLLTLLFA    59
rat_gammaENaC    ----------------PTIKDLMHWYCMNTNTHGCRRIVVS-RGRLRRLLWIAFTLTAV    64
human_ASIC1      -------------------VSIQAFASSSTLHGLAHIFSYERLSLKRALWAICFLGSL    54
chicken_ASIC1    -------------------VSIQAFASSSTLHGISHIFSYERLSLKRVVWAICFMGSL    55
                                   :   :.. .:.  **  ::.      :  .*    :

                       TM1
rat_alphaENaC    GMMYWQFALLFEEYLSYP-VSLNINLNSDKLVFPAVTVCTLNPYRYTEIKEELEELDRIT   179
rat_betaENaC     CLVCWQWGVFIQTYLSWE-VSVSLSMGFKTMNFPAVTVCNSSPFQYSKVKHLLKDLYKLM   118
rat_gammaENaC    ALIIWQCALLVFSF--YT-VSVSIKVHFQKLDFPAVTICNINPYKYSAVSDLLTDLDSET   121
human_ASIC1      AVLLCVCTERVQYYFHYHHVTKLDEVAASQLTFPAVTLCNLNEFRFSQVSK--NDLYHAG   112
chicken_ASIC1    ALLALVCTNRIQYYFLYPHVTKLDEVAATRLTFPAVTFCNLNEFRFSRVTK--NDLYHAG   113
                  ::    .    :  :  *:   .:    : *****.*. . :::: :.. :*

rat_alphaENaC    E--QTLFDLYKYNSSYT-RQAGARRRSSRDL----LGAFPHPLQRLRTPPP--P-YSGRT   229
rat_betaENaC     E--AVLDKILAPKSSHT-NTTSTLNFTIWN-------HTPLVLIDERNPDH--PVVLNLF   167
rat_gammaENaC    K--QALLSLYGVKESRKRREAGSMPSTLEGTPPRFFKLIPLLVFNENEKGKARDFFTGRK   179
human_ASIC1      ELLALLNNRYEIPDTQMA-DEK--QLEILQD--------------------------   140
chicken_ASIC1    ELLALLNNRYEIPDTQTA-DEK--QLEILQD--------------------------   141
                 :    *  .      .:

rat_alphaENaC    AR-SGSSSVR-DNNPQVDRKDWKIGFQLCNQNKSDCFYQTYSSGVDAVREWYRFHYINIL   287
rat_betaENaC     GD-SHNSSNP-APGSTCNAQGCKVAMRLCSANGTVCTFRNFTSATQAVTEWYILQATNIF   225
rat_gammaENaC    RKISGKIIHKASNVMHVHESKKLVGFQLCSNDTSDCATYTFSSGINAIQEWYKLHYMNIM   239
human_ASIC1      --------------------------------KANFRSFKPKPFNMREFYDR------   160
chicken_ASIC1    --------------------------------KANFRNFKPKPFNMLEFYDR------   161
                                                 .   .:..   : *:*

rat_alphaENaC    SRLSDTSPALEEEALGNFIFTCRFNQAPCNQANYSKFHHPMYGNCYTFNDKNNSNL-WMS   346
rat_betaENaC     SQVLPQDLVGMGYAPDRIILACLFGTEPCSHRNFTPIFYPDYGNCYIFNWGMTEKA-LPS   284
rat_gammaENaC    AQVPLEKKINMSYSAEELLVTCFFDGMSCDARNFTLFHHPMYGNCYTFNNKENATI-LST   298
human_ASIC1      ---------AGHDIRDMLLSCHFRGEVCSAEDFKVV-FTRYGKCYTFNSGRDGRPRLKT   209
chicken_ASIC1    ---------AGHDIREMLLSCFFRGEQCSPEDFKVV-FTRYGKCYTFNAGQDGKPRLIT   210
                          ::.:* *   *.  ::. . .. **:** **           :
```

```
rat_alphaENaC    SMPGVNNGLSLTLRTEQNDFIPLLST------VTGARVMVHGQDEPAFMDDGGFNLRPGV  400
rat_betaENaC     ANPGTEFGLKLILDIGQEDYVPFLAS------TAGARLMLHEQRTYPFIREEGIYAMAGT  338
rat_gammaENaC    SMGGSEYGLQVILYINEDEYNPFLVS------STGAKVLIHQQNEYPFIEDVGMEIETAM  352
human_ASIC1      MKDGTGNGLEIMLDIQQDEYLPVWGETDETSFEAGIKVQIHSQDEPPFIDQLGFGVAPGF  261
chicken_ASIC1    MKGGTGNGLEIMLDIQQDEYLPVWGETDETSFEAGIKVQIHSQDEPPLIDQLGFGVAPGF  270
                  *    **.: *   :::: *.           :* :: :* *    .:: : *:    ..

rat_alphaENaC    ETSISMRKEALDSLGGNYGDCTENGSDVPVKNL---YPSKYTQQVCIHSCFQENMIKKCG  457
rat_betaENaC     ETSIGVLLDKLQGKGEPYSPCTMNGSDVAIQNLYSDYNTTYSIQACLHSCFQDHMIHNCS  398
rat_gammaENaC    STSIGMHLTESFKLSEPYSQCTEDGSDVPVTNI---YNAAYSLQICLYSCFQTKMVEKCG  409
human_ASIC1      QTFVACQEQRLIYLPPPWGTCKAVTMDSDL-----DFFDSYSITACRIDCETRYLVENCN  324
chicken_ASIC1    QTFVSCQEQRLIYLPPPWGDCKATTGDS-------EFYDTYSITACRIDCETRYLVENCN  323
                 .* :.             :. *.    *         :   *:   *  .*     ::.:*.

rat_alphaENaC    CAYIFYPKPKGVEFCDYRKQSSWGYCYYKLQGAFSLDSLGCFSKCRKPCSVINYKLSAGY  517
rat_betaENaC     CGHYLYPLPAGEKYCNNRDFPDWAYCYLSLQMS-VVQRETCLSMCKESCNDTQYKMTISM  457
rat_gammaENaC    CAQYSQPLPPAANYCNYQQHPNWMYCYYQLYQAFVREELGCQSVCKQSCSFKEWTLTTSL  469
human_ASIC1      CRMVH--MPGDAPYCTPEQYKECADPA---LD-FLVEKDQEYCVCEMPCNLTRYGKELSM  378
chicken_ASIC1    CRMVH--MPGDAPYCTPEQYKECADPA---LD-FLVEKDNEYCVCEMPCNVTRYGKELSM  377
                 *       *      :*   ..  .              :         . *. .*.  .:

                                                                        TM2
rat_alphaENaC    SRWPSVKSQDWIFEMLSLQNNYTINN--KRNGVAKLNIFFKELNYKTNSESPSVTMVSLL  575
rat_betaENaC     ADWPSEASEDWILHVLSQERDQSSNITLSRKGIVKLNIYFQEFNYRTIEESPANNIVWLL  517
rat_gammaENaC    AQWPSEASEKWLLNVLTWDQSQQINKKLNKTDLAKLLIFYKDLNQRSIMESPANSIEMLL  529
human_ASIC1      VKIPSKASAKYLAKKFNKSEQY------IGENILVLDIFFEVLNYETIEQKKAYEIAGLL  432
chicken_ASIC1    VKIPSKASAKYLAKKYNKSEQY------IGENILVLDIFFEALNYETIEQKKAYEVAGLL  431
                   **   *   .::  ...         .:  * *:::  :* .:   :.  :   :  **
     DEG     Amil.       TM2
rat_alphaENaC    SNLGSQWSLWFGSSVLSVVEMAELIF-DLLVITLLMLLRRFR---SRYW-SPGRGARGA-  629
rat_betaENaC     SNLGGQFGFWMGGSVLCLIEFGEIII-DFIWITVIKLVASCKGLRRRRPQAPYTGPPPTV  576
rat_gammaENaC    SNFGGQLGLWMSCSVVCVIEIIEVFFIDFFSIIARRQWHKAKDWWARRQTPPSTETPS--  587
human_ASIC1      GDIGGQMGLFIGASILTVLELFDYAY-EVIKHK---ICRRGKCKEAKRSSADKGVALSL   488
chicken_ASIC1    GDIGGQMGLFIGASILTVLELFDYAY-EVIKHR---ICRRGKCKNHKRNNTDKGVALSM   487
                 .::*.* .:::. *:: .::*: :          :.:           :           .
                     Selectivity filter                       PY motif
rat_alphaENaC    REV--AS-TPASSFPSRFCPHPTSPPPSLPQQGMTPPLALTAPPPAYATLGPSAPP-LDS  685
rat_betaENaC     AELVEAHTNFGF-QPDTT-SCRPNAEVYPDQQTLPIPG---TPPPNYDSLR--LQP-LDT  628
rat_gammaENaC    SRQ-GQD-NPALDTDDDL-PTFTSAMRLPPAPGSTVPG---TPPPRYNTLR--LDRAFSS  639
human_ASIC1      DDV-KRH-NPC-----------ESLRGHPA-GMTYAAN--------------ILP-HHP   518
chicken_ASIC1    DDV-KRH-NPC-----------ESLRGHPA-GMTYAAN--------------ILP-HHP   517
                  .        ..          .. .          . .                   .

rat_alphaENaC    AAPDCSACALAAL  698
rat_betaENaC     MESDSE---VEAI  638
rat_gammaENaC    QLTDTQ--LTNEL  650
human_ASIC1      ARG---TFEDFTC  528
chicken_ASIC1    ARG---TFEDFTC  527
```

REFERENCE LIST

1. **Amorim JB and Malnic G**. V(1) receptors in luminal action of vasopressin on distal K(+) secretion. *Am J Physiol Renal Physiol* 278: F809-F816, 2000.

2. **Anantharam A and Palmer LG**. Determination of epithelial Na+ channel subunit stoichiometry from single-channel conductances. *J Gen Physiol* 130: 55-70, 2007.

3. **Anantharam A, Tian Y and Palmer LG**. Open probability of the epithelial sodium channel is regulated by intracellular sodium. *J Physiol* 574: 333-347, 2006.

4. **Armstrong C**. The vision of the pore. *Science* 280: 56-57, 1998.

5. **Auberson M, Hoffmann-Pochon N, Vandewalle A, Kellenberger S and Schild L**. Epithelial Na+ channel mutants causing Liddle's syndrome retain ability to respond to aldosterone and vasopressin. *Am J Physiol Renal Physiol* 285: F459-F471, 2003.

6. **Babini E, Geisler HS, Siba M and Grunder S**. A new subunit of the epithelial Na+ channel identifies regions involved in Na+ self-inhibition. *J Biol Chem* 278: 28418-28426, 2003.

7. **Bankir L**. Antidiuretic action of vasopressin: quantitative aspects and interaction between V1a and V2 receptor-mediated effects. *Cardiovasc Res* 51: 372-390, 2001.

8. **Berdiev BK, Cormet-Boyaka E, Tousson A, Qadri YJ, Oosterveld-Hut HM, Hong JS, Gonzales PA, Fuller CM, Sorscher EJ, Lukacs GL and Benos DJ**. Molecular proximity of cystic fibrosis transmembrane conductance regulator and epithelial sodium channel assessed by fluorescence resonance energy transfer. *J Biol Chem* 282: 36481-36488, 2007.

9. **Bertog M, Cuffe JE, Pradervand S, Hummler E, Hartner A, Porst M, Hilgers KF, Rossier BC and Korbmacher C**. Aldosterone responsiveness of the epithelial sodium channel (ENaC) in colon is increased in a mouse model for Liddle's syndrome. *J Physiol* 586: 459-475, 2008.

10. **Bhalla V, Soundararajan R, Pao AC, Li H and Pearce D**. Disinhibitory pathways for control of sodium transport: regulation of ENaC by SGK1 and GILZ. *Am J Physiol Renal Physiol* 291: F714-F721, 2006.

11. **Bize V and Horisberger JD**. Sodium self-inhibition of human epithelial sodium channel: selectivity and affinity of the extracellular sodium sensing site. *Am J Physiol Renal Physiol* 293: F1137-F1146, 2007.

12. **Bonny O, Chraibi A, Loffing J, Jaeger NF, Grunder S, Horisberger JD and Rossier BC**. Functional expression of a pseudohypoaldosteronism type I mutated epithelial Na+ channel lacking the pore-forming region of its alpha subunit. *J Clin Invest* 104: 967-974, 1999.

13. **Bonny O, Knoers N, Monnens L and Rossier BC**. A novel mutation of the epithelial Na+ channel causes type 1 pseudohypoaldosteronism. *Pediatr Nephrol* 17: 804-808, 2002.

14. **Boucher RC**. New concepts of the pathogenesis of cystic fibrosis lung disease. *Eur Respir J* 23: 146-158, 2004.

15. **Boucher RC**. Airway surface dehydration in cystic fibrosis: pathogenesis and therapy. *Annu Rev Med* 58: 157-170, 2007.

16. **Breyer MD and Ando Y**. Hormonal signaling and regulation of salt and water transport in the collecting duct. *Annu Rev Physiol* 56: 711-739, 1994.

17. **Bruns JB, Carattino MD, Sheng S, Maarouf AB, Weisz OA, Pilewski JM, Hughey RP and Kleyman TR**. Epithelial Na+ channels are fully activated by furin- and prostasin-dependent release of an inhibitory peptide from the gamma-subunit. *J Biol Chem* 282: 6153-6160, 2007.

18. **Caldwell RA, Boucher RC and Stutts MJ**. Serine protease activation of near-silent epithelial Na+ channels. *Am J Physiol Cell Physiol* 286: C190-C194, 2004.

19. **Canessa CM, Horisberger JD and Rossier BC**. Epithelial sodium channel related to proteins involved in neurodegeneration. *Nature* 361: 467-470, 1993.

20. **Canessa CM, Schild L, Buell G, Thorens B, Gautschi I, Horisberger JD and Rossier BC**. Amiloride-sensitive epithelial Na+ channel is made of three homologous subunits. *Nature* 367: 463-467, 1994.

21. **Carattino MD, Hughey RP and Kleyman TR**. Proteolytic processing of the epithelial sodium channel gamma subunit has a dominant role in channel activation. *J Biol Chem* 2008.

22. **Carattino MD, Sheng S, Bruns JB, Pilewski JM, Hughey RP and Kleyman TR**. The epithelial Na+ channel is inhibited by a peptide derived from proteolytic processing of its alpha subunit. *J Biol Chem* 281: 18901-18907, 2006.

23. **Chalfie M and Wolinsky E**. The identification and suppression of inherited neurodegeneration in Caenorhabditis elegans. *Nature* 345: 410-416, 1990.

24. **Chen LM, Skinner ML, Kauffman SW, Chao J, Chao L, Thaler CD and Chai KX**. Prostasin is a glycosylphosphatidylinositol-anchored active serine protease. *J Biol Chem* 276: 21434-21442, 2001.

25. **Chen SY, Bhargava A, Mastroberardino L, Meijer OC, Wang J, Buse P, Firestone GL, Verrey F and Pearce D**. Epithelial sodium channel regulated by aldosterone-induced protein sgk. *Proc Natl Acad Sci U S A* 96: 2514-2519, 1999.

26. **Chraibi A and Horisberger JD**. Na self inhibition of human epithelial Na channel: temperature dependence and effect of extracellular proteases. *J Gen Physiol* 120: 133-145, 2002.

27. **Chraibi A, Vallet V, Firsov D, Hess SK and Horisberger JD**. Protease modulation of the activity of the epithelial sodium channel expressed in Xenopus oocytes. *J Gen Physiol* 111: 127-138, 1998.

28. **Collier DM and Snyder PM**. Extracellular protons regulate human ENaC by modulating Na+ self-inhibition. *J Biol Chem* 284: 792-798, 2009.

29. **Coscoy S, Lingueglia E, Lazdunski M and Barbry P**. The Phe-Met-Arg-Phe-amide-activated sodium channel is a tetramer. *J Biol Chem* 273: 8317-8322, 1998.

30. **Debonneville C, Flores SY, Kamynina E, Plant PJ, Tauxe C, Thomas MA, Munster C, Chraibi A, Pratt JH, Horisberger JD, Pearce D, Loffing J and Staub O**. Phosphorylation of Nedd4-2 by Sgk1 regulates epithelial Na(+) channel cell surface expression. *EMBO J* 20: 7052-7059, 2001.

31. **Diakov A, Bera K, Mokrushina M, Krueger B and Korbmacher C**. Cleavage in the {gamma}-subunit of the epithelial sodium channel (ENaC) plays an important role in the proteolytic activation of near-silent channels. *J Physiol* 2008.

32. **Diakov A and Korbmacher C**. A novel pathway of epithelial sodium channel activation involves a serum- and glucocorticoid-inducible kinase consensus motif in the C terminus of the channel's alpha-subunit. *J Biol Chem* 279: 38134-38142, 2004.

33. **Dijkink L, Hartog A, van Os CH and Bindels RJ**. The epithelial sodium channel (ENaC) is intracellularly located as a tetramer. *Pflugers Arch* 444: 549-555, 2002.

34. **Doyle DA, Morais CJ, Pfuetzner RA, Kuo A, Gulbis JM, Cohen SL, Chait BT and MacKinnon R**. The structure of the potassium channel: molecular basis of K+ conduction and selectivity. *Science* 280: 69-77, 1998.

35. **Fakitsas P, Adam G, Daidie D, van Bemmelen MX, Fouladkou F, Patrignani A, Wagner U, Warth R, Camargo SM, Staub O and Verrey F**. Early aldosterone-induced gene product regulates the epithelial sodium channel by deubiquitylation. *J Am Soc Nephrol* 18: 1084-1092, 2007.

36. **Fejes-Toth G, Frindt G, Naray-Fejes-Toth A and Palmer LG**. Epithelial Na+ channel activation and processing in mice lacking SGK1. *Am J Physiol Renal Physiol* 2008.

37. **Firsov D, Gautschi I, Merillat AM, Rossier BC and Schild L**. The heterotetrameric architecture of the epithelial sodium channel (ENaC). *EMBO J* 17: 344-352, 1998.

38. **Firsov D, Robert-Nicoud M, Gruender S, Schild L and Rossier BC**. Mutational analysis of cysteine-rich domains of the epithelium sodium channel (ENaC). Identification of cysteines essential for channel expression at the cell surface. *J Biol Chem* 274: 2743-2749, 1999.

39. **Firsov D, Schild L, Gautschi I, Merillat AM, Schneeberger E and Rossier BC**. Cell surface expression of the epithelial Na channel and a mutant causing Liddle syndrome: a quantitative approach. *Proc Natl Acad Sci U S A* 93: 15370-15375, 1996.

40. **Fotia AB, Dinudom A, Shearwin KE, Koch JP, Korbmacher C, Cook DI and Kumar S**. The role of individual Nedd4-2 (KIAA0439) WW domains in binding and regulating epithelial sodium channels. *FASEB J* 17: 70-72, 2003.

41. **Frindt G, Ergonul Z and Palmer LG**. Surface expression of epithelial Na channel protein in rat kidney. *J Gen Physiol* 131: 617-627, 2008.

42. **Garcia-Anoveros J, Derfler B, Neville-Golden J, Hyman BT and Corey DP**. BNaC1 and BNaC2 constitute a new family of human neuronal sodium channels related to degenerins and epithelial sodium channels. *Proc Natl Acad Sci U S A* 94: 1459-1464, 1997.

43. **Garty H and Palmer LG**. Epithelial sodium channels: function, structure, and regulation. *Physiol Rev* 77: 359-396, 1997.

44. **Grunder S, Firsov D, Chang SS, Jaeger NF, Gautschi I, Schild L, Lifton RP and Rossier BC**. A mutation causing pseudohypoaldosteronism type 1 identifies a conserved glycine that is involved in the gating of the epithelial sodium channel. *EMBO J* 16: 899-907, 1997.

45. **Grunder S, Jaeger NF, Gautschi I, Schild L and Rossier BC**. Identification of a highly conserved sequence at the N-terminus of the epithelial Na+ channel alpha subunit involved in gating. *Pflugers Arch* 438: 709-715, 1999.

46. **Guex N and Peitsch MC**. SWISS-MODEL and the Swiss-PdbViewer: an environment for comparative protein modeling. *Electrophoresis* 18: 2714-2723, 1997.

47. **Hamilton KL and Eaton DC**. Single-channel recordings from amiloride-sensitive epithelial sodium channel. *Am J Physiol* 249: C200-C207, 1985.

48. **Hansson JH, Nelson-Williams C, Suzuki H, Schild L, Shimkets R, Lu Y, Canessa C, Iwasaki T, Rossier B and Lifton RP**. Hypertension caused by a truncated epithelial sodium channel gamma subunit: genetic heterogeneity of Liddle syndrome. *Nat Genet* 11: 76-82, 1995.

49. **Hansson JH, Schild L, Lu Y, Wilson TA, Gautschi I, Shimkets R, Nelson-Williams C, Rossier BC and Lifton RP**. A de novo missense mutation of the beta subunit of the epithelial sodium channel causes hypertension and Liddle syndrome, identifying a proline-rich segment critical for regulation of channel activity. *Proc Natl Acad Sci U S A* 92: 11495-11499, 1995.

50. **Hanukoglu A**. Type I pseudohypoaldosteronism includes two clinically and genetically distinct entities with either renal or multiple target organ defects. *J Clin Endocrinol Metab* 73: 936-944, 1991.

51. **Harris M, Firsov D, Vuagniaux G, Stutts MJ and Rossier BC**. A novel neutrophil elastase inhibitor prevents elastase activation and surface cleavage of the epithelial sodium channel expressed in Xenopus laevis oocytes. *J Biol Chem* 282: 58-64, 2007.

52. **Harris M, Garcia-Caballero A, Stutts MJ, Firsov D and Rossier BC**. Preferential assembly of epithelial sodium channel (ENaC) subunits in Xenopus oocytes: role of furin-mediated endogenous proteolysis. *J Biol Chem* 283: 7455-7463, 2008.

53. **Harvey BJ, Thomas SR and Ehrenfeld J**. Intracellular pH controls cell membrane Na+ and K+ conductances and transport in frog skin epithelium. *J Gen Physiol* 92: 767-791, 1988.

54. **Helms MN, Jain L, Self JL and Eaton DC**. Redox Regulation of Epithelial Sodium Channels Examined in Alveolar Type 1 and 2 Cells Patch-clamped in Lung Slice Tissue. *J Biol Chem* 283: 22875-22883, 2008.

55. **Henry PC, Kanelis V, O'Brien MC, Kim B, Gautschi I, Forman-Kay J, Schild L and Rotin D**. Affinity and specificity of interactions between Nedd4 isoforms and the epithelial Na+ channel. *J Biol Chem* 278: 20019-20028, 2003.

56. **Hiltunen TP, Hannila-Handelberg T, Petajaniemi N, Kantola I, Tikkanen I, Virtamo J, Gautschi I, Schild L and Kontula K**. Liddle's syndrome associated with a point mutation in the extracellular domain of the epithelial sodium channel gamma subunit. *J Hypertens* 20: 2383-2390, 2002.

57. **Hirsh AJ, Zhang J, Zamurs A, Fleegle J, Thelin WR, Caldwell RA, Sabater JR, Abraham WM, Donowitz M, Cha B, Johnson KB, St George JA, Johnson MR and Boucher RC**. Pharmacological properties of N-(3,5-diamino-6-chloropyrazine-2-carbonyl)-N'-4-[4-(2,3-dihydroxypropoxy) phenyl]butyl-guanidine methanesulfonate (552-02), a novel epithelial sodium channel blocker with potential clinical efficacy for cystic fibrosis lung disease. *J Pharmacol Exp Ther* 325: 77-88, 2008.

58. **Hughey RP, Bruns JB, Kinlough CL, Harkleroad KL, Tong Q, Carattino MD, Johnson JP, Stockand JD and Kleyman TR**. Epithelial sodium channels are activated by furin-dependent proteolysis. *J Biol Chem* 279: 18111-18114, 2004.

59. **Hughey RP, Bruns JB, Kinlough CL and Kleyman TR**. Distinct pools of epithelial sodium channels are expressed at the plasma membrane. *J Biol Chem* 279: 48491-48494, 2004.

60. **Hughey RP, Mueller GM, Bruns JB, Kinlough CL, Poland PA, Harkleroad KL, Carattino MD and Kleyman TR**. Maturation of the epithelial Na+ channel involves proteolytic processing of the alpha- and gamma-subunits. *J Biol Chem* 278: 37073-37082, 2003.

61. **Jasti J, Furukawa H, Gonzales EB and Gouaux E**. Structure of acid-sensing ion channel 1 at 1.9 A resolution and low pH. *Nature* 449: 316-323, 2007.

62. **Kabra R, Knight KK, Zhou R and Snyder PM**. Nedd4-2 induces endocytosis and degradation of proteolytically cleaved epithelial Na+ channels. *J Biol Chem* 283: 6033-6039, 2008.

63. **Kellenberger S, Auberson M, Gautschi I, Schneeberger E and Schild L**. Permeability properties of ENaC selectivity filter mutants. *J Gen Physiol* 118: 679-692, 2001.

64. **Kellenberger S, Gautschi I, Pfister Y and Schild L**. Intracellular thiol-mediated modulation of epithelial sodium channel activity. *J Biol Chem* 280: 7739-7747, 2005.

65. **Kellenberger S, Gautschi I, Rossier BC and Schild L**. Mutations causing Liddle syndrome reduce sodium-dependent downregulation of the epithelial sodium channel in the Xenopus oocyte expression system. *J Clin Invest* 101: 2741-2750, 1998.

66. **Kellenberger S, Gautschi I and Schild L**. Mutations in the epithelial Na+ channel ENaC outer pore disrupt amiloride block by increasing its dissociation rate. *Mol Pharmacol* 64: 848-856, 2003.

67. **Kellenberger S, Gautschi I and Schild L**. An external site controls closing of the epithelial Na+ channel ENaC. *J Physiol* 543: 413-424, 2002.

68. **Kellenberger S, Gautschi I and Schild L**. A single point mutation in the pore region of the epithelial Na+ channel changes ion selectivity by modifying molecular sieving. *Proc Natl Acad Sci U S A* 96: 4170-4175, 1999.

69. **Kellenberger S, Hoffmann-Pochon N, Gautschi I, Schneeberger E and Schild L**. On the molecular basis of ion permeation in the epithelial Na+ channel. *J Gen Physiol* 114: 13-30, 1999.

70. **Kellenberger S and Schild L**. Epithelial sodium channel/degenerin family of ion channels: a variety of functions for a shared structure. *Physiol Rev* 82: 735-767, 2002.

71. **Knight KK, Olson DR, Zhou R and Snyder PM**. Liddle's syndrome mutations increase Na+ transport through dual effects on epithelial Na+ channel surface expression and proteolytic cleavage. *Proc Natl Acad Sci U S A* 103: 2805-2808, 2006.

72. **Knight KK, Wentzlaff DM and Snyder PM**. Intracellular sodium regulates proteolytic activation of the epithelial sodium channel. *J Biol Chem* 2008.

73. **Kosari F, Sheng S, Li J, Mak DO, Foskett JK and Kleyman TR**. Subunit stoichiometry of the epithelial sodium channel. *J Biol Chem* 273: 13469-13474, 1998.

74. **Ladner CL, Yang J, Turner RJ and Edwards RA**. Visible fluorescent detection of proteins in polyacrylamide gels without staining. *Anal Biochem* 326: 13-20, 2004.

75. **Li J, Sheng S, Perry CJ and Kleyman TR**. Asymmetric organization of the pore region of the epithelial sodium channel. *J Biol Chem* 278: 13867-13874, 2003.

76. **Li SS**. Specificity and versatility of SH3 and other proline-recognition domains: structural basis and implications for cellular signal transduction. *Biochem J* 390: 641-653, 2005.

77. **Liddle G.W., Bledsoe T. and Coppage W.S.Jr**. A familial renal disorder simulating primary aldosteronism but with negligible aldosterone secretion. *Trans Assoc Am Physicians* 76: 199-213, 1963.

78. **Lingueglia E**. Acid-sensing ion channels in sensory perception. *J Biol Chem* 282: 17325-17329, 2007.

79. **Lingueglia E, Champigny G, Lazdunski M and Barbry P**. Cloning of the amiloride-sensitive FMRFamide peptide-gated sodium channel. *Nature* 378: 730-733, 1995.

80. **Loffing J, Zecevic M, Feraille E, Kaissling B, Asher C, Rossier BC, Firestone GL, Pearce D and Verrey F**. Aldosterone induces rapid apical translocation of ENaC in early portion of renal collecting system: possible role of SGK. *Am J Physiol Renal Physiol* 280: F675-F682, 2001.

81. **Lott JS, Coddington-Lawson SJ, Teesdale-Spittle PH and McDonald FJ**. A single WW domain is the predominant mediator of the interaction between the human ubiquitin-protein ligase Nedd4 and the human epithelial sodium channel. *Biochem J* 361: 481-488, 2002.

82. **Lu C, Jiang C, Pribanic S and Rotin D**. CFTR stabilizes ENaC at the plasma membrane. *J Cyst Fibros* 6: 419-422, 2007.

83. **Maarouf AB, Sheng N, Chen J, Winarski KL, Okumura S, Carattino MD, Boyd CR, Kleyman TR and Sheng S**. Novel determinants of epithelial sodium channel gating within extracellular thumb domains. *J Biol Chem* 2009.

84. **Mall M, Grubb BR, Harkema JR, O'Neal WK and Boucher RC**. Increased airway epithelial Na+ absorption produces cystic fibrosis-like lung disease in mice. *Nat Med* 10: 487-493, 2004.

85. **Masilamani S, Kim GH, Mitchell C, Wade JB and Knepper MA**. Aldosterone-mediated regulation of ENaC alpha, beta, and gamma subunit proteins in rat kidney. *J Clin Invest* 104: R19-R23, 1999.

86. **May A, Puoti A, Gaeggeler HP, Horisberger JD and Rossier BC**. Early effect of aldosterone on the rate of synthesis of the epithelial sodium channel alpha subunit in A6 renal cells. *J Am Soc Nephrol* 8: 1813-1822, 1997.

87. **McDonald FJ**. A new SGK1 knockout mouse. *Am J Physiol Renal Physiol* 2008.

88. **Mikosz CA, Brickley DR, Sharkey MS, Moran TW and Conzen SD**. Glucocorticoid receptor-mediated protection from apoptosis is associated with induction of the serine/threonine survival kinase gene, sgk-1. *J Biol Chem* 276: 16649-16654, 2001.

89. **Myerburg MM, Butterworth MB, McKenna EE, Peters KW, Frizzell RA, Kleyman TR and Pilewski JM**. Airway surface liquid volume regulates ENaC by altering the serine protease-protease inhibitor balance: a mechanism for sodium hyperabsorption in cystic fibrosis. *J Biol Chem* 281: 27942-27949, 2006.

90. **Naray-Fejes-Toth A, Canessa C, Cleaveland ES, Aldrich G and Fejes-Toth G**. sgk is an aldosterone-induced kinase in the renal collecting duct. Effects on epithelial na+ channels. *J Biol Chem* 274: 16973-16978, 1999.

91. **Nesterov V, Dahlmann A, Bertog M and Korbmacher C**. Trypsin can activate the epithelial sodium channel (ENaC) in microdissected mouse distal nephron. *Am J Physiol Renal Physiol* 2008.

92. **Palmer LG and Andersen OS**. Interactions of amiloride and small monovalent cations with the epithelial sodium channel. Inferences about the nature of the channel pore. *Biophys J* 55: 779-787, 1989.

93. **Palmer LG and Frindt G**. Amiloride-sensitive Na channels from the apical membrane of the rat cortical collecting tubule. *Proc Natl Acad Sci U S A* 83: 2767-2770, 1986.

94. **Palmer LG and Frindt G**. Conductance and gating of epithelial Na channels from rat cortical collecting tubule. Effects of luminal Na and Li. *J Gen Physiol* 92: 121-138, 1988.

95. **Pfister Y, Gautschi I, Takeda AN, van BM, Kellenberger S and Schild L**. A gating mutation in the internal pore of ASIC1a. *J Biol Chem* 281: 11787-11791, 2006.

96. **Poet M, Tauc M, Lingueglia E, Cance P, Poujeol P, Lazdunski M and Counillon L**. Exploration of the pore structure of a peptide-gated Na+ channel. *EMBO J* 20: 5595-5602, 2001.

97. **Pradervand S, Vandewalle A, Bens M, Gautschi I, Loffing J, Hummler E, Schild L and Rossier BC**. Dysfunction of the epithelial sodium channel expressed in the kidney of a mouse model for Liddle syndrome. *J Am Soc Nephrol* 14: 2219-2228, 2003.

98. **Quinby WC, Dexter L, Sandmeyer JA and Haynes FW**. The renal humoral pressor mechanism in man. II. The effect of transitory complete constriction of the human renal artery on blood pressure and on the concentration of renin, hypertensinogen, and hypertensinase of renal arterial and venous blood, with animal observations. *J Clin Invest* 24: 69-74, 1945.

99. **Raikwar NS and Thomas CP**. Nedd4-2 isoforms ubiquitinate individual epithelial sodium channel subunits and reduce surface expression and function of the epithelial sodium channel. *Am J Physiol Renal Physiol* 294: F1157-F1165, 2008.

100. **Robert-Nicoud M, Flahaut M, Elalouf JM, Nicod M, Salinas M, Bens M, Doucet A, Wincker P, Artiguenave F, Horisberger JD, Vandewalle A, Rossier BC and Firsov D**. Transcriptome of a mouse kidney cortical collecting duct cell line: effects of aldosterone and vasopressin. *Proc Natl Acad Sci U S A* 98: 2712-2716, 2001.

101. **Rossier BC and Stutts MJ**. Activation of the Epithelial Sodium Channel (ENaC) by Serine Proteases. *Annu Rev Physiol* 2008.

102. **Rost B, Yachdav G and Liu J**. The PredictProtein server. *Nucleic Acids Res* 32: W321-W326, 2004.

103. **Schaedel C, Marthinsen L, Kristoffersson AC, Kornfalt R, Nilsson KO, Orlenius B and Holmberg L**. Lung symptoms in pseudohypoaldosteronism type 1 are associated with deficiency of the alpha-subunit of the epithelial sodium channel. *J Pediatr* 135: 739-745, 1999.

104. **Schild L, Canessa CM, Shimkets RA, Gautschi I, Lifton RP and Rossier BC**. A mutation in the epithelial sodium channel causing Liddle disease increases channel activity in the Xenopus laevis oocyte expression system. *Proc Natl Acad Sci U S A* 92: 5699-5703, 1995.

105. **Schild L, Schneeberger E, Gautschi I and Firsov D**. Identification of amino acid residues in the alpha, beta, and gamma subunits of the epithelial sodium channel (ENaC) involved in amiloride block and ion permeation. *J Gen Physiol* 109: 15-26, 1997.

106. **Sheng S, Bruns JB and Kleyman TR**. Extracellular histidine residues crucial for Na+ self-inhibition of epithelial Na+ channels. *J Biol Chem* 279: 9743-9749, 2004.

107. **Sheng S, Carattino MD, Bruns JB, Hughey RP and Kleyman TR**. Furin cleavage activates the epithelial Na+ channel by relieving Na+ self-inhibition. *Am J Physiol Renal Physiol* 290: F1488-F1496, 2006.

108. **Sheng S, Li J, McNulty KA, Avery D and Kleyman TR**. Characterization of the selectivity filter of the epithelial sodium channel. *J Biol Chem* 275: 8572-8581, 2000.

109. **Sheng S, Li J, McNulty KA, Kieber-Emmons T and Kleyman TR**. Epithelial sodium channel pore region. structure and role in gating. *J Biol Chem* 276: 1326-1334, 2001.

110. **Sheng S, Maarouf AB, Bruns JB, Hughey RP and Kleyman TR**. Functional role of extracellular loop cysteine residues of the epithelial Na+ channel in Na+ self-inhibition. *J Biol Chem* 2007.

111. **Sheng S, McNulty KA, Harvey JM and Kleyman TR**. Second transmembrane domains of ENaC subunits contribute to ion permeation and selectivity. *J Biol Chem* 276: 44091-44098, 2001.

112.	**Sheng S, Perry CJ, Kashlan OB and Kleyman TR**. Side chain orientation of residues lining the selectivity filter of epithelial Na+ channels. *J Biol Chem* 280: 8513-8522, 2005.

113.	**Sheng S, Perry CJ and Kleyman TR**. Extracellular Zn2+ activates epithelial Na+ channels by eliminating Na+ self-inhibition. *J Biol Chem* 279: 31687-31696, 2004.

114.	**Shi PP, Cao XR, Sweezer EM, Kinney TS, Williams NR, Husted RF, Nair R, Weiss RM, Williamson RA, Sigmund CD, Snyder PM, Staub O, Stokes JB and Yang B**. Salt-sensitive hypertension and cardiac hypertrophy in mice deficient in the ubiquitin ligase Nedd4-2. *Am J Physiol Renal Physiol* 295: F462-F470, 2008.

115.	**Shimkets RA, Warnock DG, Bositis CM, Nelson-Williams C, Hansson JH, Schambelan M, Gill JR, Jr., Ulick S, Milora RV, Findling JW and .** Liddle's syndrome: heritable human hypertension caused by mutations in the beta subunit of the epithelial sodium channel. *Cell* 79: 407-414, 1994.

116.	**Snyder PM, Bucher DB and Olson DR**. Gating induces a conformational change in the outer vestibule of ENaC. *J Gen Physiol* 116: 781-790, 2000.

117.	**Snyder PM, Olson DR and Thomas BC**. Serum and glucocorticoid-regulated kinase modulates Nedd4-2-mediated inhibition of the epithelial Na+ channel. *J Biol Chem* 277: 5-8, 2002.

118.	**Staruschenko A, Adams E, Booth RE and Stockand JD**. Epithelial Na+ channel subunit stoichiometry. *Biophys J* 88: 3966-3975, 2005.

119. **Staruschenko A, Pochynyuk O, Vandewalle A, Bugaj V and Stockand JD**. Acute regulation of the epithelial Na+ channel by phosphatidylinositide 3-OH kinase signaling in native collecting duct principal cells. *J Am Soc Nephrol* 18: 1652-1661, 2007.

120. **Staub O, Gautschi I, Ishikawa T, Breitschopf K, Ciechanover A, Schild L and Rotin D**. Regulation of stability and function of the epithelial Na+ channel (ENaC) by ubiquitination. *EMBO J* 16: 6325-6336, 1997.

121. **Stockand JD**. New ideas about aldosterone signaling in epithelia. *Am J Physiol Renal Physiol* 282: F559-F576, 2002.

122. **Stutts MJ, Canessa CM, Olsen JC, Hamrick M, Cohn JA, Rossier BC and Boucher RC**. CFTR as a cAMP-dependent regulator of sodium channels. *Science* 269: 847-850, 1995.

123. **Sutherland SP, Benson CJ, Adelman JP and McCleskey EW**. Acid-sensing ion channel 3 matches the acid-gated current in cardiac ischemia-sensing neurons. *Proc Natl Acad Sci U S A* 98: 711-716, 2001.

124. **Takeda AN, Gautschi I, van Bemmelen MX and Schild L**. Cadmium trapping in an epithelial sodium channel pore mutant. *J Biol Chem* 282: 31928-31936, 2007.

125. **Verrey F, Fakitsas P, Adam G and Staub O**. Early transcriptional control of ENaC (de)ubiquitylation by aldosterone. *Kidney Int* 73: 691-696, 2008.

126. **Vuagniaux G, Vallet V, Jaeger NF, Hummler E and Rossier BC**. Synergistic activation of ENaC by three membrane-bound channel-activating serine proteases (mCAP1, mCAP2, and mCAP3) and serum- and glucocorticoid-regulated kinase (Sgk1) in Xenopus Oocytes. *J Gen Physiol* 120: 191-201, 2002.

127. **Vuagniaux G, Vallet V, Jaeger NF, Pfister C, Bens M, Farman N, Courtois-Coutry N, Vandewalle A, Rossier BC and Hummler E**. Activation of the amiloride-sensitive epithelial sodium channel by the serine protease mCAP1 expressed in a mouse cortical collecting duct cell line. *J Am Soc Nephrol* 11: 828-834, 2000.

128. **Waldmann R, Champigny G, Bassilana F, Heurteaux C and Lazdunski M**. A proton-gated cation channel involved in acid-sensing. *Nature* 386: 173-177, 1997.

129. **Waldmann R and Lazdunski M**. H(+)-gated cation channels: neuronal acid sensors in the NaC/DEG family of ion channels. *Curr Opin Neurobiol* 8: 418-424, 1998.

130. **Wang HC, Zentner MD, Deng HT, Kim KJ, Wu R, Yang PC and Ann DK**. Oxidative stress disrupts glucocorticoid hormone-dependent transcription of the amiloride-sensitive epithelial sodium channel alpha-subunit in lung epithelial cells through ERK-dependent and thioredoxin-sensitive pathways. *J Biol Chem* 275: 8600-8609, 2000.

131. **Wang S, Publicover S and Gu Y**. An oxygen-sensitive mechanism in regulation of epithelial sodium channel. *Proc Natl Acad Sci U S A* 2009.

132. **Wemmie JA, Price MP and Welsh MJ**. Acid-sensing ion channels: advances, questions and therapeutic opportunities. *Trends Neurosci* 29: 578-586, 2006.

133. **Wulff P, Vallon V, Huang DY, Volkl H, Yu F, Richter K, Jansen M, Schlunz M, Klingel K, Loffing J, Kauselmann G, Bosl MR, Lang F and Kuhl D**. Impaired renal Na(+) retention in the sgk1-knockout mouse. *J Clin Invest* 110: 1263-1268, 2002.

134. **Xiong ZG, Pignataro G, Li M, Chang SY and Simon RP**. Acid-sensing ion channels (ASICs) as pharmacological targets for neurodegenerative diseases. *Curr Opin Pharmacol* 8: 25-32, 2008.